AFFDL-TR-71-62
VOLUME IV
Part I

Volume IV. Wind Tunnel Test of the Conversion Process of a Folding Tilt-Rotor Aircraft Using a Semispan Unpowered Model

Part I. Analysis and Results

John Magee
Robert Taylor
The Boeing Company, Vertol Division
Philadelphia, Pennsylvania

TECHNICAL REPORT AFFDL-TR-71-62, VOLUME IV, PART I

August 1971

Air Force Flight Dynamics Laboratory
Air Force Systems Command
Wright-Patterson Air Force Base, Ohio

Security Classification

DOCUMENT CONTROL DATA - R & D

(Security classification of title, body of abstract and indexing annotation must be entered when the overall report is classified)

ORIGINATING ACTIVITY (Corporate author) The Boeing Company, Vertol Division Boeing Center P. O. Box 16858 Philadelphia, Pa. 19142	2a. REPORT SECURITY CLASSIFICATION 2b. GROUP

REPORT TITLE

WIND TUNNEL TEST OF THE CONVERSION PROCESS OF A FOLDING TILT ROTOR AIRCRAFT USING A SEMISPAN UNPOWERED MODEL

Part I Analysis and Results

DESCRIPTIVE NOTES (Type of report and inclusive dates)

Final Report

AUTHOR(S) (First name, middle initial, last name)

John Magee

Robert Taylor

REPORT DATE	7a. TOTAL NO. OF PAGES	7b. NO. OF REFS
August 1971	135	2

a. CONTRACT OR GRANT NO. F33615-69-C-1577	9a. ORIGINATOR'S REPORT NUMBER(S) D213-10000-4, Volume IV, Part I
b. PROJECT NO.	
c.	9b. OTHER REPORT NO(S) (Any other numbers that may be assigned this report) AFFDL-TR-71-62, Volume IV, Part I
d.	

10. DISTRIBUTION STATEMENT

Approved for Public Release Distribution Unlimited

11. SUPPLEMENTARY NOTES	12. SPONSORING MILITARY ACTIVITY Air Force Flight Dynamics Laboratory Air Force Systems Command Wright-Patterson Air Force Base,Ohio

13. ABSTRACT

Wind tunnel test data obtained with a 33.75-inch diameter nonarticulated folding tilt rotor mounted on a semispan wing show the effects of collective pitch schedule variations on transient lift, drag, and pitching moment of the aircraft. Blade loads data presented show that loads do not limit the conversion process. The model was configured with prop/rotor blades which had an in-plane natural frequency of less than 1.0/rev. The testing included study of the aerodynamics and dynamics of rotor spin-up, spin-down, stopping, and steady windmilling. Correlation with predictions of transient aerodynamic performance, static derivatives of the prop/rotor, and blade loads are included.

DD FORM 1 NOV 68 1473 REPLACES DD FORM 1473, 1 JAN 64, WHICH IS OBSOLETE FOR ARMY USE.

Security Classification

NOTICE

When Government drawings, specifications, or other data are used for any purpose other than in connection with a definitely related Government procurement operation, the United States Government thereby incurs no responsibility nor any obligation whatsoever; and the fact that the government may have formulated, furnished, or in any way supplied the said drawings, specifications, or other data, is not to be regarded by implication or otherwise as in any manner licensing the holder or any other person or corporation, or conveying any rights or permission to manufacture, use, or sell any patented invention that may in any way be related thereto.

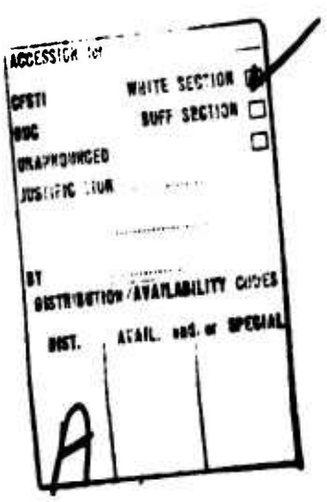

Copies of this report should not be returned unless return is required by security considerations, contractual obligations, or notice on a specific document.

KEY WORDS	LINK A		LINK B		LINK C	
	ROLE	WT	ROLE	WT	ROLE	WT
Nonarticulated folding tilt rotor						
Blade loads						
Prop/rotor						
Rotor spin-up						
Rotor spin-down						

Volume VIII Summary of Structural Design Criteria and Aerodynamic Prediction Techniques

The contractor's report number is D213-10000-4.

This technical report has been reviewed and is approved.

ERNEST J. CROSS, JR.
Lt. Colonel, USAF
Chief, V/STOL Technology Division

AFFDL-TR-71-62
Volume IV
Part I

VOLUME IV. WIND TUNNEL TEST OF THE CONVERSION PROCESS OF A FOLDING TILT-ROTOR AIRCRAFT USING A SEMISPAN UNPOWERED MODEL

Part I. Analysis and Results

John Magee

Robert Taylor

The Boeing Company, Vertol Division

Philadelphia, Pennsylvania

TECHNICAL REPORT AFFDL-TR-71-62, VOLUME IV, PART I

August 1971

Air Force Flight Dynamics Laboratory

Air Force Systems Command

Wright-Patterson Air Force Base, Ohio

D213-10000-4

FOREWORD

This report was prepared by The Boeing Company, Vertol Division, Philadelphia, Pennsylvania, for the Air Force Flight Dynamics Laboratory, Wright-Patterson Air Force Base, Ohio, under Phase II of Contract F33615-69-C-1577. The contract was initiated under Project 69BT, "US/FRG Technology - V/STOL Aircraft Task 02," Prop/Rotor Technology. The contract objective is to develop design criteria and aerodynamic prediction techniques for the folding tilt-rotor concept through a program of model testing and analysis. This covers the first of four test programs which will be reported in separate volumes of the final report. Part II of this volume presents the blade stress analyses, model details, and bench tests. It was submitted by the authors in June 1971. The contract was administered by the Air Force Flight Dynamics Laboratory, Wright-Patterson Air Force Base, Ohio, with Mr. Daniel E. Fraga (AFFDL/FV) as Project Engineer.

The reports published under this contract for design studies and model tests of the Stowed Tilt Rotor concept are:

Volume I	Parametric Design Studies
Volume II	Component Design Studies
Volume III	Performance Data for Parametric Study Aircraft
Volume IV	Wind Tunnel Test of the Conversion Process of a Folding Tilt-Rotor Aircraft Using a Semispan Unpowered Model
Volume V	Wind Tunnel Test of a Powered Tilt Rotor Performance Model
Volume VI	Wind Tunnel Test of a Powered Tilt Rotor Dynamic Model on a Simulated Free Flight Suspension System
Volume VII	Wind Tunnel Test of the Dynamics and Aerodynamics of Rotor Spinup, Stopping and Folding on a Semispan Folding Tilt Rotor Model

ABSTRACT

Wind tunnel test data obtained with a 33.75-inch diameter nonarticulated folding tilt rotor mounted on a semispan wing show the effects of collective pitch schedule variations on transient lift, drag, and pitching moment of the aircraft. Blade loads data presented show that loads do not limit the conversion process. The model was configured with prop/rotor blades which had an in-plane natural frequency of less than 1.0/rev. The testing included study of the aerodynamics and dynamics of rotor spin-up, spin-down, stopping, and steady windmilling. Correlation with predictions of transient aerodynamic performance, static derivatives of the prop/rotor, and blade loads are included.

CONTENTS

ILLUSTRATIONS

LIST OF SYMBOLS

b	Number of blades	—
c	Blade chord	ft
$\bar{c}$	Wing mean aerodynamic chord	ft
C_D	Drag coefficient $\frac{D}{qS}$	—
C_L	Lift coefficient $\frac{L}{qS}$	—
C_M	Pitching moment coefficient $\frac{M}{qS\bar{c}}$	—
D	Aerodynamic drag parallel to wind axis	lb
E	Modulus of elasticity (Young's Modulus)	lb/in^2
f_t	Tensile stress	lb/in^2
f_b	Bending stress	lb/in^2
GJ	Blade torsional stiffness	$lb\text{-}in^2$
I	Moment of inertia	$lb\text{-}ft\text{-}sec^2$
J	Propeller advance ratio, $\pi V/\Omega R$	—
k_θ	Spring rate	in-lb
L	Aerodynamic lift	lb
M	Aerodynamic pitching moment	ft-lb
M_c	Chord bending moment	in-lb

LIST OF SYMBOLS (Continued)

M_f	Flap bending moment	in-lb
q	Freestream dynamic pressure, $1/2\rho V^2$	lb/ft^2
r	Radius to a blade station	ft
R	Blade radius	ft
S	Wing reference area	ft^2
t	Blade section thickness	ft
V	Tunnel speed	ft/sec
W	Running blade weight	lb/in
x	Distance from blade centroid to vertical station	in
α	Wing and/or rotor angle of attack	degrees
δ	Wing flap deflection angle	degrees
ρ	Air density	$slugs/ft^3$
σ	Rotor solidity, $\frac{bc}{\pi R}$	—
θ_{75}	Blade collective pitch at .75R	degrees
θ_T	Blade twist caused by load application	degrees
Ω	Rotor angular velocity	rad/sec
ω_L	First mode, in-plane blade natural frequency	rad/sec

LIST OF SYMBOLS (Continued)

ω_β	First mode, flapwise blade natural frequency	rad/sec
$\Delta\theta$	Torsional deflection	degrees
Δf	Flapwise displacement	in
Δc	Chordwise deflection	in

SECTION I

INTRODUCTION

This report presents a portion of a continuing effort to acquire the technology required for development of a stowed/tilt-rotor concept aircraft. A design study[1] of this aircraft was completed in September 1969. The work reported herein is part of Phase II of Contract F33615-69-C-1577 which is aimed at developing the design criteria and substantiated prediction methodology required for this aircraft development.

The stowed/tilt-rotor concept aircraft hovers and makes a transition to forward flight with the rotor shaft horizontal, in the same manner as a pure tilt-rotor aircraft. However, when the aircraft reaches a flight airspeed of 120 to 180 knots, the rotors are feathered and stopped and the blades are folded back into wingtip-mounted nacelles. Power is provided by convertible engines which are capable of proving shaft power for the rotor drive or fan power for cruise flight with the rotors folded.

Investigations of the concept has steadily advanced to the point where preliminary wind tunnel tests of the folding tilt rotor have been completed. However, much remains to be done to establish a firm base of technical data and design criteria for further development of the concept. Under USAF Flight Dynamics Laboratory Contract, Boeing is conducting a program of parametric design, analysis, and wind tunnel testing to establish design criteria for the stowed/tilt-rotor stoppable rotor concept. The test program reported is the first of four tests being conducted. This test was designed to provide the following information:

a. The development of a collective pitch schedule that minimizes transient longitudinal force and blade loads during rotor spin-up and stopping

---

1. Fry, B.L., DESIGN STUDIES AND MODEL TESTS OF THE STOWED TILT ROTOR CONCEPT, D213-10000-1, The Boeing Company, Vertol Division, Philadelphia, Pennsylvania, September 1969 (R&D Interim Report of Phase I).

b. Measurement of rotor force and moment stability derivatives of a hingeless rotor with flap frequency of about 1.25 per rev, including variations in rpm from design rpm down to zero rpm

c. Measurement of soft in-plane rotor blade loads during steady windmilling and conversion

d. Validation of analysis used for predictions of transient drag and blade loads during steady windmilling and conversion.

SECTION II

SUMMARY

A model consisting of an unpowered hingeless propeller/rotor mounted at the tip of a semispan wing has been tested to devise a collective pitch schedule that provides minimum drag changes and minimum blade loads during the spin-up and spin-down (feathering) processes required for stowing the rotor. Tests were conducted at various wing/propeller shaft angle-of-attack values appropriate to essentially axial flight and with various wing flap settings appropriate to trim and accelerated flight. Data obtained show that acceptably small values of transient drag can be obtained with a nonlinear collective schedule and with a spin-up or spin-down time equivalent to about 10 seconds full scale. This process is not restrained by blade loads for a hingeless propeller/rotor of the soft in-plane design. Steady windmilling vibratory blade loads were larger than predicted in the first phase of testing. They were caused by the proximity of rotating-blade chordwise natural frequency to 1 per rev. Tip tuning weights were added to reduce the blade chordwise frequency from 0.94 per rev to 0.74 per rev at design rpm. The retuned blades reduced the chordwise loads to predicted levels.

Collective pitch rates tested included linear and nonlinear schedules of various time durations. A summary of the schedules tested is presented in Figure 1. Linear schedules were tested for correlation with analysis. Schedules with a concave time history were predicted to cause minimum transient drag variations. Some of the tested schedules also had convex time histories. The significance of these variations is illustrated by the data given in Figure 2 for the more critical spin-up transient. The convex collective time history of the run 49 data is shown to produce a thrust transient (decreased C_D) at a model time of about 0.8 second and a drag peak at 2.0 seconds equivalent to 0.1 g's longitudinal acceleration of an aircraft. A concave time history illustrated by the run 58 data shows a drag variation equivalent to about 0.02 g.

Peak drag change data obtained in collective pitch schedule optimization testing are shown as a function of model lift in Figure 3. From the pretest predictions and the initial testing, a conversion time of two seconds was shown to produce acceptable transient drag peak with a linear schedule. As shown in

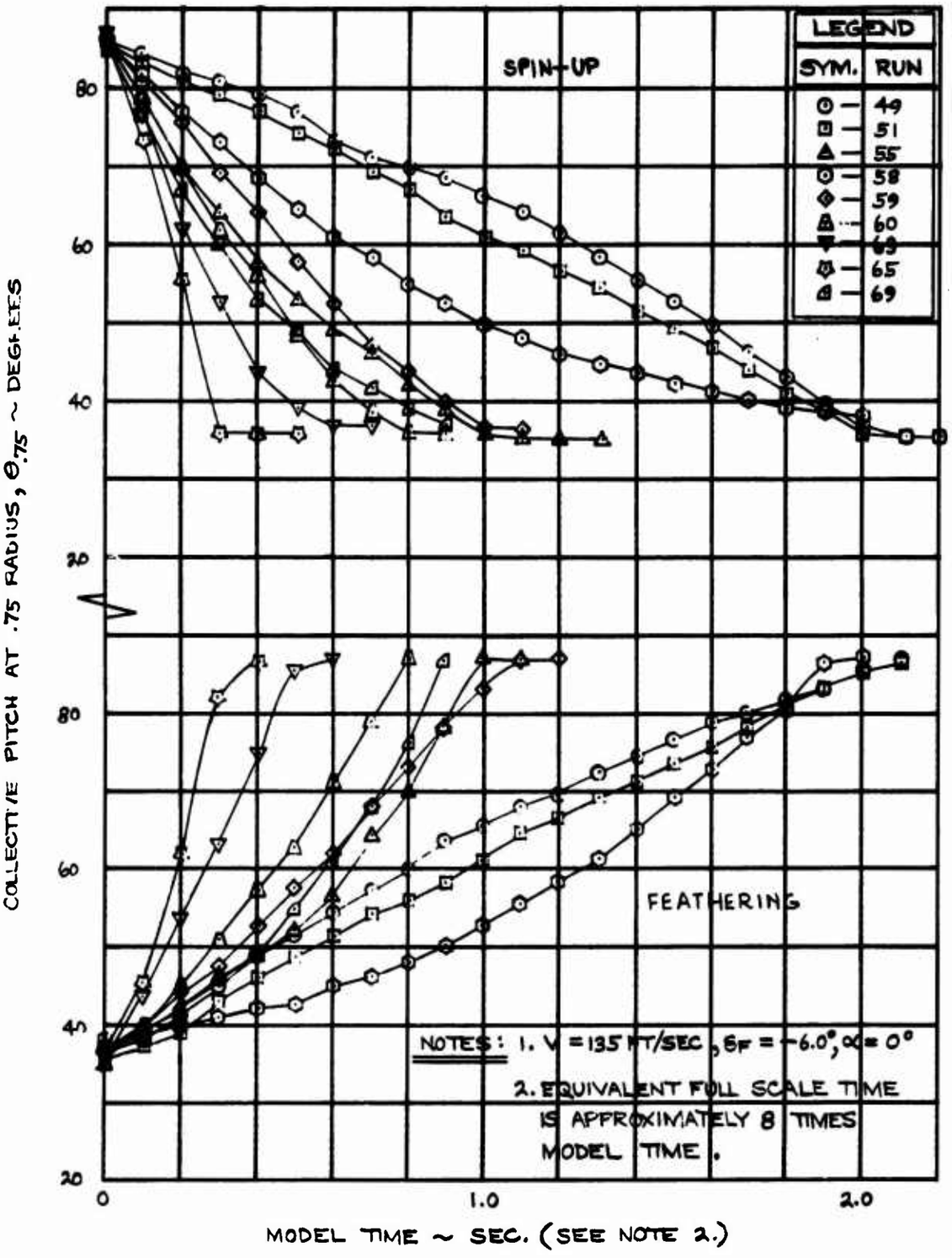

Figure 1. Summary of Transient Collective Pitch Schedules Tested at J=1.6 with Zero Wing Lift.

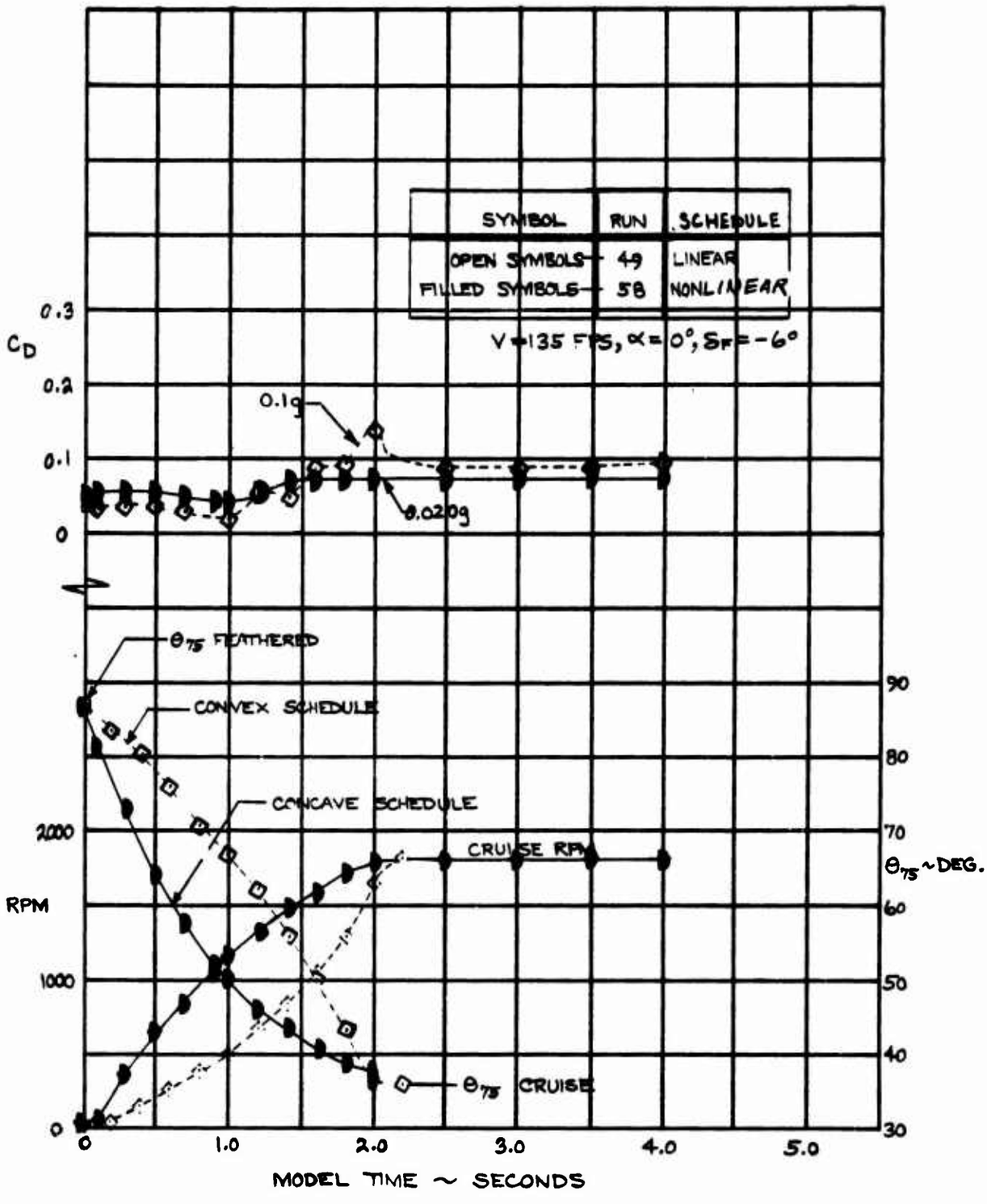

Figure 2. Transient Drag During Spin-up to Cruise Flight at J=1.6 Resulting from Collective Pitch Schedule Variations.

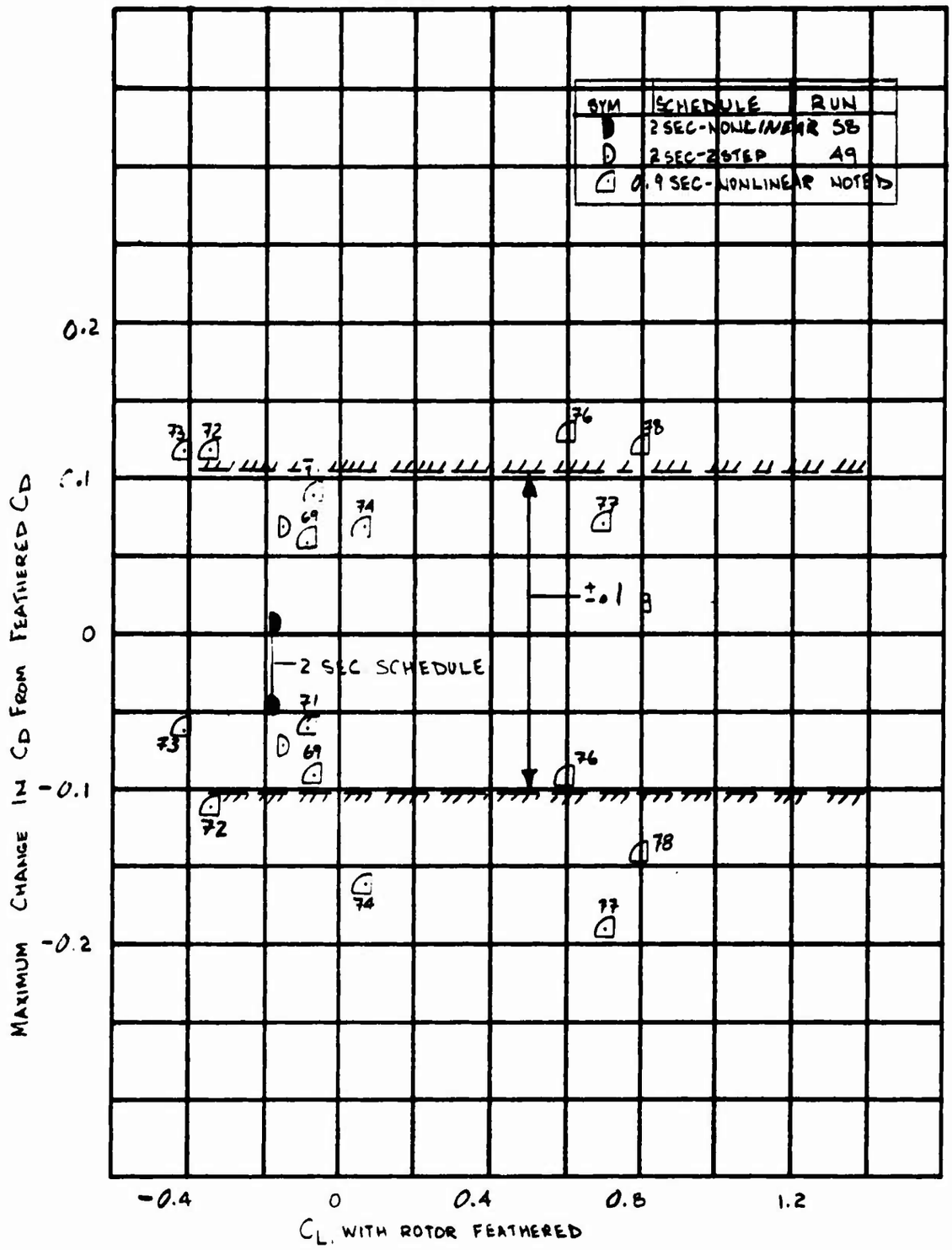

Figure 3. Variation of Peak Transient Drag in Conversion with Model Lift for Best Conversion Schedules.

the figure, use of a nonlinear schedule at two-second duration reduced the peak drag to well within the objective drag criterion. The drag time histories for these transients show drag peaks which can be reduced by further tailoring the schedule. A more gradual approach to the cruise collective is desirable.

Vibratory blade loads were measured during steady windmilling, spin-up, and spin-down. The maximum values recorded during spin-up and spin-down were only slightly higher than those in steady windmilling, as shown in Figure 4, and did not vary significantly. This indicates that the schedule will not be constrained by blade loads.

The blade and wing loads data provide information useful in the dynamic design of the rotor/wing system. Resonance crossings of individual modes with integers of rpm could be clearly identified. The blade loads were insensitive to wing frequencies, but were sensitive to blade frequency near the 1-per-rev crossing as expected. The vibratory wing loads showed amplification at the crossings of the wing frequencies with integers of the rotor rpm. Such conditions should be avoided in the full-scale design in the operating rpm range to minimize wing alternating loads.

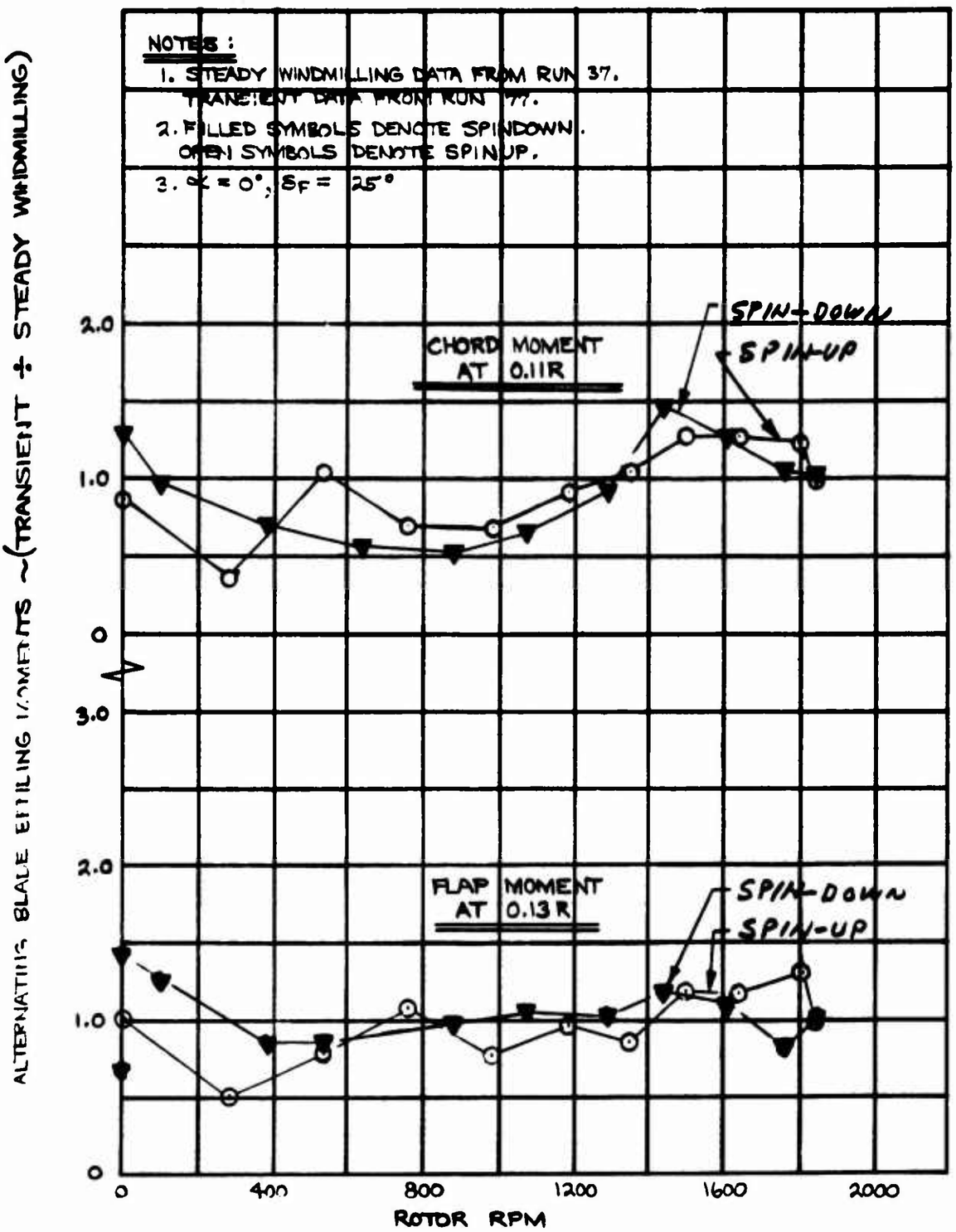

Figure 4. Small Changes between Blade Bending Loads in Transient and Steady Windmilling Blade Loads are Produced with Collective Schedule that Produces Minimum Drag Variations.

SECTION III

MODEL AND WIND TUNNEL

1. MODEL DESCRIPTION

1.1 GENERAL

The model tested consisted of a semispan wing/nacelle assembly and a three-bladed unpowered rotor. The model blades were of the hingeless, soft in-plane type and were dynamically representative of a typical folding tilt-rotor design. The rotor diameter was 33.75 inches and the rotor solidity was 0.102. Figure 5 illustrates the general arrangement of the model and Figure 6 shows the model mounted in the test section of the Princeton University wind tunnel. Model dimensions are given in Table I. Further details of the model may be found in Volume II of this report.

1.1.1 Wing/Nacelle Details

The model wing had an NACA 63A415.5 section and a 0.3 chord, single-slotted, full-span flap, manually adjustable over a ±30° range. The wing was geometrically scaled only and the nacelle was oversized (compared to a typical full-scale design) in order to accommodate sliprings, instrumentation, and the collective pitch actuating system.

The wing was not dynamically scaled and was sufficiently flexible such that mounting frequencies which coupled with the rotor resulted. Consequently, dynamic data relating to these modes are not scalable to full scale. The responses which did occur, however, were useful since they illustrate the existence of coupling phenomena which must be treated in the full-scale design analysis.

The wing airfoil was removable, as illustrated in Figure 6b, to allow isolation of the effect of the wing aerodynamics on the rotor.

Prior to the test program the stiffnesses of the model wing and support structure were measured, giving the following results:

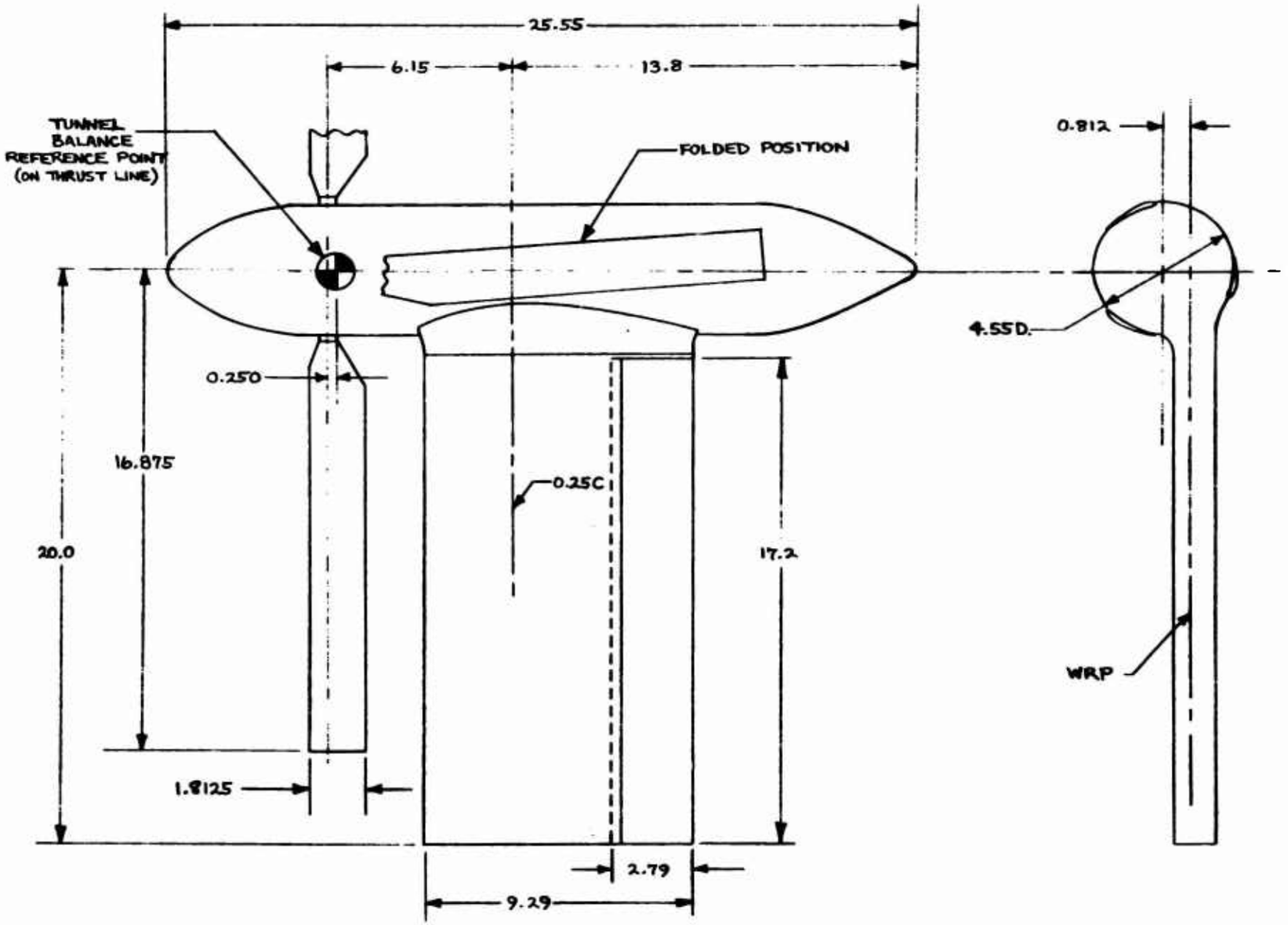

Figure 5. Semispan Folding Tilt Rotor Model Test Setup.

a. Model With Blades in Feathered Position and Flap Setting of 18.6°.

b. Model With Wing Airfoil Removed.

Figure 6. Model 213, 1/16-Scale Semispan Conversion Model Installed in Princeton University Low-speed Wind Tunnel.

TABLE I

MODEL DIMENSIONS

ROTOR

Number of Blades	3
Disc Area	894.62 $in.^2$
Solidity	0.102
Blade Radius	16.875 in.
Blade Chord	1.813 in.
Blade Airfoil Sections (XX = 100 t/c)	230XX

Blade Characteristics

r/R	Twist, Deg.	Thickness, t/c
0.2	24.2	0.250
0.3	20.75	0.143
0.4	17.3	0.127
0.5	13.8	0.120
0.6	10.35	0.115
0.7	6.9	0.109
0.8	3.45	0.103
0.9	0	0.097
1.0	-3.45	0.090

WING

Airfoil	NACA 63A415.5
Span (℄ Nacelle to Tunnel Floor)	20.0 in.
Chord (Constant)	9.29 in.
Area	185.8 $in.^2$
Aspect Ratio	2.15
Flap	0.3 Chord, Single-Slotted

NACELLE (Not Scaled)

Overall Length	25.55 in.
Maximum Diameter	4.55 in.
Angle of Incidence (WRT Wing)	0.0°

Chordwise	1,430 lb/in.
Lift	800 lb/in.
Torsion	65,000 in.-lb/radian

The deflections are rotor hub deflections or angular motions of the rotor shaft respectively. To further define the aeroelastic/dynamic properties of the wing, tests were performed to measure the natural frequencies of the wing with the nonrotating rotor. These tests were performed at various times during the test program. The results presented in Table II show the effects of changes made to the wing during testing. Testing prior to run 84 with the wing airfoil removed shows lower-than-expected frequencies. Wires were added to the model prior to run 95 to increase the wing chordwise stiffness.

At the end of phase 1 testing (i.e., after run 97) some additional testing was performed (run log Appendix) with different wing stiffnesses to evaluate the impact of wing frequencies on blade loads data. Three wing stiffnesses were considered with measured frequencies, as shown in Table II.

1.2 INSTRUMENTATION

Two of the three rotor blades used in the test program were instrumented to measure torsion, chordwise bending, and flapwise bending. The third and spare blades were uninstrumented. Instrumentation details may be found in Volume II.

The complete wing-nacelle-rotor system was mounted on a three-component strain-gage balance system designed to measure the transient lift, drag, and pitching moment of the model as a function of rotor speed and acceleration. The system consisted of two parallel plates connected by flexural supports. The lower plate was secured to the tunnel floor and the upper plate was restrained from in-plane translation by means of two orthogonal strain gages measuring body axis lift and drag forces. Rotation in the plane was resisted by a third gage which measured pitching moment.

The model nacelle contained instrumentation to measure blade collective pitch, blade azimuth position, and angular velocity. The blade pitch control system follow-up potentiometer was also used as the collective pitch data instrument.

TABLE II

WING NATURAL FREQUENCY TEST HISTORY

TEST WAS PERFORMED BEFORE RUN	MODEL CONFIGURATION	PHASE 1 TESTS NATURAL FREQUENCIES, CPS CHORDWISE	FLAPWISE	TORSION
23	Airfoil On	31.6	24.0	42.8
Repeat	Airfoil On	30.0	24.0	42.8
84	Airfoil Off	26.7	22.2	41.1
85	Airfoil Off	30.0	23.1	37.9
95	Airfoil Off (Chordwise-Stiffened)	33.3	-	41.1
Repeat	Airfoil Off	35.1	-	-
Repeat	Airfoil Off	33.3	-	-

	PHASE 2 TESTS NATURAL FREQUENCIES, CPS ORIGINAL	BRACED	SOFT
Flapwise bending	23.5	50.0	6.0
Chordwise bending	30.0	60.0	7.0
Torsion	42.4	66.7	15.0

NOTE: Model installed in tunnel with rotor not rotating.

1.3 BLADE PITCH CONTROL SYSTEM

The blade pitch control system was a high-gain, proportional-feed-back control system. Its function was to position the blade pitch control acutation mechanism in proportion to any combination of a number of command signals.

The system was designed to control the rotor in either of two modes of operations, rate (windmilling rpm) or position (feathered-rotor azimuthal position). In the rate mode, the rotor angular velocity was sensed and summed to command blade pitch angle. In the position mode, both angular velocity and rotor azimuth were sensed and summed to command the blade pitch angle.

The basic blade pitch angle control system had a saturating-integrator, ramp-input generator whose rate and amplitude could be adjusted independently.

The function generator gave a ramp output consisting of 10 potentiometer-adjustable slopes between 11 evenly spaced breakpoints. The output of these devices in turn was used as the command signal for the blade collective pitch positioning system. In use, a desired collective schedule was synthesized by assuming approximate potentiometer settings for the various slopes between breakpoints and then iterating to the final desired schedule.

To control the blade collective closely in following the commanded programs, it was necessary to increase greatly both the bandwidth and damping of the positioning servo inner loop. This was accomplished by incorporating into the blade positioning system a DC tachometer whose output was used as a damping signal for the blade pitch servo.

1.4 ROTOR DYNAMICS

Rotor chord- and flap-bending frequencies calculated from blade properties available before the bench test program using the collective pitch schedule required for windmilling conditions are shown in Figure 8.

The blade loads data obtained in Phase I testing indicated that the rotating-blade chordwise natural frequency at design rpm was closer to 1 per rev than desired, and closer than the initial blade properties showed. After the airplane force

tests were complete, a baffle test was run to accurately measure the rotating-blade natural frequencies. The baffle test consists of mounting pie-shaped baffles behind the rotor and measuring the rotor loads over an rpm sweep. The blade loads spike sharply at the rpm at which the blade frequencies are integers times the number of baffles used. Figure 7 is a photograph of the baffle test arrangement with four-per-rev baffles fitted. The blade loads are used to identify integer crossings of blade frequency; the results of these tests for the original blades in Phase 1 tests and for the subsequently tuned blades in Phase 2 tests are shown in Figure 9.

The blade chordwise rotating natural frequency for the original blades was 0.94 per rev at design rpm and, after the addition of 11 grams of tuning weight distributed over the outermost three inches of the blade at 12-percent chord, the rotating-blade chordwise frequency was dropped to 0.71 per rev.

1.5 ROTOR-WING DYNAMICS

The interaction of rotor and wing frequencies may be seen in Figure 74. Shown on this figure are the wing torsion and bending modes along with the rotor frequencies at 1/, 2/, and 3/rev. The effects of dynamic coupling on rotor blade loads will be discussed in Section V-3.

2. WIND TUNNEL TEST FACILITY

The wind tunnel used for these experiments is located on the Forrestal Campus of Princeton University. The tunnel itself is conventional in most respects. Pertinent characteristics are as follows:

a. Test section size - 4 feet high x 5 feet wide

b. Working medium - unconditioned air

c. Maximum steady velocity - 185 ft/sec

d. Minimum steady velocity - 30 ft/sec

e. Closed circuit - oriented in a vertical plane with the return below the test section

f. Closed test section - unvented and nonporous

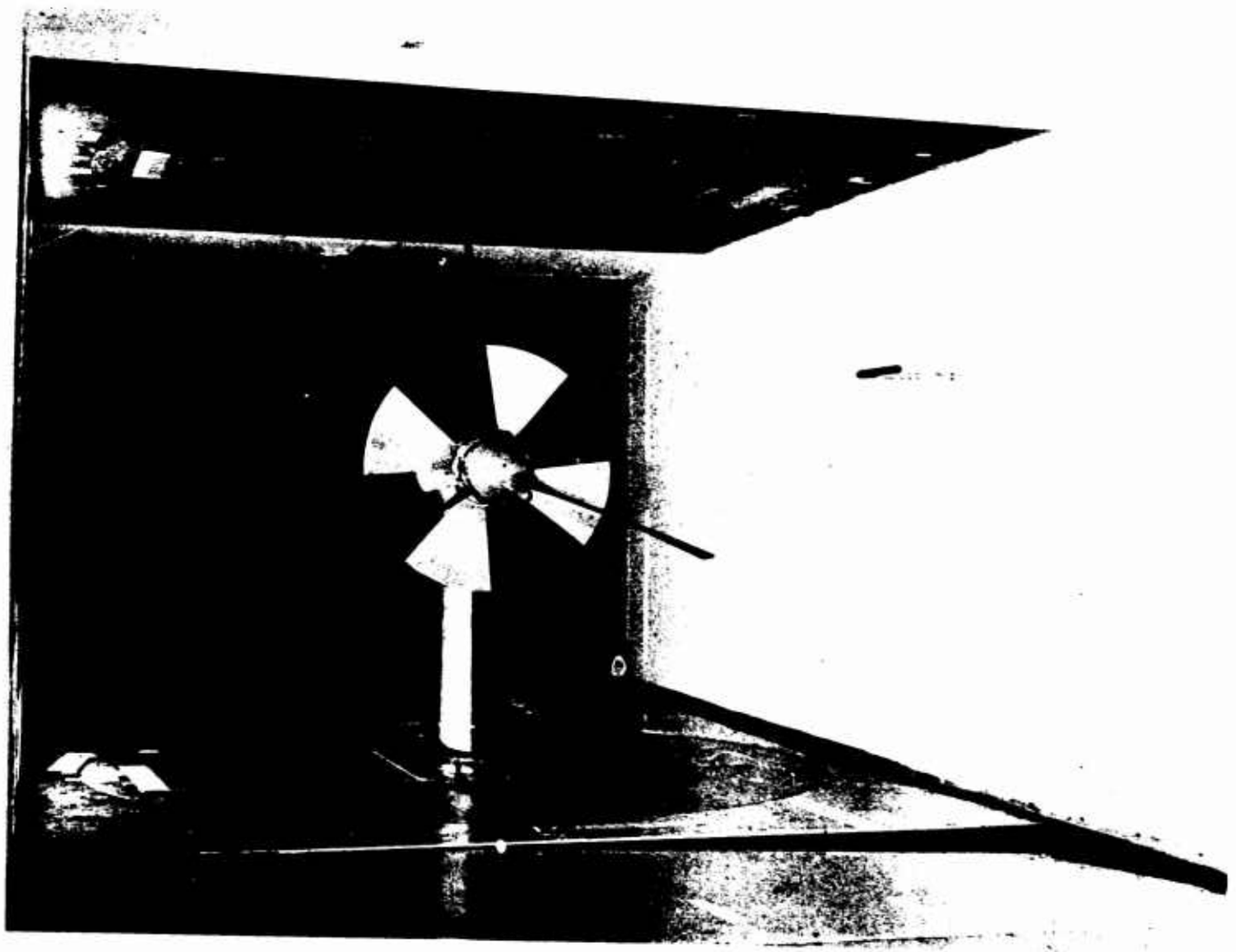

Figure 7. Model 213, 1/16 Scale Semispan Conversion Model with 4/Rev Baffle.

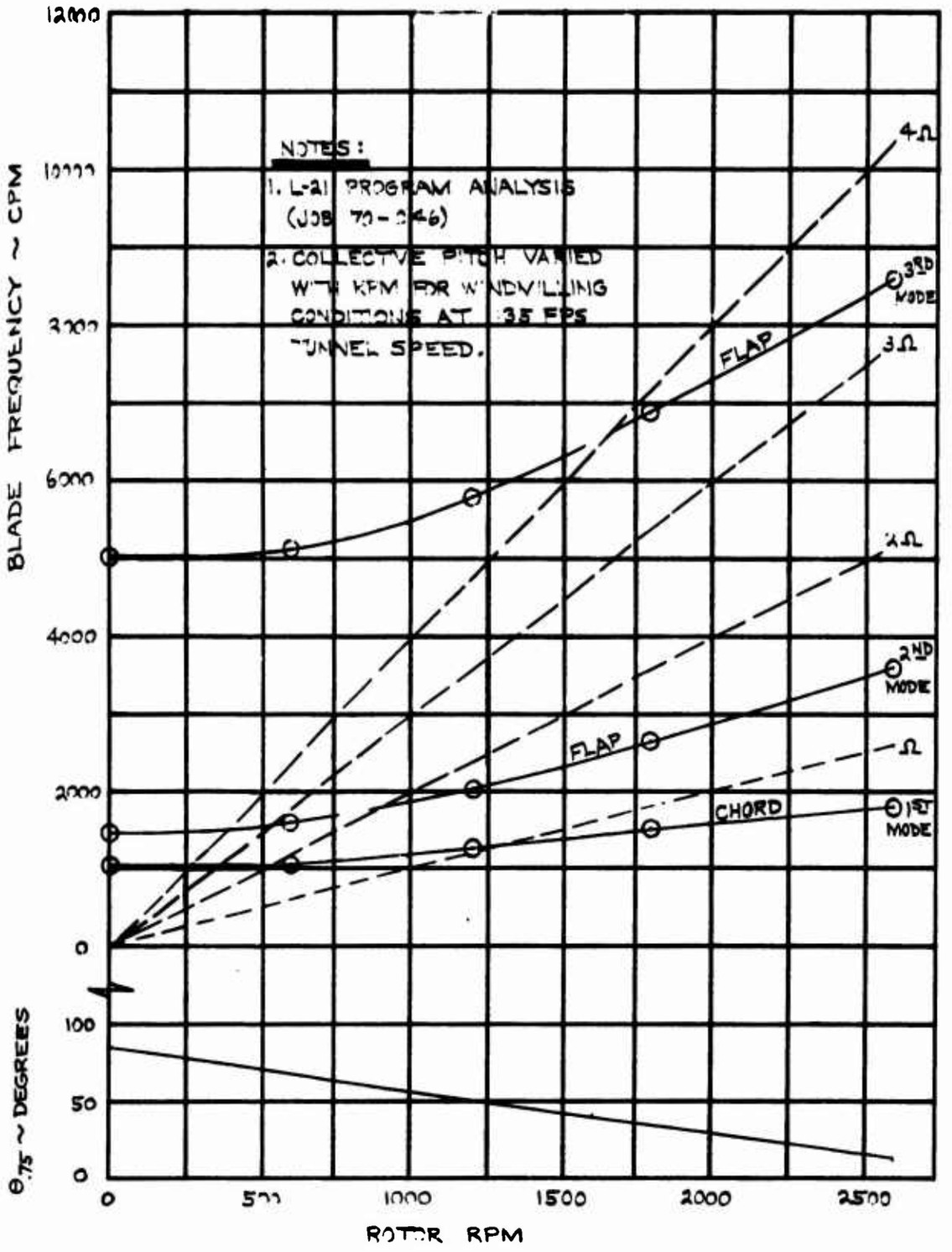

Figure 8. Blade Natural Frequency Spectrum for Phase 1 Tests.

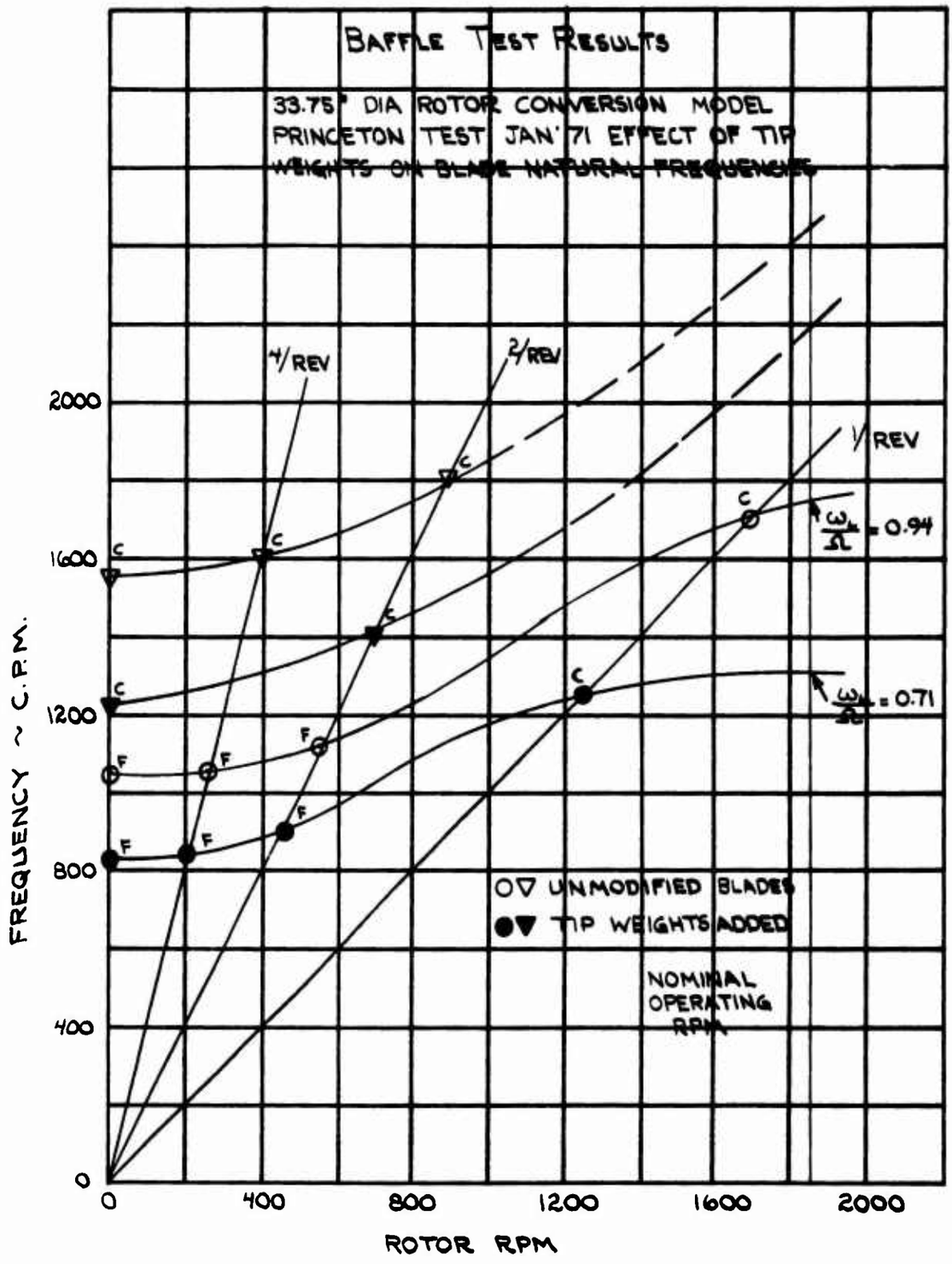

Figure 9. Blade Natural Frequency Spectrum from Baffle Test in Phase 2.

g. Settling chamber at atmospheric pressure

h. Eddy current clutch controlled

i. Six-component virtual center balance with dial readouts

Both tunnel and balance system have been in continuous use since 1950 and have been proven to be reliable and accurate.

3. TEST PROCEDURE

Prior to the start of a test run, the ground-adjustable model controls (angle of attack, flap setting, hub precone) were set to the required values. The rotor blades were placed in the feathered position and the tunnel was started and brought up to the test velocity. In a steady windmilling run, rotor rpm was varied from zero to approximately 1,800 by means of changes in blade collective pitch. After the rotor had stabilized at a given rpm, oscillograph records were taken of the various blade and model balance strain-gage signals. Rotor blade and total model static and dynamic loads were then obtained from the oscillograph traces. At the conclusion of the run, the rotor was stopped by feathering and the tunnel velocity was brought to zero.

In tests of the various conversion collective pitch schedules, the tunnel was again brought up to test velocity with the rotor in the feathered position. A rotor spin-up to 1,800 was then conducted with the rotor collective pitch variation governed by the electronic collective pitch control system. After the rotor rpm had stabilized, a spin-down to zero rpm was conducted, again controlled by the electronic system. The spin-up-steady windmilling-spin-down sequence was repeated twice, once taking oscillograph data at a high paper speed and once at a low paper speed.

During the course of the test program, static disturbance tests of the instrumented blades and the wing were frequently conducted to measure natural frequencies and viscous damping. Wind-off data points were taken prior to and at the conclusion of each test series involving tunnel operation.

SECTION IV

TEST OBJECTIVES

The major objective of this test program was to develop a collective pitch schedule which would minimize the peak drag produced during conversion. Rotor blade loads data were also required to ensure that such a schedule does not cause blade motion irregularities or blade-bending loads which could cause fatigue damage. Based on these broad objectives, a series of specific questions was formulated which were to be answered in this test program. The test results relative to these questions are presented in Section V.

It was the objective of this test to obtain data which would answer the following questions:

a. What are stopped blade loads?

b. What are blade loads in steady windmilling and their variation with rotor speed down to zero rpm?

c. What are the effects of aircraft angle of attack on blade loads in steady windmilling at cruise conditions?

d. What are the effects of wing flap deflection on blade loads during steady windmilling operation?

e. What is model drag for various collective pitch schedules?

f. Are blade loads during conversion limiting?

g. Are blade load predictions that are based on a quasi-static approach substantiated by test?

h. What is the effect of increased wing lift and angle of attack on transient blade loads and rotor wing drag during conversion?

i. How do soft in-plane blade loads compare with the existing stiff in-plane blade loads data under identical conditions?

j. What is the effect of increased drive system inertia on transient drag?

k. What are model lift, drag, and moment variations with angle of attack and flap setting?

l. What effect does the wing exert on blade loads and rotor derivatives?

m. Does rotor hub pre-cone setting influence windmilling blade loads?

SECTION V

DISCUSSION OF TEST RESULTS

The results of these tests include aerodynamic performance and blade loads. Some data and analysis of the dynamics of the test model are included in this section.

1. AERODYNAMICS

From an aerodynamic viewpoint, the conversion process tested consists of an energy exchange as the kinetic energy of rotation of the prop/rotor varies from and to zero. The energy involved is taken from the airstream as the kinetic energy of the prop/rotor increases during spin-up and therefore a transient drag force is produced. Energy is given up to the airstream as the prop/rotor is feathered, resulting in a transient propulsive thrust force. Scheduling of the prop/rotor blade collective pitch variations provides the means for reducing sudden changes in drag or thrust to levels which will not cause piloting problems or crew discomfort. As shown in Figure 3, less than 0.05g peak axial acceleration can be achieved with an equivalent full-scale conversion time of 10 seconds.

1.1 MODEL SCALE CONSIDERATIONS

Testing of the model was performed at a principal test speed of 135 feet per second. The variations of Reynolds number for this primary test condition are shown in Figure 10. This resulted in adequately large Reynolds number conditions at all of the blade stations, even with zero rpm. Data obtained at various tunnel speeds on the complete model with zero rpm are plotted in Figure 11. These data show the variations of the lift, drag, and moment coefficients are approaching asymptotes at a speed of 145 feet per second. From these data, it appears that the data obtained at 135 feet per second can be extrapolated to full scale with confidence.

As discussed in a recent technical paper[2], the natural frequency of the first-mode flapwise (out-of-plane) blade bending has a significant effect on the forces and moments produced by the prop/rotor. When operating at rpm close to the 1st chordwise (in-plane) blade-bending, 1-per-rev frequency crossing, the lag motion of the blade has a large stabilizing impact on the rotor stability derivatives. The measured model blade frequencies are given in Figure 9.

---

2. Magee, J. P. and Pruyn, R. R., PREDICTION OF THE STABILITY DERIVATIVES OF LARGE FLEXIBLE PROP/ROTORS BY A SIMPLIFIED ANALYSIS, Presented at the 26th Annual National Forum, AHS, June 1970, Preprint No. 443.

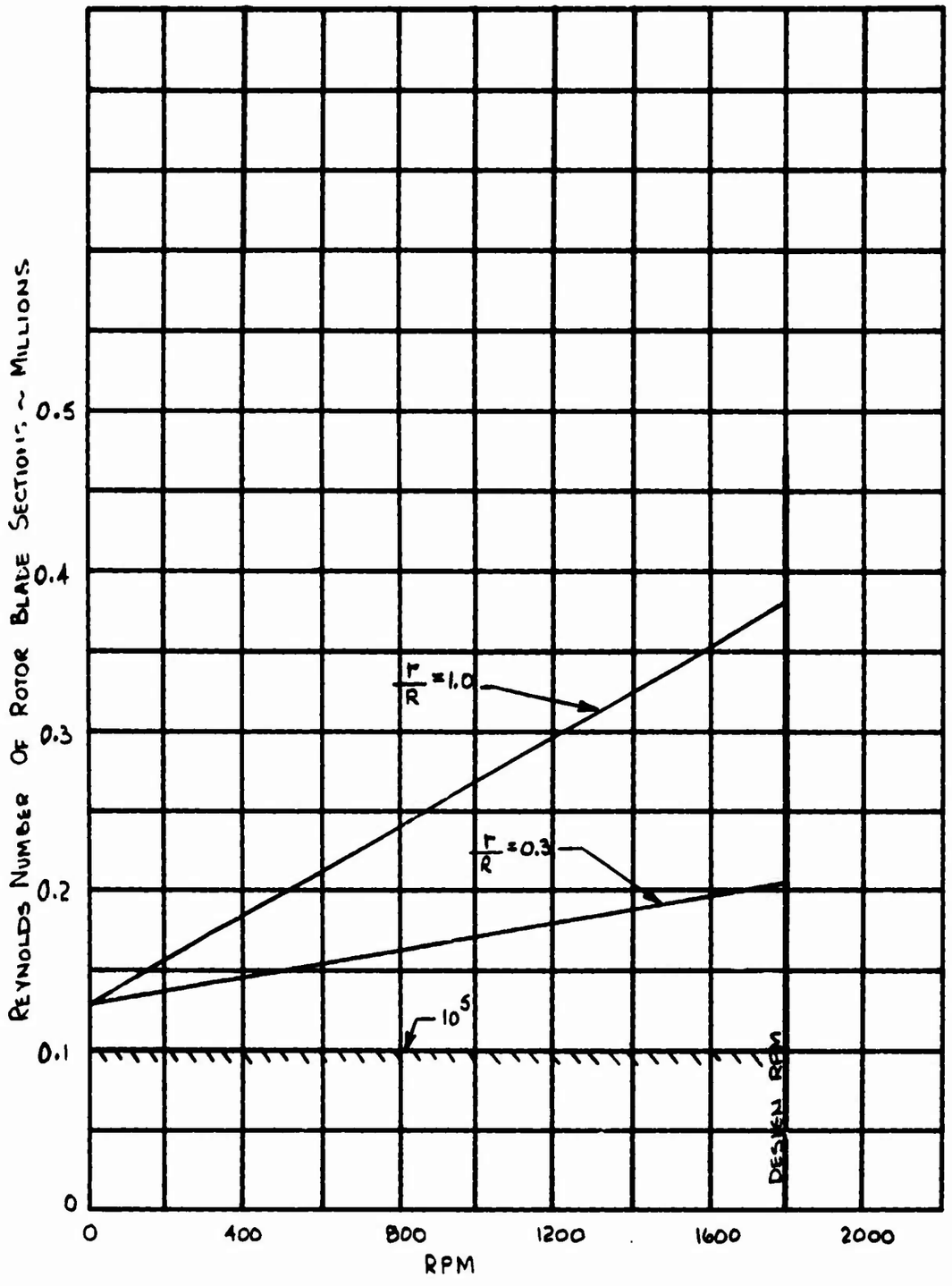

Figure 10. Blade Section Reynolds Numbers all Exceed 10^5 at the Test Speed of 135 Feet Per Second.

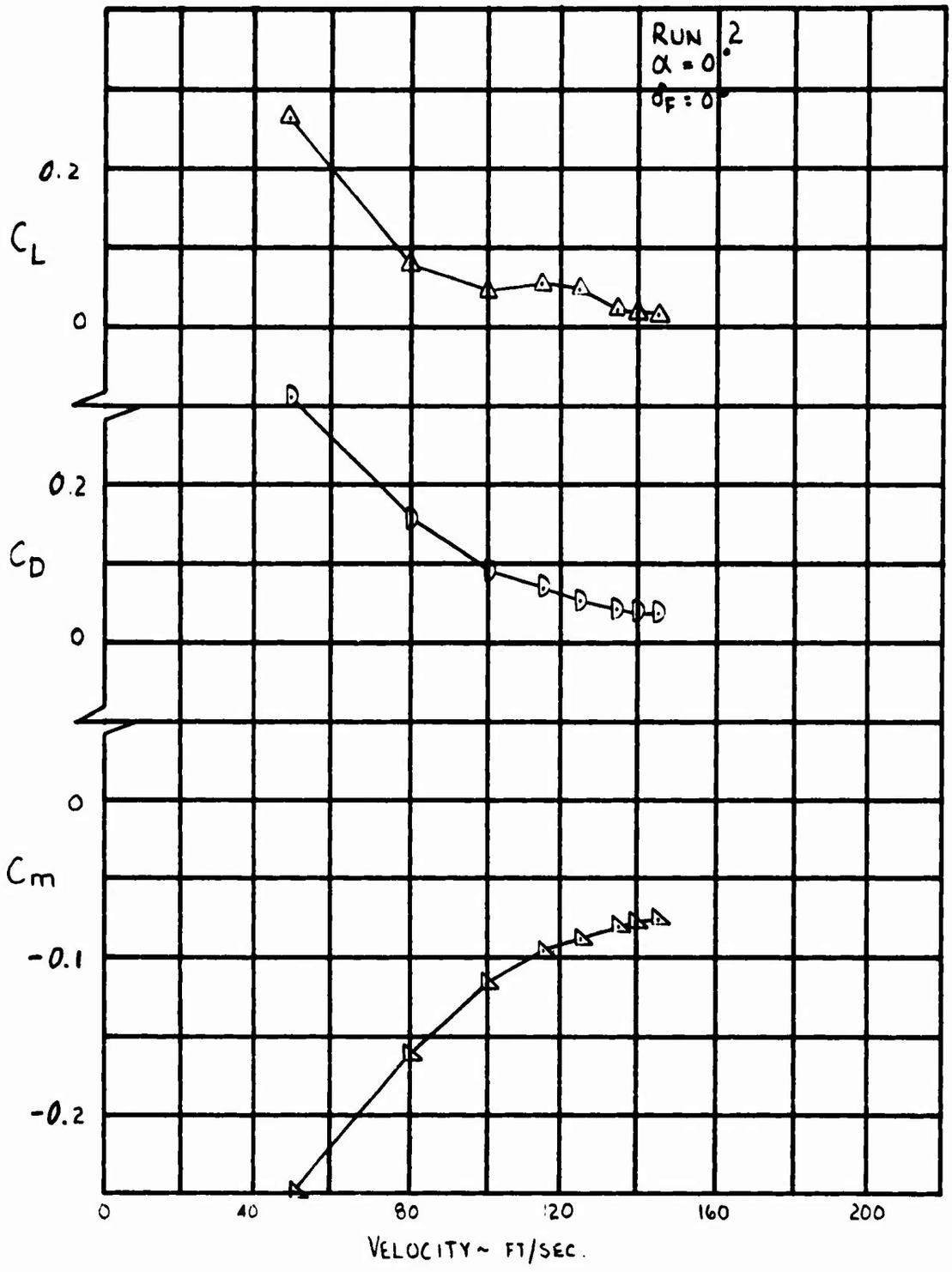

Figure 11. Aerodynamic Data on Model with Stopped Blades Approach Asymptotes at 135 Feet Per Second.

To put the test data into perspective, the approximate scale factors were developed by assuming the full-scale aircraft to be a 67,000-pound vehicle with a pitch inertia of 250,000 slug-ft^2 which will execute conversion at 170 knots. The resulting model scale is 1/16. Time is scaled based on the time for a rotor revolution so that, at design rpm, one second model scale is equivalent to 7.9 seconds full scale. The resolution of the model balance for steady loads is about one pound of force or one inch-pound of moment. This resolution scales and reduces to coefficient form as follows:

MODEL DATA RESOLUTION

Type of Load	Model Scale Value	Acceleration	Load	Coefficient
Lift or Drag	1 pound	0.034 g's	2,250 lb	0.036
Moment	1 inch-pound	0.012 rad/sec^2	3,080 ft-lb	0.0039

1.2 STEADY WINDMILLING

In steady windmilling (with zero rotor shaft torque), a unique relationship exists between rotor rpm and rotor blade collective pitch angle at constant airspeed. This relationship is defined by the blade twist and chord distributions and the airfoil sectional characteristics which provide that the integrated distribution of torque along the blade be zero. The test data for steady windmilling are compared with prediction in Figure 12. The largest difference in collective pitch at a specified rpm is 10 percent between prediction and test.

The wing balance recorded the lift, drag, and pitching moment of the wing, nacelle, and rotor combination. Data are presented in Figures 13 through 16 for steady windmilling operation at wing and rotor anbles of attack between zero and -6 degrees. The steady pitching moment is practically independent of rpm; thus, trim changes on a full-scale aircraft would cause small pitch accelerations requiring minimal control to trim.

The wing and rotor lift is shown to systematically increase with increasing rpm. The lift coefficient increment increases as the angle of attack is reduced. A similar trend of smaller magnitude is also shown in the data obtained with the wing aerodynamic surface removed. These data are presented in Figure 17. The trend of increased lift with increased rpm at negative angles of attack may be due to the reduction in the prop/rotor normal force as the rpm increases. The same trend occurs at zero angle of attack; this is thought to be due to

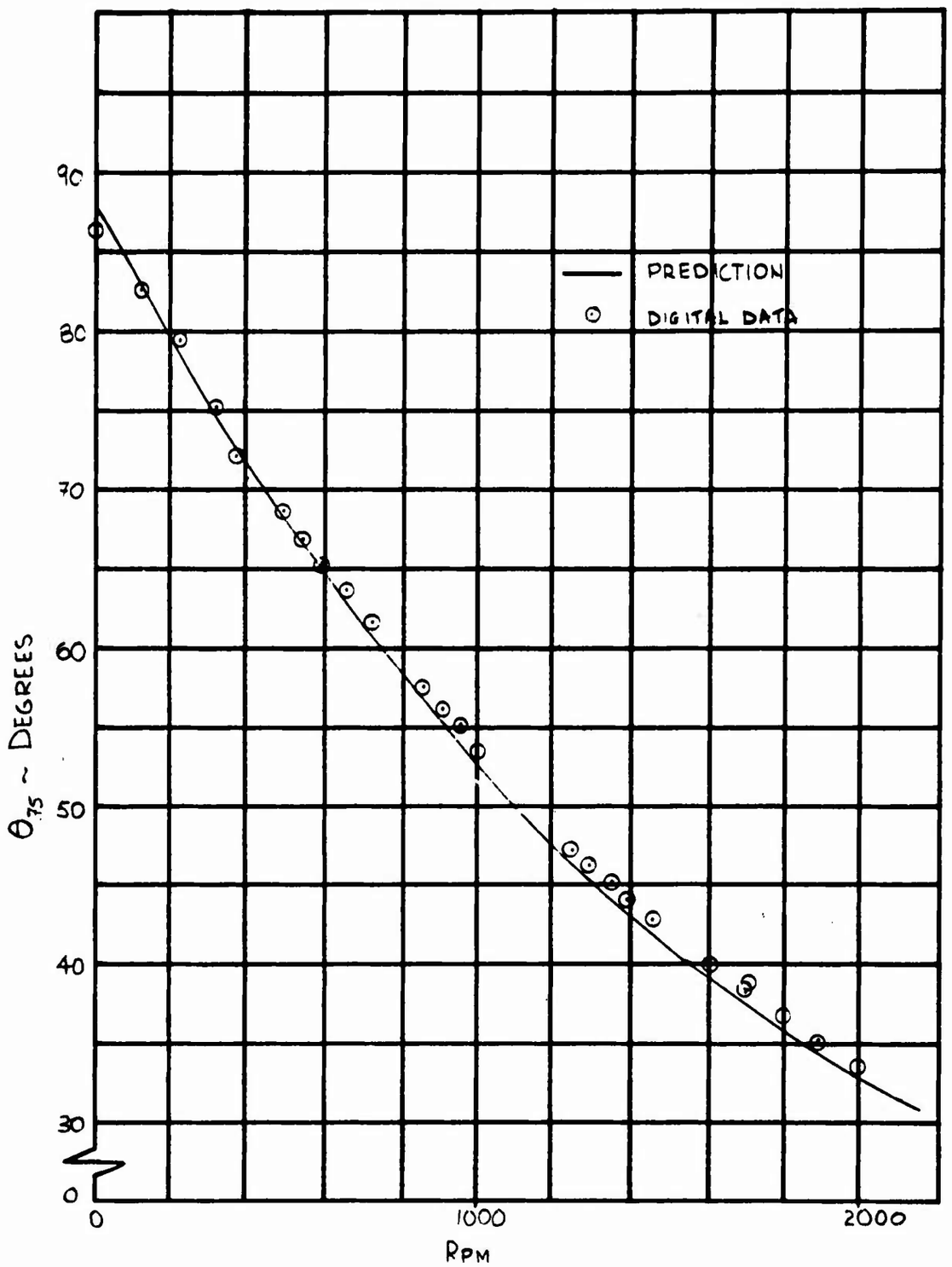

Figure 12. Relationship between RPM and Collective Pitch at 135 Feet Per Second Airspeed.

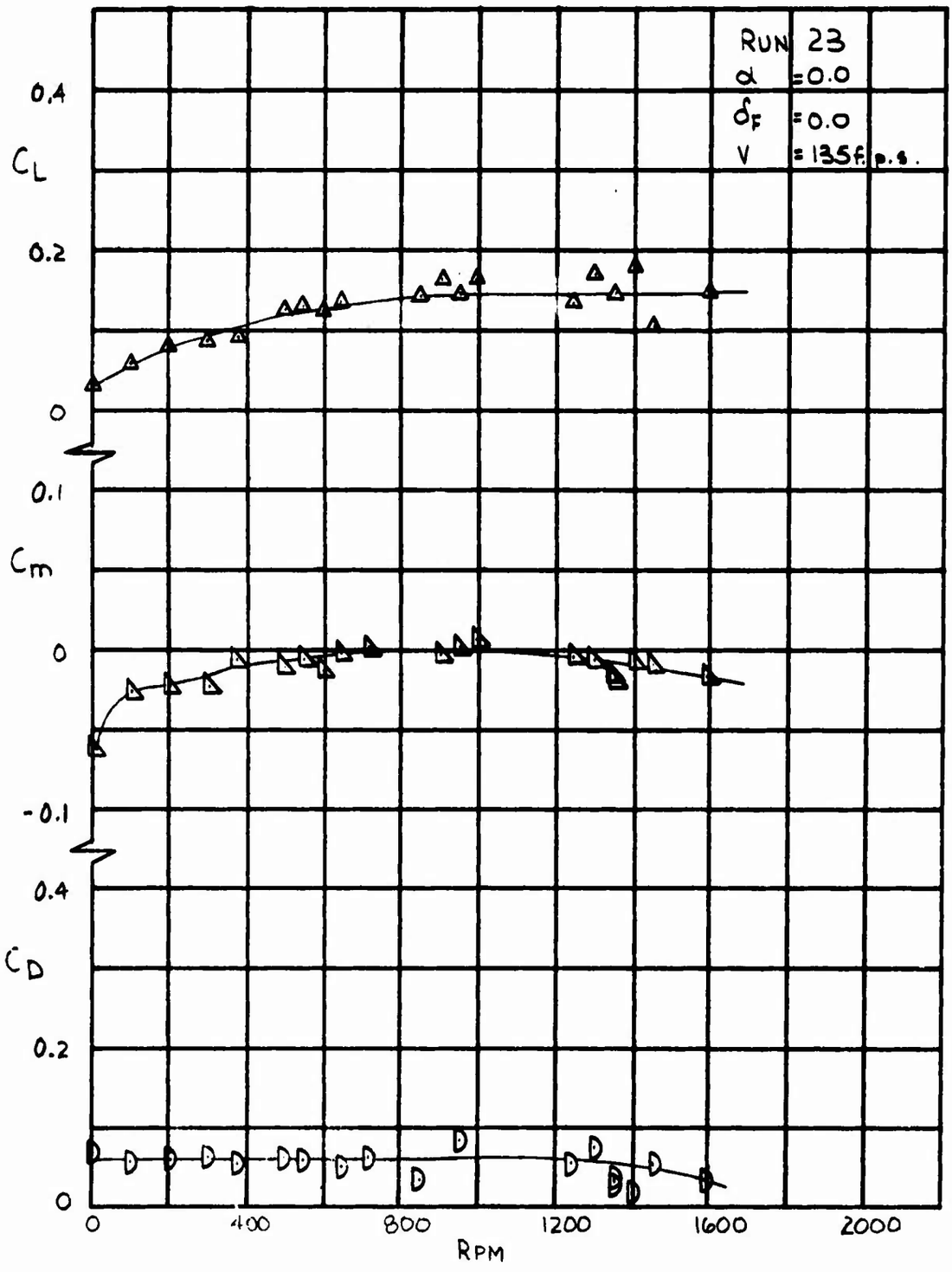

Figure 13. Effect of Steady Windmilling RPM on Lift, Drag and Pitching Moment, $\alpha = 0$, $\delta f = 0$.

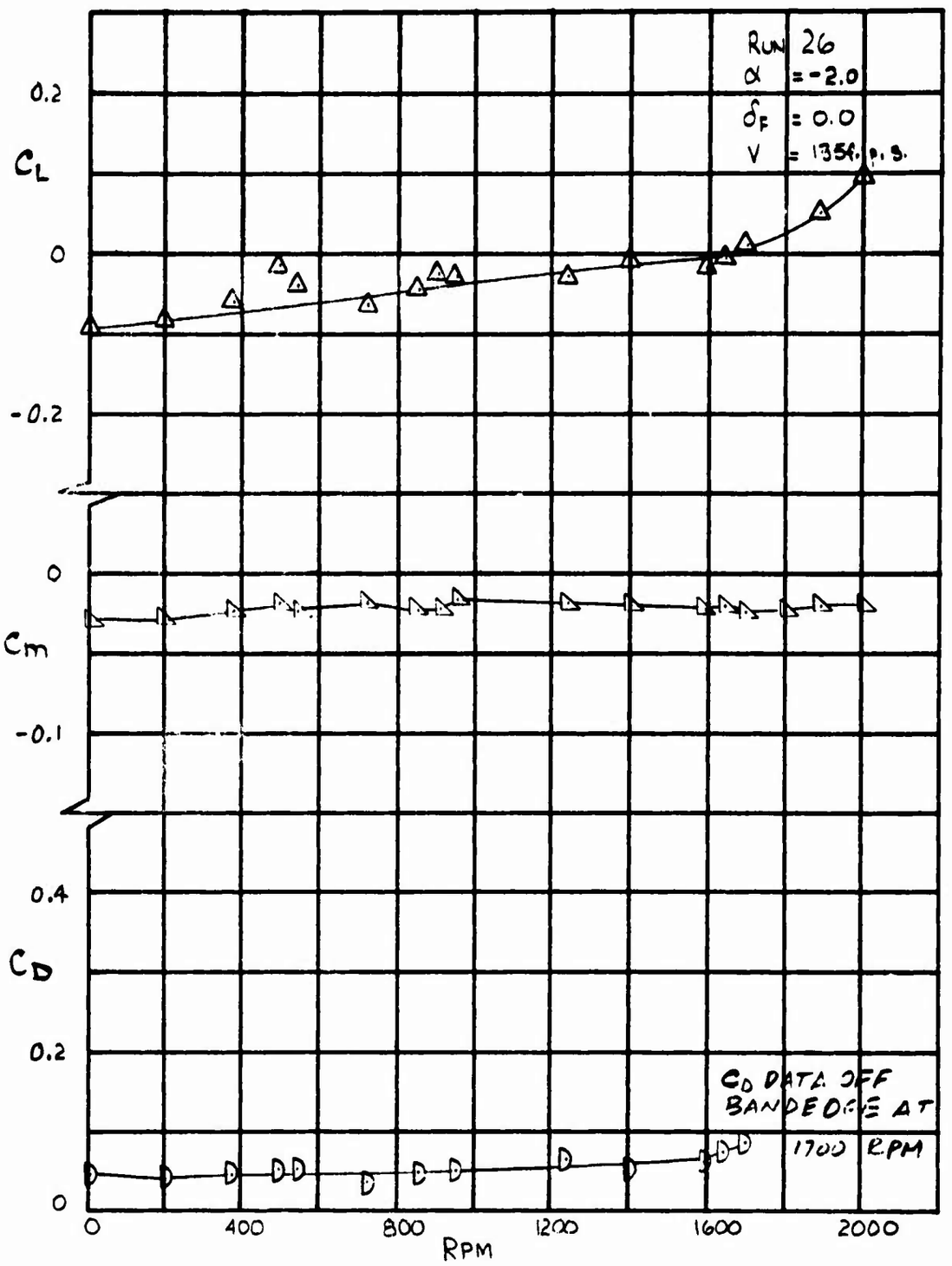

Figure 14. Effect of Steady Windmilling RPM on Lift, Drag and Pitching Moment, α = -2.0, δ_f = 0.

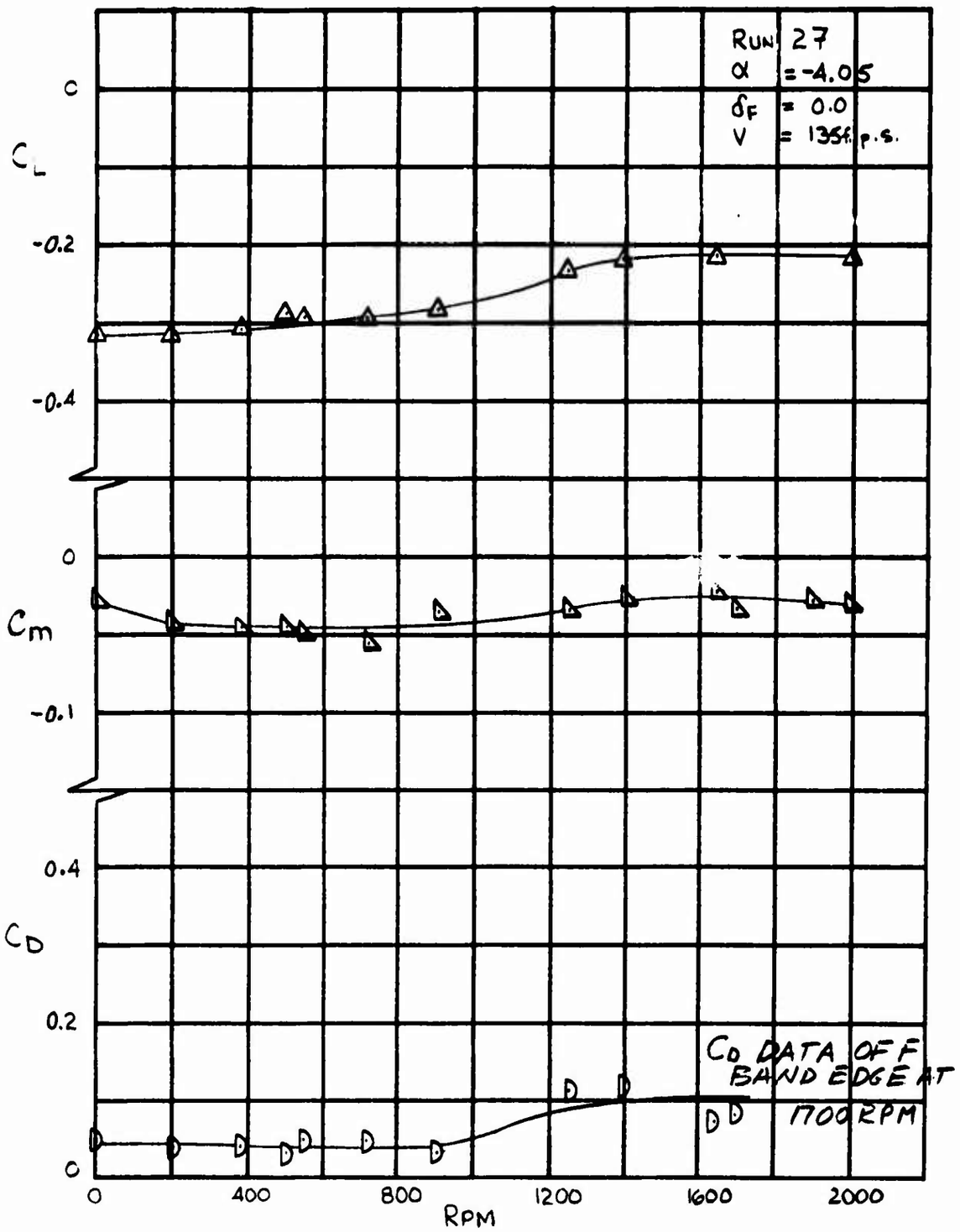

Figure 15. Effect of Steady Windmilling RPM on Lift, Drag and Pitching Moment, α =-4.05, δf = 0.

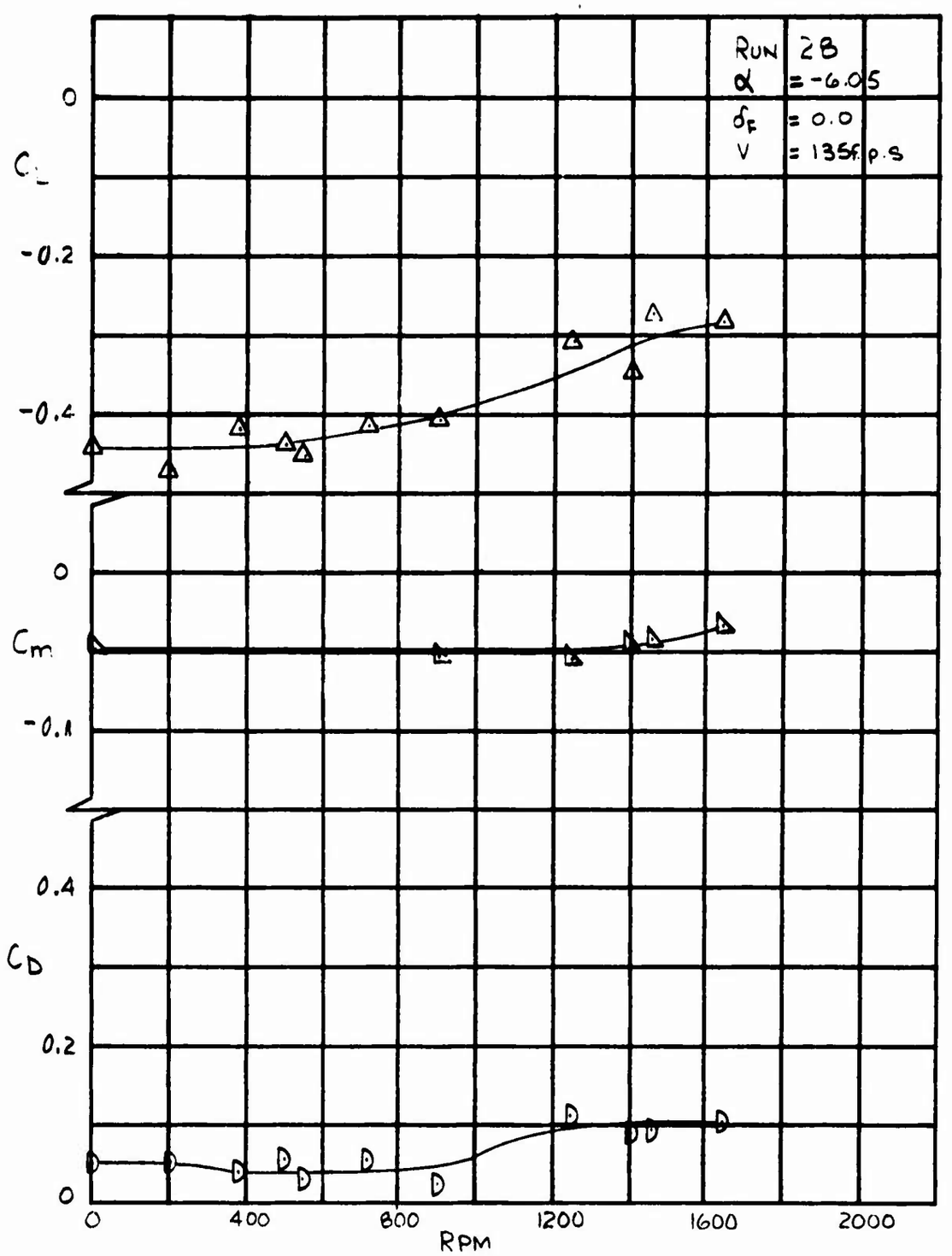

Figure 16. Effect of Steady Windmilling RPM on Lift, Drag and Pitching Moment, α = -6.06, δf = 0.

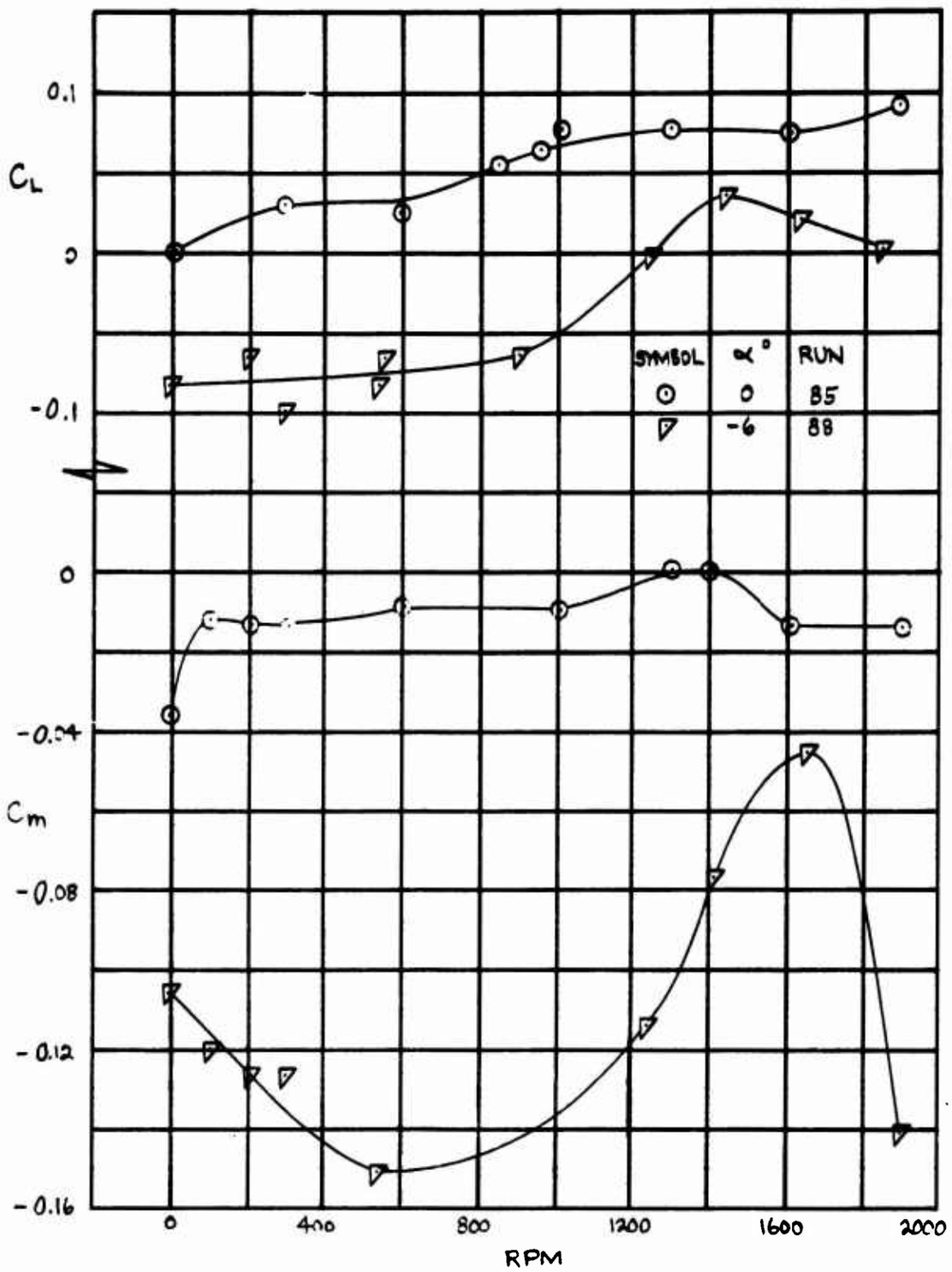

Figure 17. Lift and Pitching Moment in Steady Windmilling with Aerodynamic Surface Removed.

rotor inflow distribution produced by wing circulation. As will be shown in the next section, this same increase in lift coefficient with increased rpm also occurs in the transient test data. It should be noted that, in the aircraft, the measured lift coefficient increment with rpm would require a trim change of less than two degrees. This trim change could easily be provided in the approximately 10 seconds required to produce the rpm change.

Figures 18 through 21 are for steady windmilling conditions with different flap deflections. The drag and pitching moment levels measured change with flap deflection as expected; the drag coefficient is almost constant while pitching moment increases with rpm. The increase in lift coefficient with rpm trend is again shown. The flap appears to stall between 25 and 30 degrees of deflection, since the C_L produced by the flap does not rise over 0.8 beyond 25 degrees of flap deflection. The model used a simple, nonslotted 30-percent flap.

The rpm range of these Phase I tests was limited by blade loads as the blade chordwise 1/rev was approached (See Figure 8).

1.3 CONVERSION TRANSIENTS

1.3.1 Effect of Spin Time

The data presented in Figures 22 through 27 are time histories of wing and rotor lift, drag, and pitching moment for linear collective pitch schedule cases. All of these cases were tested with the nominal angle of attack of zero and a flap deflection of -6.0° to minimize blade loads, which were high during the Phase I tests. During the spin-up operation, the drag increased to a maximum and then settled down to the windmilling drag level. The increment in drag between the feathered case (i.e., zero rpm) and the peak of the transient data will provide a deceleration to the aircraft. The slope of the drag curve with time indicates how fast the decelerating force will be applied. The test target for drag increment has been established at 0.05 g's full-scale or approximately a drag coefficient increase of 0.054. It should be noted that the difference in steady drag in the feathered and windmilling conditions is equivalent to about 0.02 g deceleration. Feathering reduces the drag on the aircraft and will cause the aircraft to accelerate. The test target for the effective thrust increment is again 0.05 g's. The effect of reducing the time during which the change in rpm is accomplished is to increase the transient drag. The peak transient drag for different spin times and linear collective schedules is summarized in Figure 28. None of the linear schedule test points comes within the 0.05 g test target; however, the test points indicate lower peak transient drag than predicted.

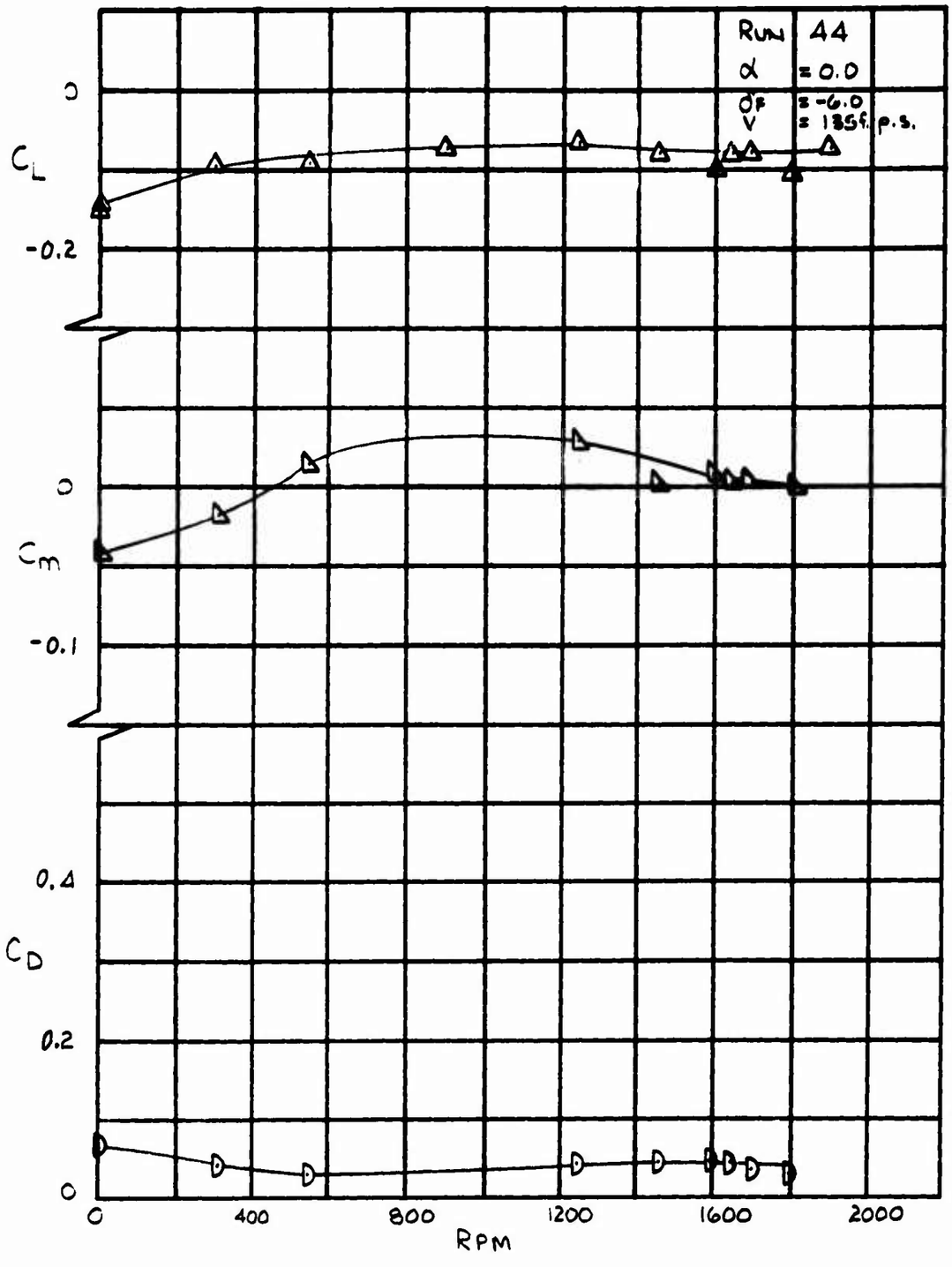

Figure 18. Effect of Steady Windmilling RPM on Lift, Drag and Pitching Moment, $\alpha = 0$, $\delta f = -6.0$.

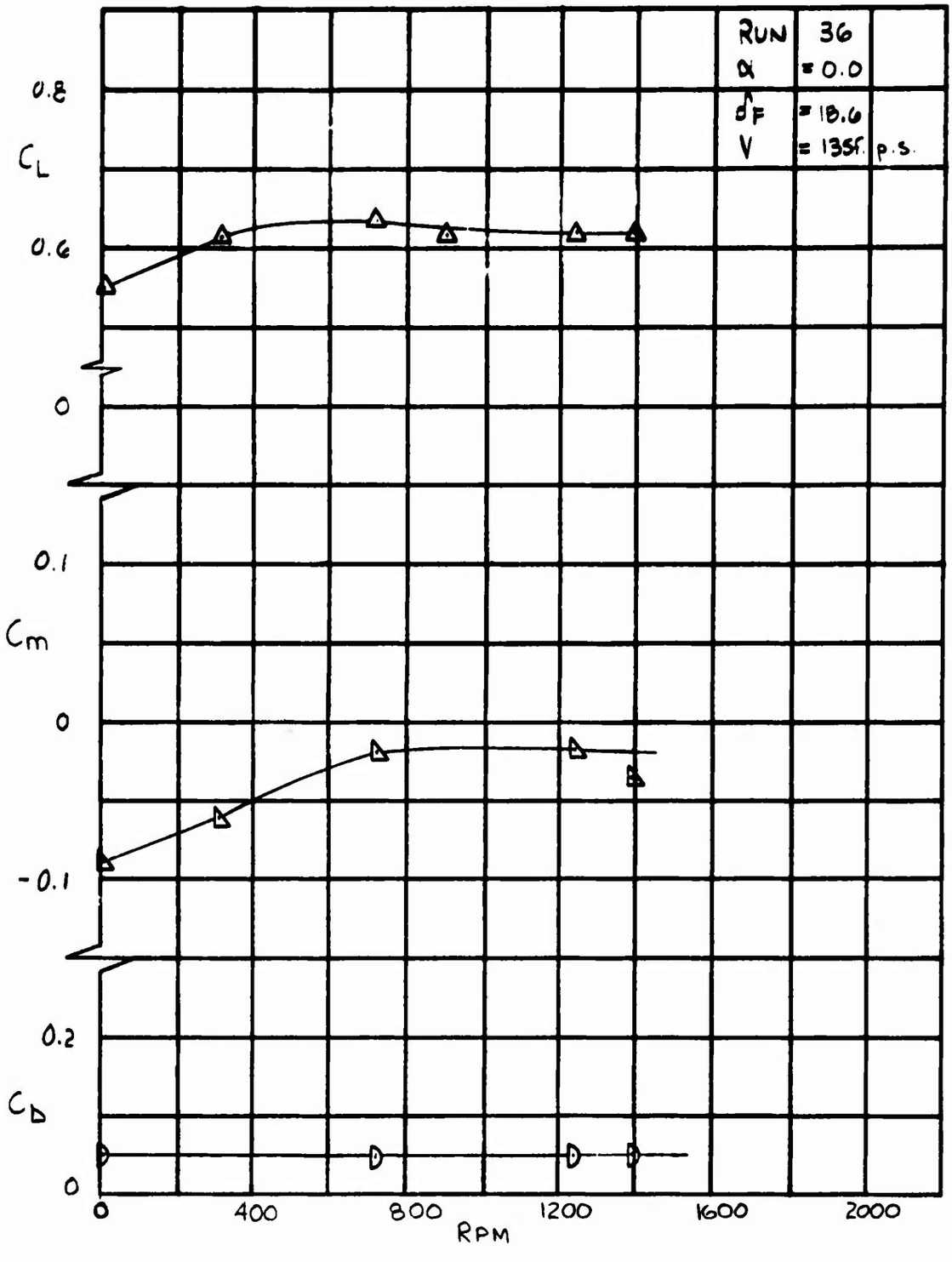

Figure 19. Effect of Steady Windmilling RPM on Lift, Drag and Pitching Moment, $\alpha = 0$, $\delta f = 18.6$.

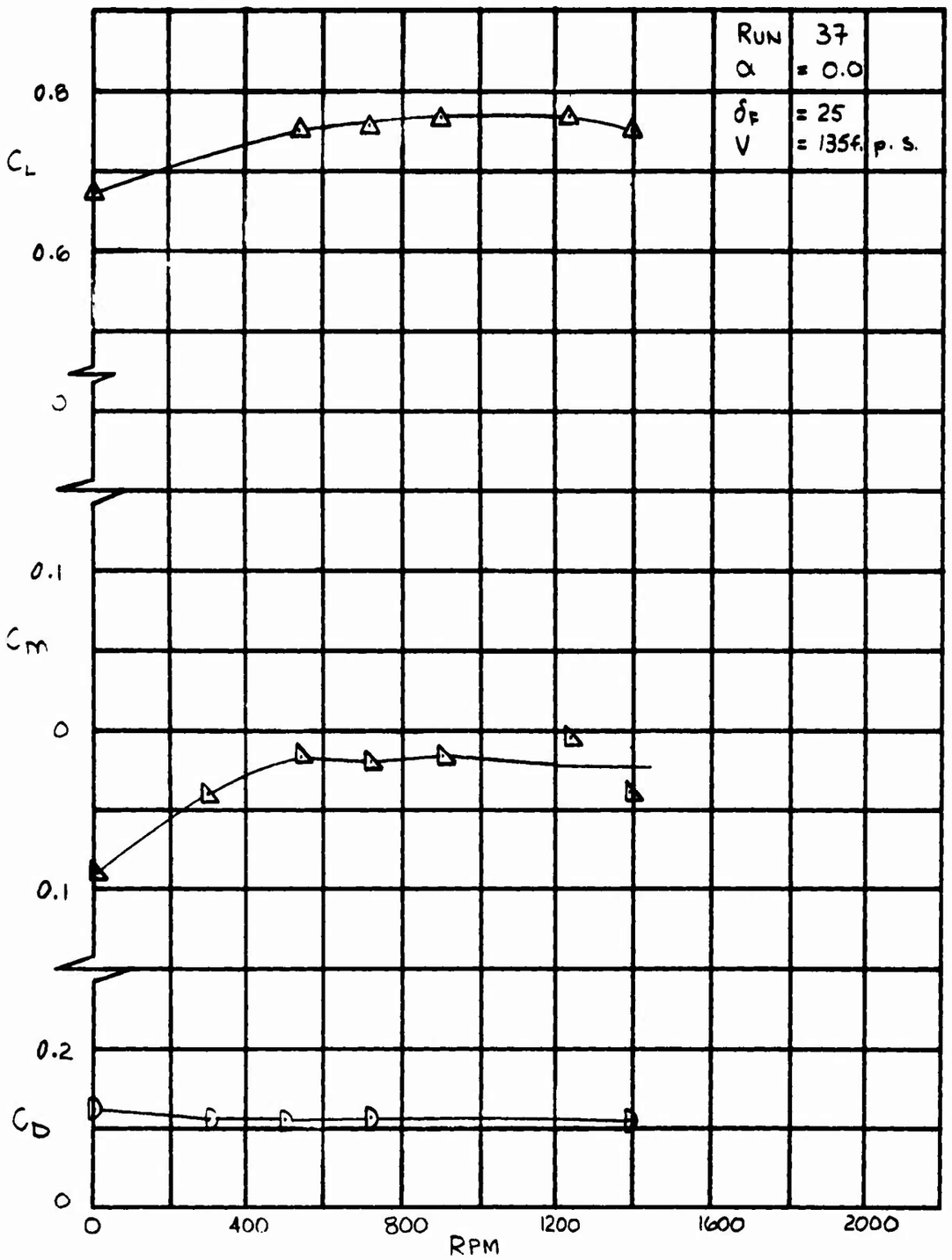

Figure 20. Effect of Steady Windmilling RPM on Lift, Drag and Pitching Moment, $\alpha = 0$, $\delta f = 25.0$.

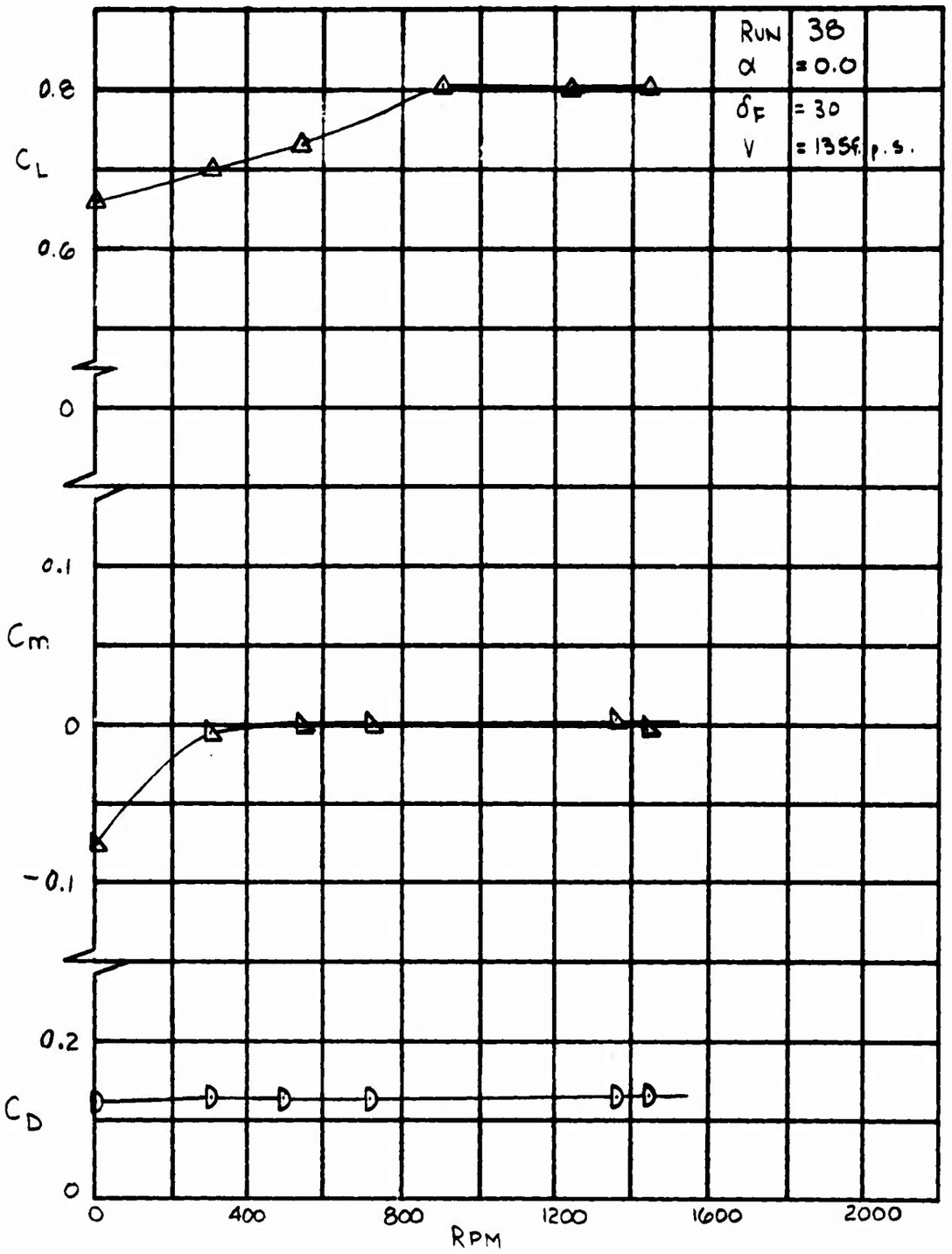

Figure 21. Effect of Steady Windmilling RPM on Lift, Drag, and Pitching Moment, $\alpha = 0$, $\delta f = 30.0$.

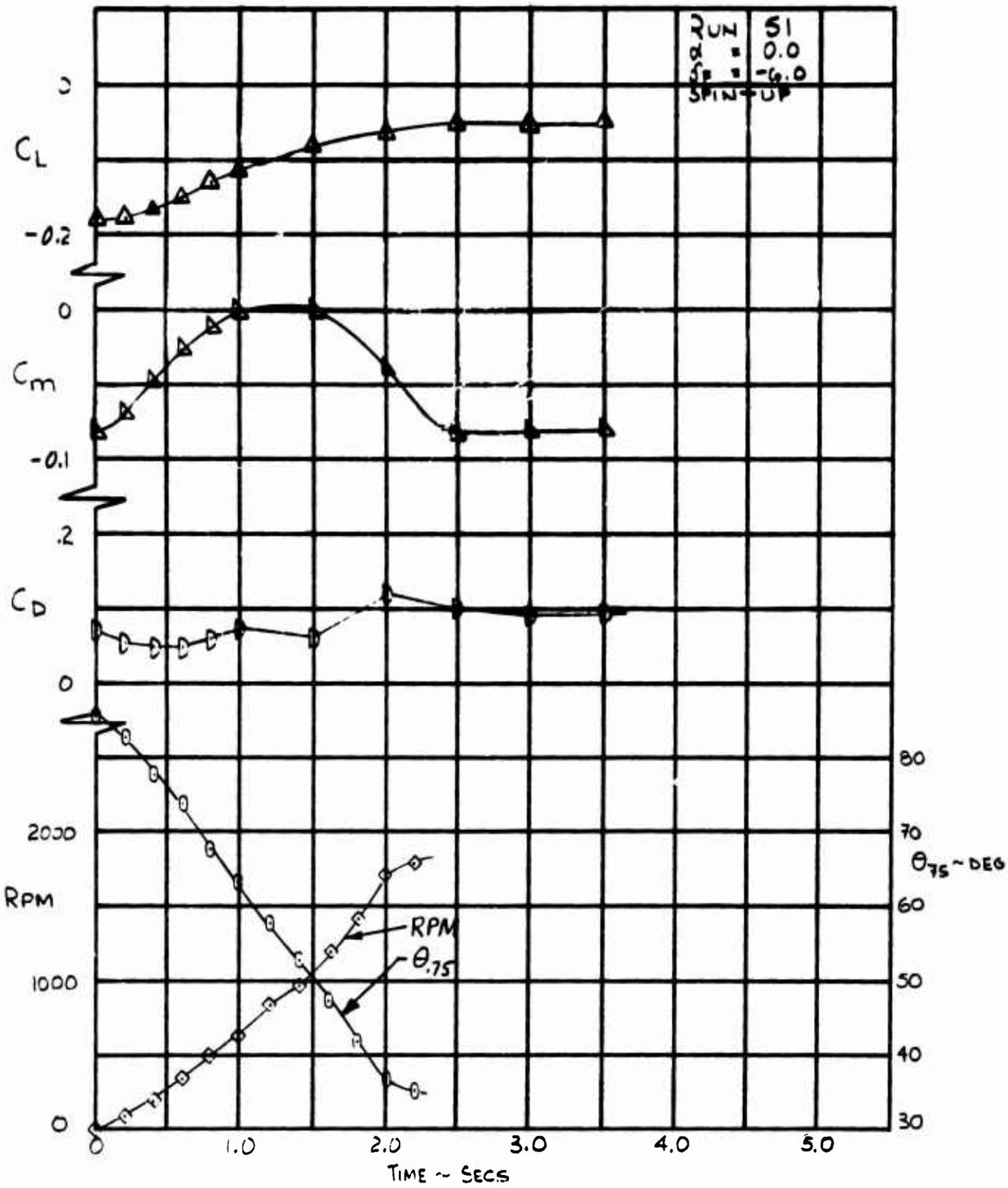

Figure 22. Variation of Drag, Lift and Pitching Moment for a 2.0 Second Linear Transient Schedule, Spin-Up

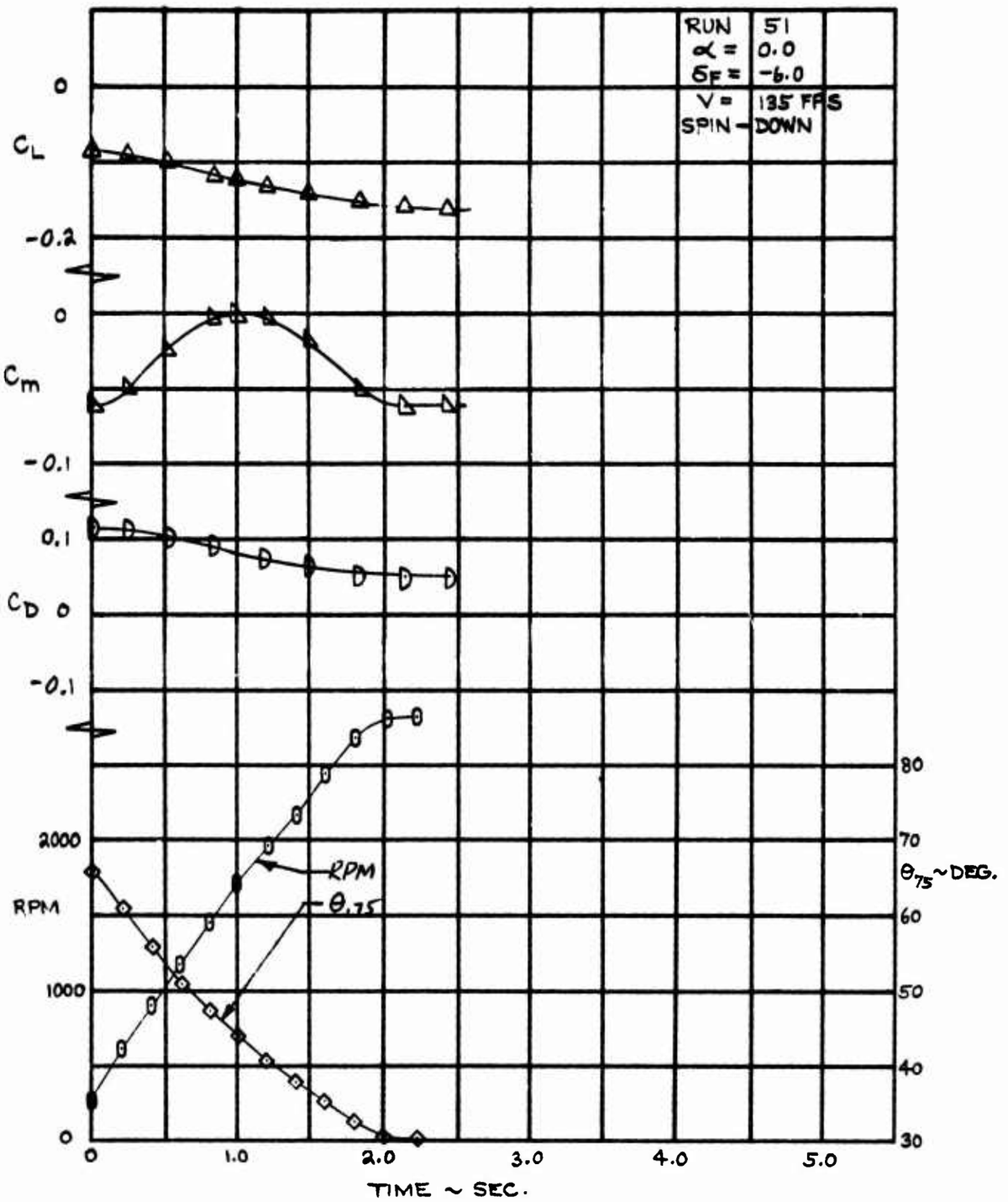

Figure 23. Variation of Drag, Lift and Pitching Moment for a 2.0 Second Linear Transient Schedule, Feathering.

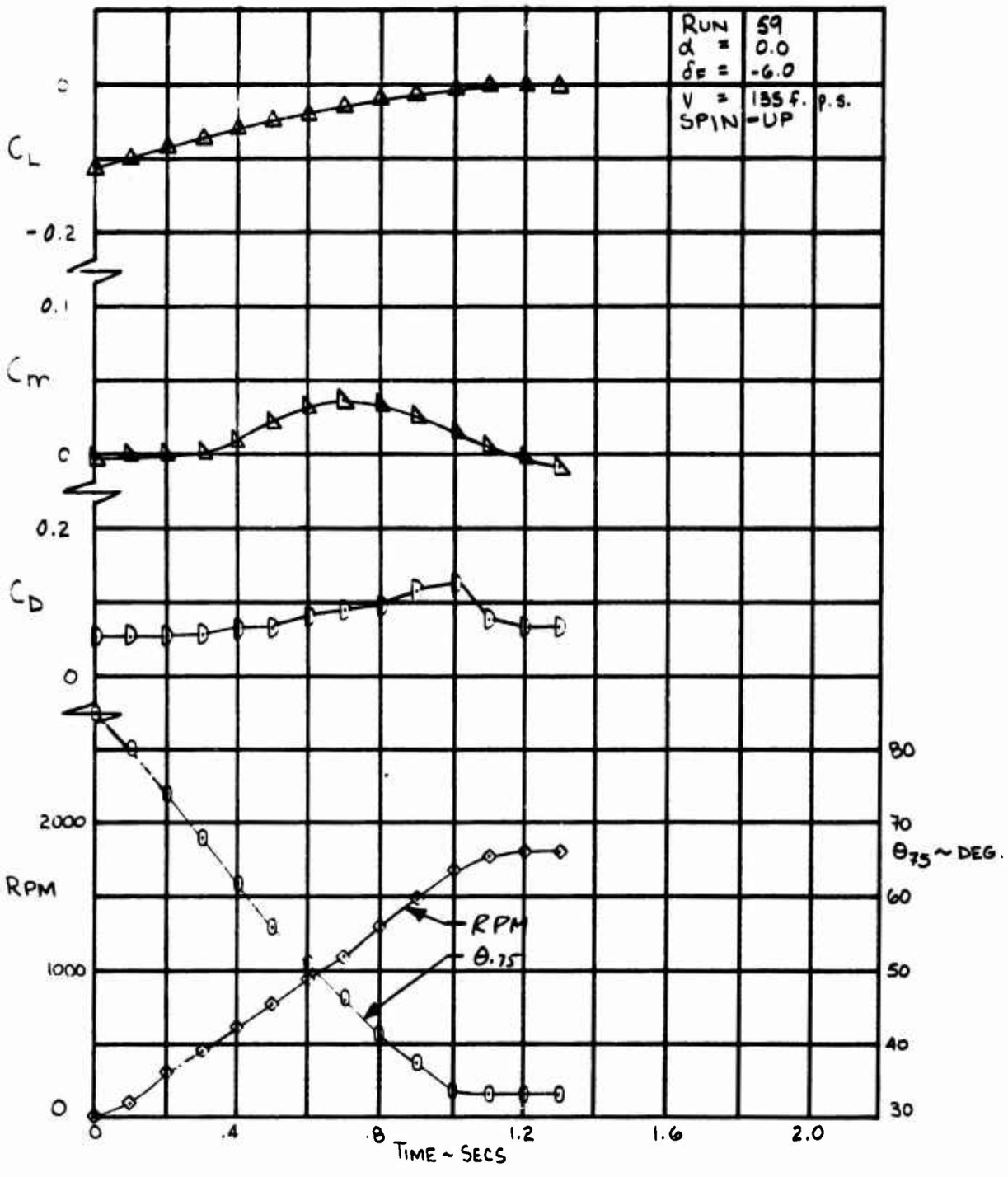

Figure 24. Variation of Drag, Lift and Pitching Moment for a 1.0 Second Linear Transient Schedule, Spin-Up.

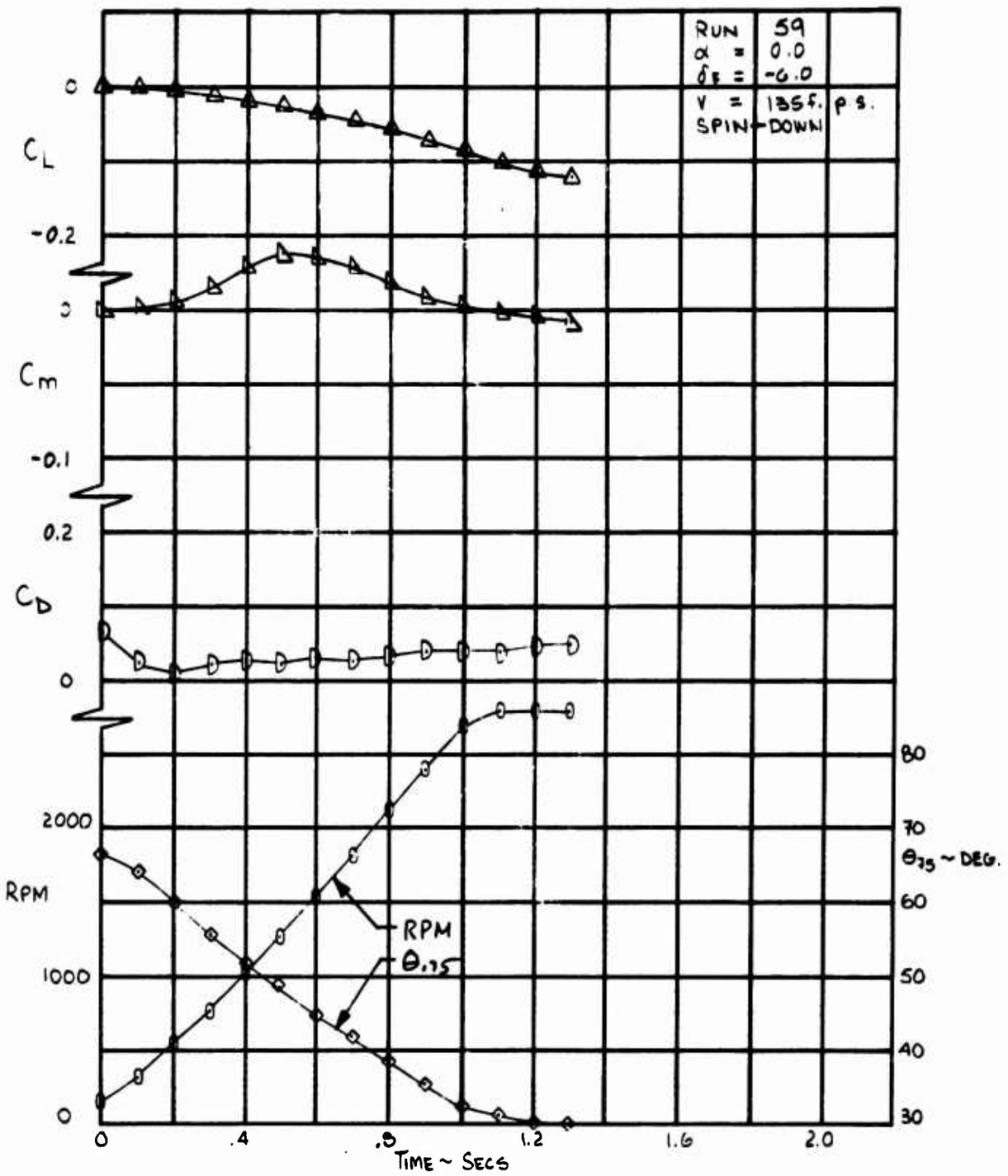

Figure 25. Variation of Drag, Lift and Pitching Moment for a 1.0 Second Linear Transient Schedule, Feathering.

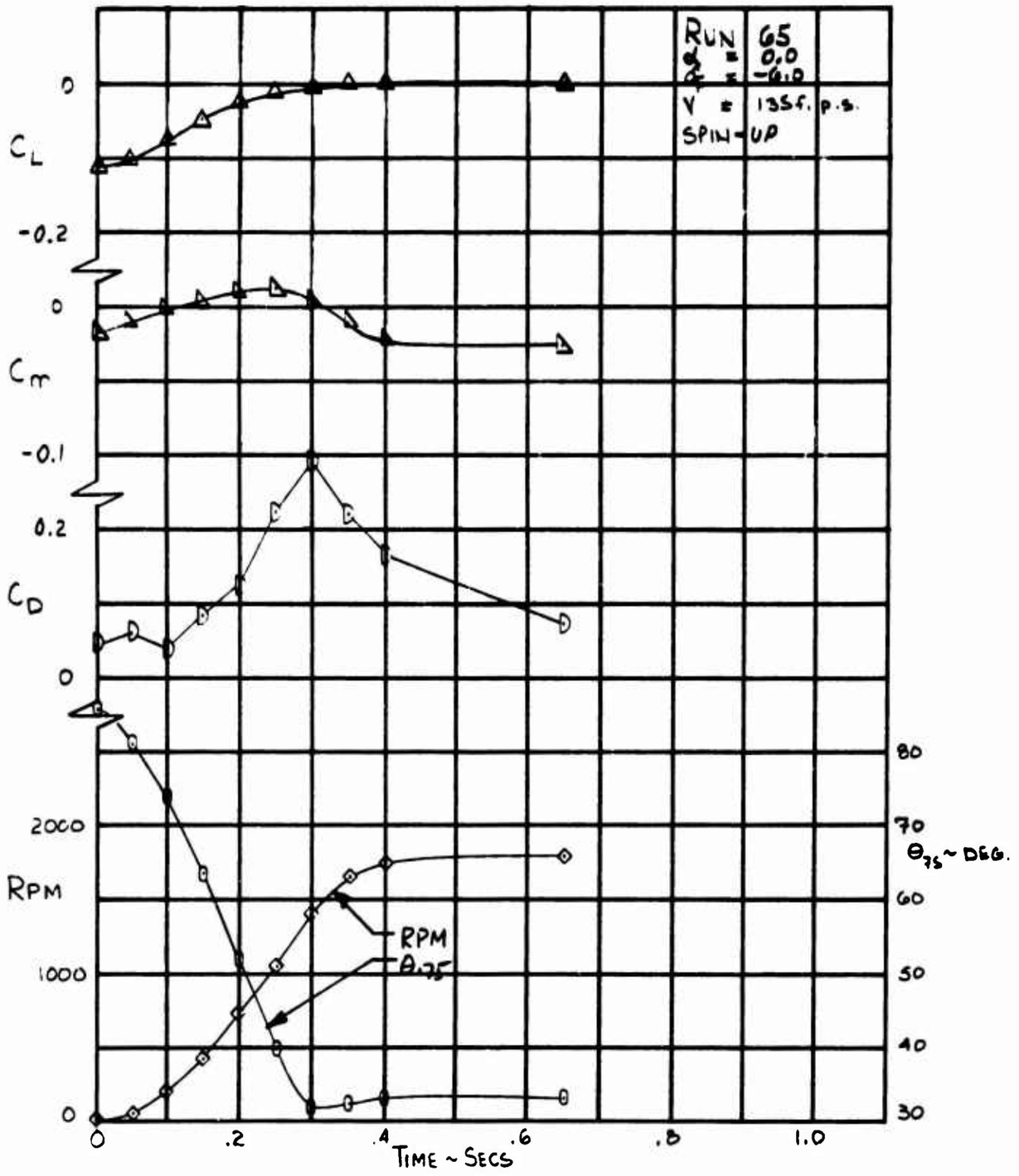

Figure 26. Variation of Drag, Lift and Pitching Moment for a 0.3 Second Linear Transient Schedule, Spin-Up.

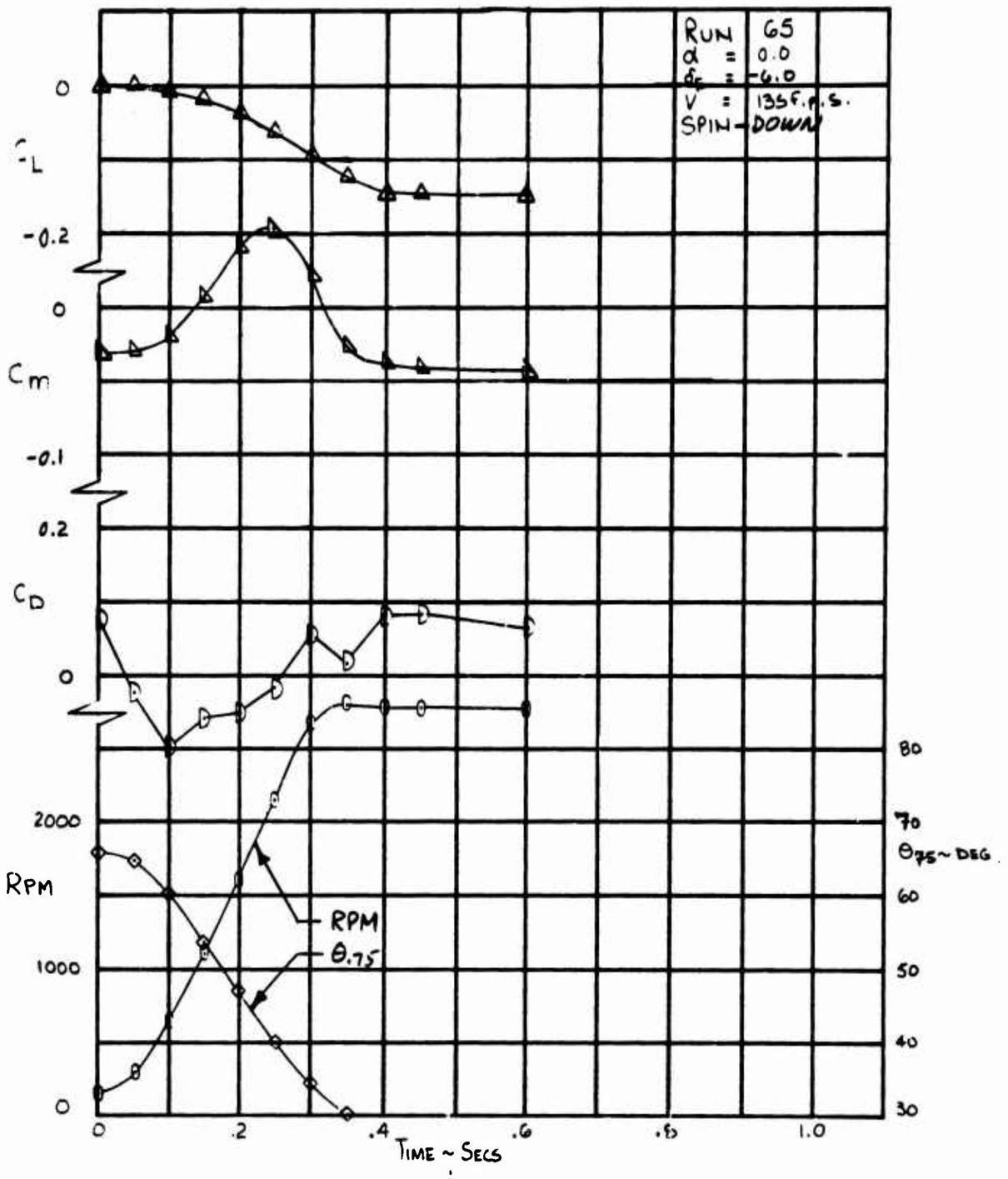

Figure 27. Variation of Drag, Lift and Pitching Moment for a 0.3 Second Linear Transient Schedule, Feathering.

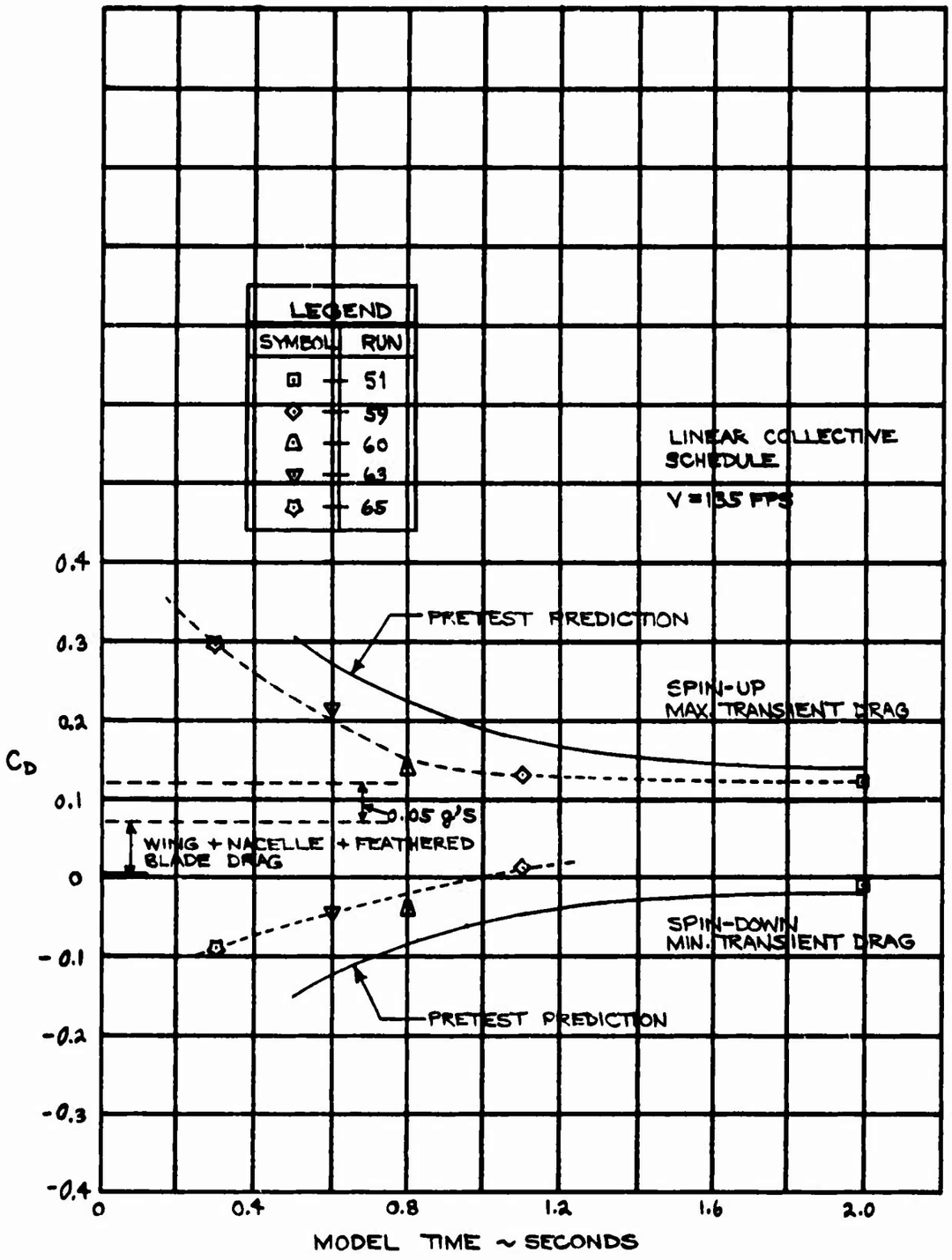

Figure 28. Correlation of Pretest Prediction of Peak Transient Drag with Test.

The discrepancy between theory and test is very small for long spin times but, as the time is reduced, the theory is conservative. The test schedules and their corresponding drag and rpm time histories have been superimposed in Figures 29 and 30. These data show that the maximum drag occurs when the rpm and the rate of change of rpm are highest. To reduce the drag, the collective pitch schedule must be tailored such that the maximum rotational acceleration occurs at the lower rpm end of the time history. An example of correlation between pretest and test data is illustrated in Figures 31 and 32 and shows the prediction to be conservative.

1.3.2 Effects of Collective Pitch Schedule

The time history of collective pitch affects the transient drag produced during conversion. By arranging the collective schedule such that the initial rotor angular acceleration is high and then reduces as the rpm increases, the transient drag and also the drag time gradient can be reduced. This effect is shown in Figures 33 and 34. The initial angular acceleration is limited by blade section stall; however, the data show no acceleration limit up to the model collective pitch actuator rate limit. The transient drag coefficient increment is reduced in the example shown from 0.08 to 0.04 by collective schedule shaping for a two-second spin time. The feathering data also show a reduction in the transient drag increment.

A further consideration in defining the collective schedule to be used is simplicity. A compromise schedule with a two-step linear segment time history was tried in a one-second spin time. This schedule provided a small reduction in transient drag over the straight linear schedule but was still not within the 0.05 g criterion. These test data are plotted in Figures 35 and 36.

Three other schedules, two nonlinear and one adverse two-step linear segmented schedule, were tested; the nonlinear collective schedules alleviate the transient drag. The two-step adverse case increased the drag peak.

The lift change during the transient cases is as previously described; however, the variation of lift with time is also shown to depend on the rpm time history. This is another clue that the lift change is coming from the rotor.

The pitching moment data increase and then decrease as the rpm is increased. This is thought to be the result of dynamics of the rotor blades as the chordwise 1/rev is crossed.

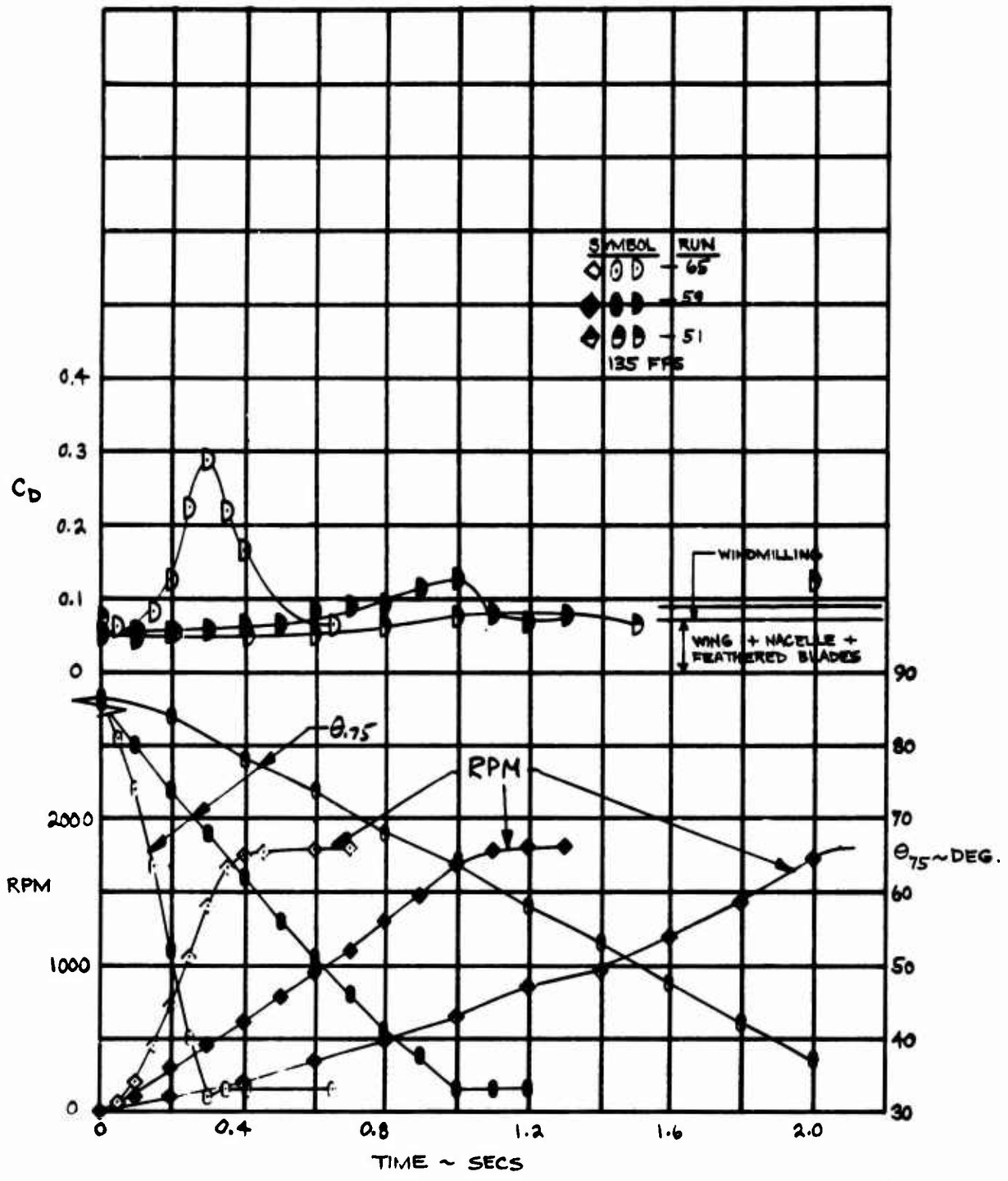

Figure 29. Effect of Transient Spin Time on Drag ~ Spin-Up.

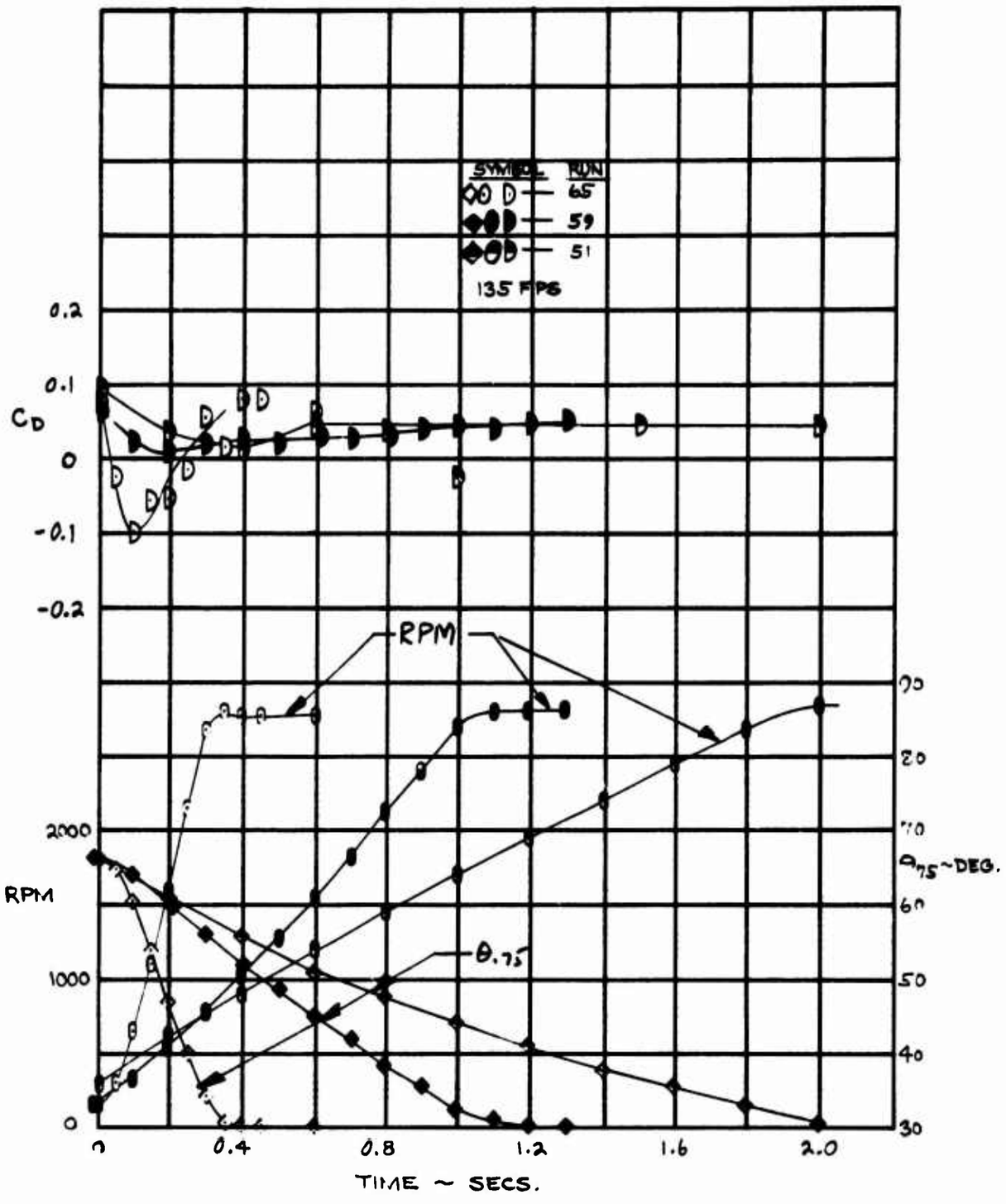

Figure 30. Effect of Transient Spin Time on Drag ~ Feathering.

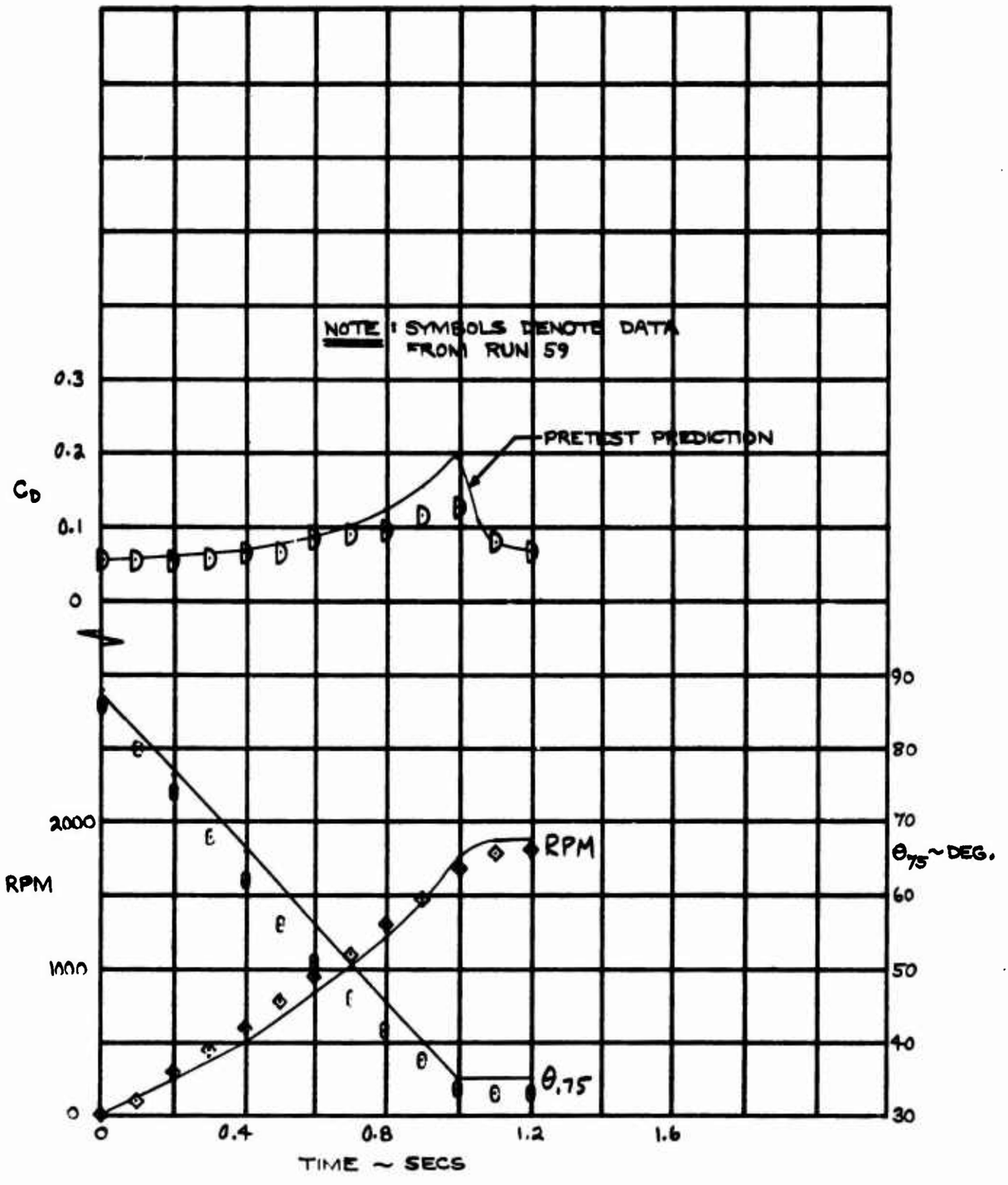

Figure 31. Transient Drag Correlation Spin-Up.

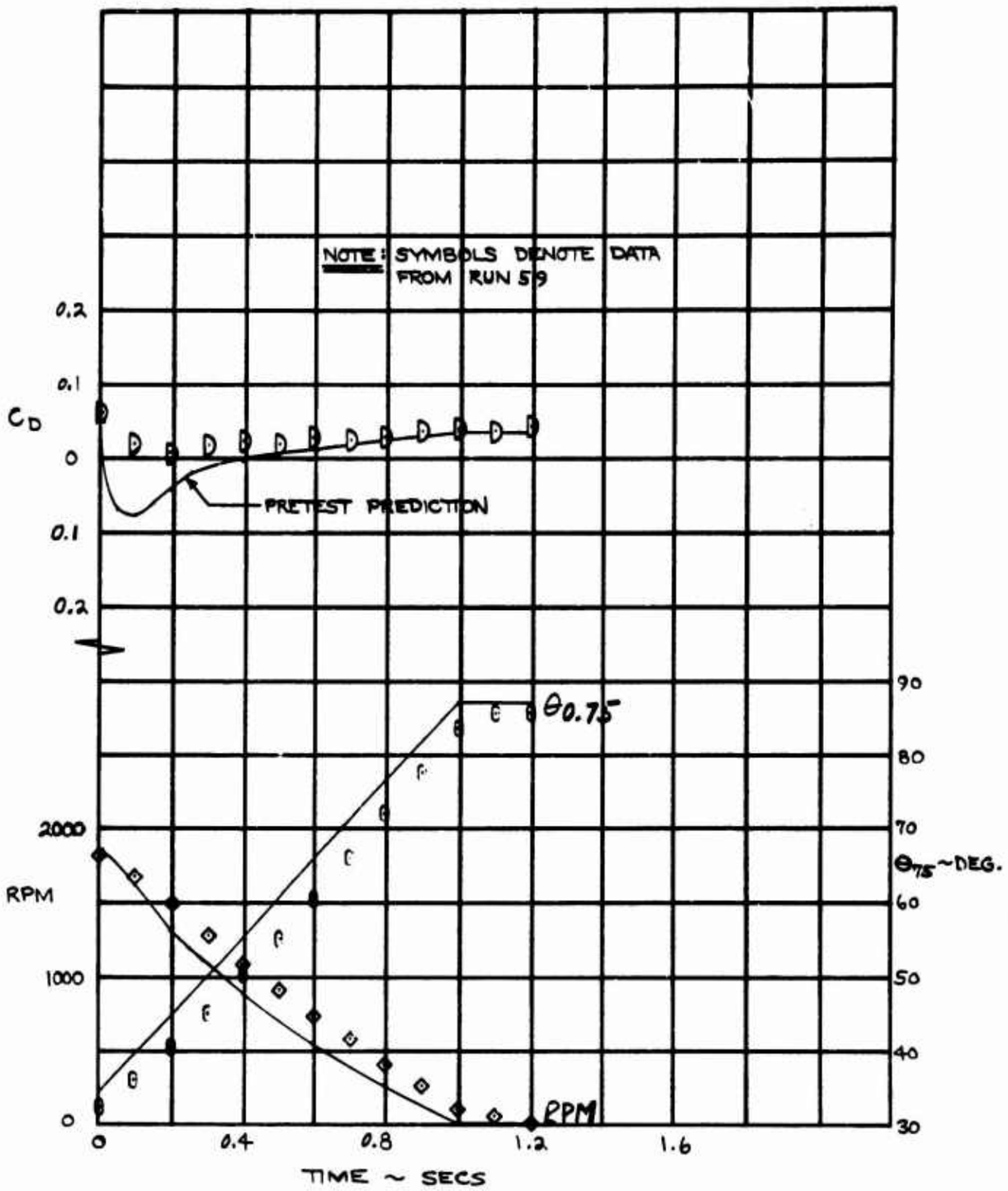

Figure 32. Transient Drag Correlation ~ Feathering.

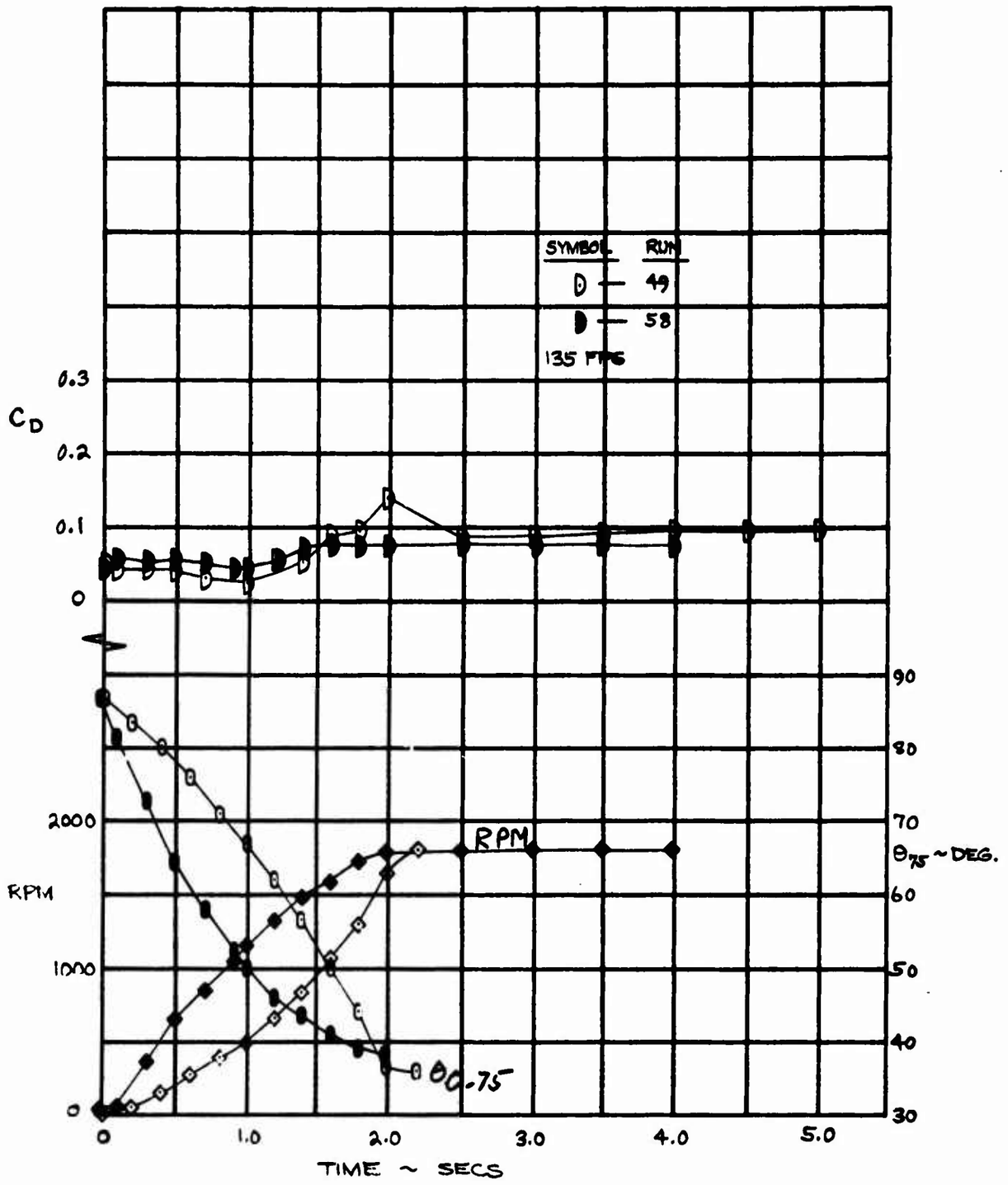

Figure 33. Effect of Conversion Schedule on Transient Drag ~ Spin-Up.

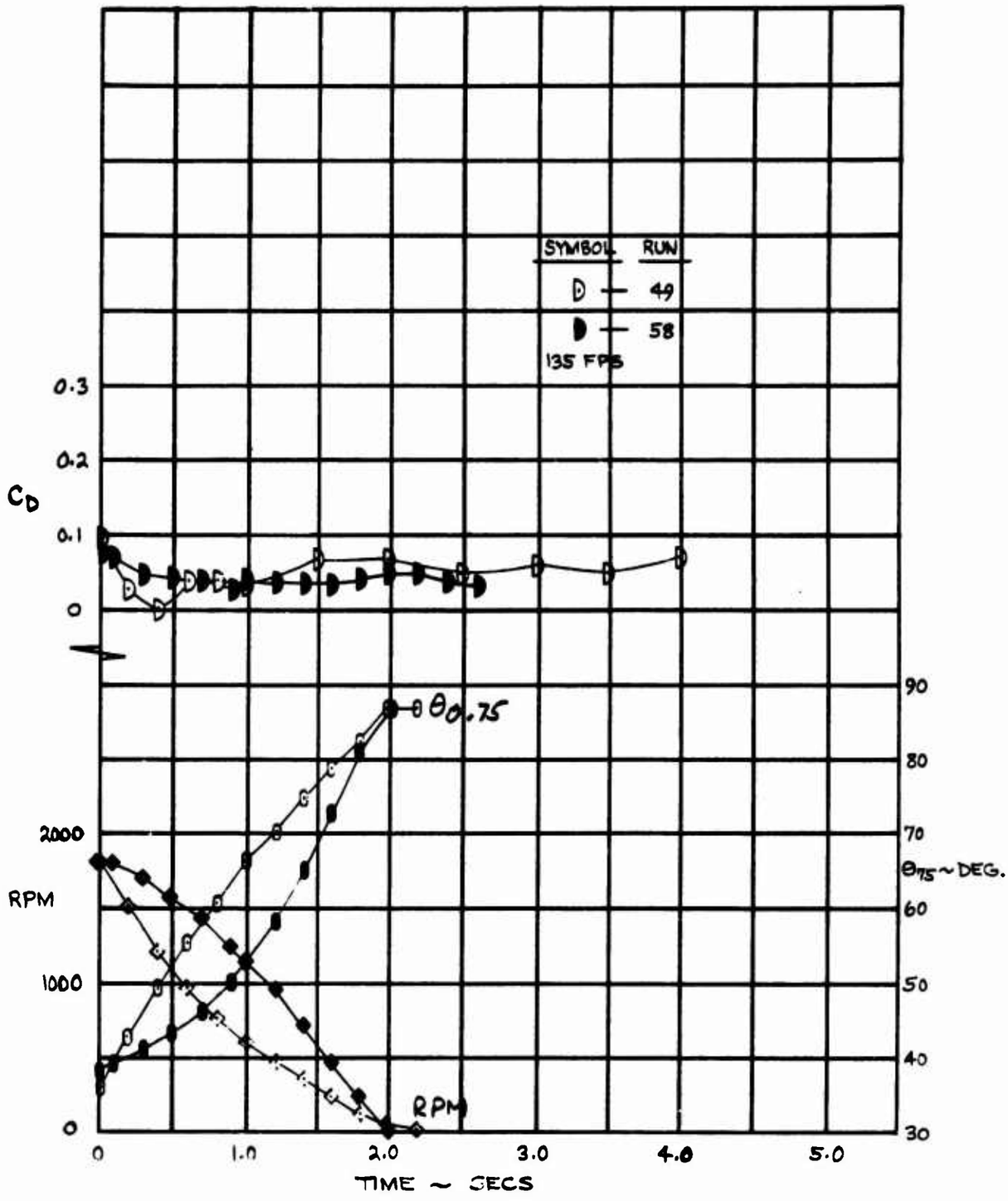

Figure 34. Effect of Conversion Schedule on Transient Drag ~ Feathering.

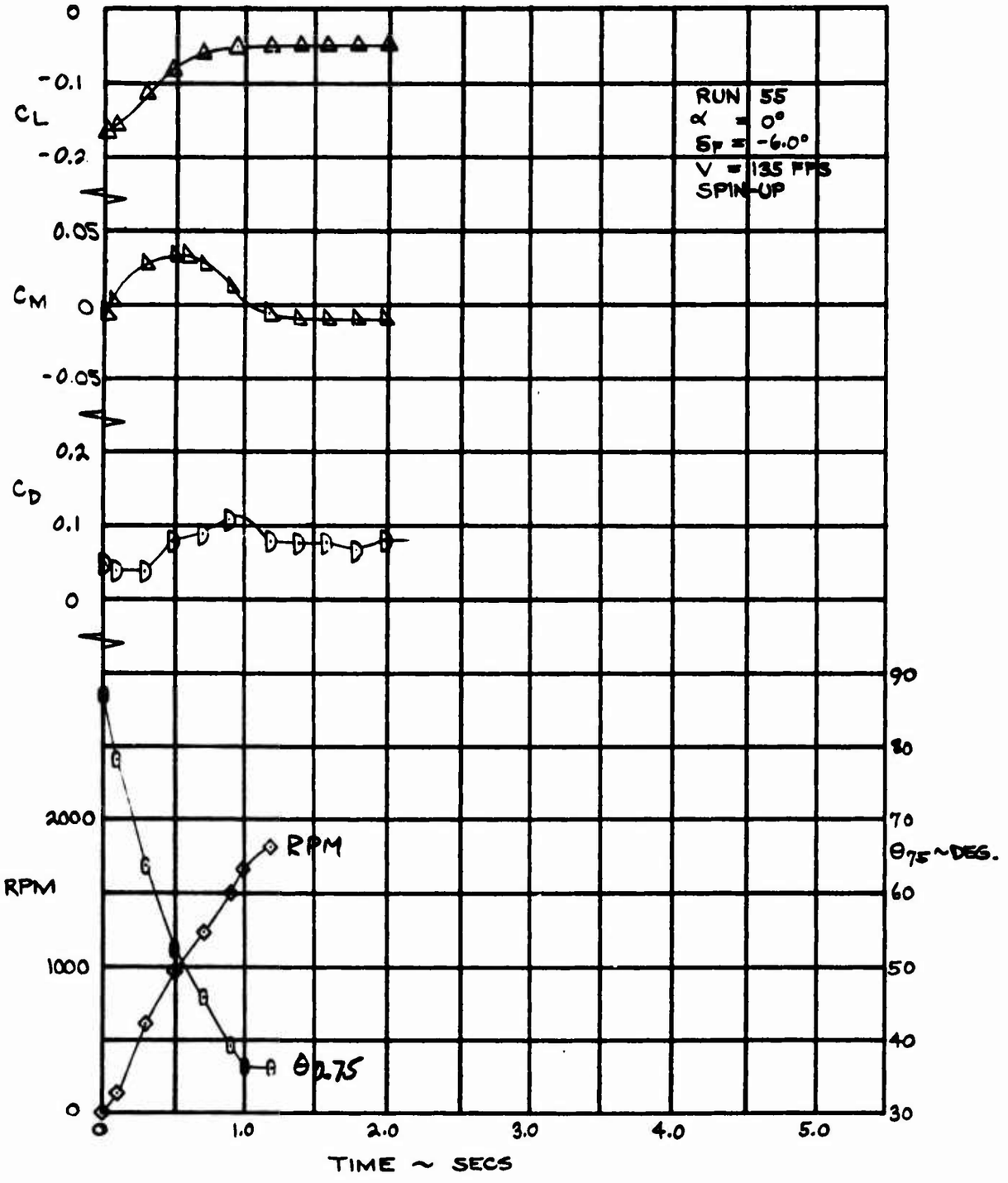

Figure 35. Drag, Lift and Pitching Moment for a 1.0 Second, 2 Step Linear Schedule, Spin-Up.

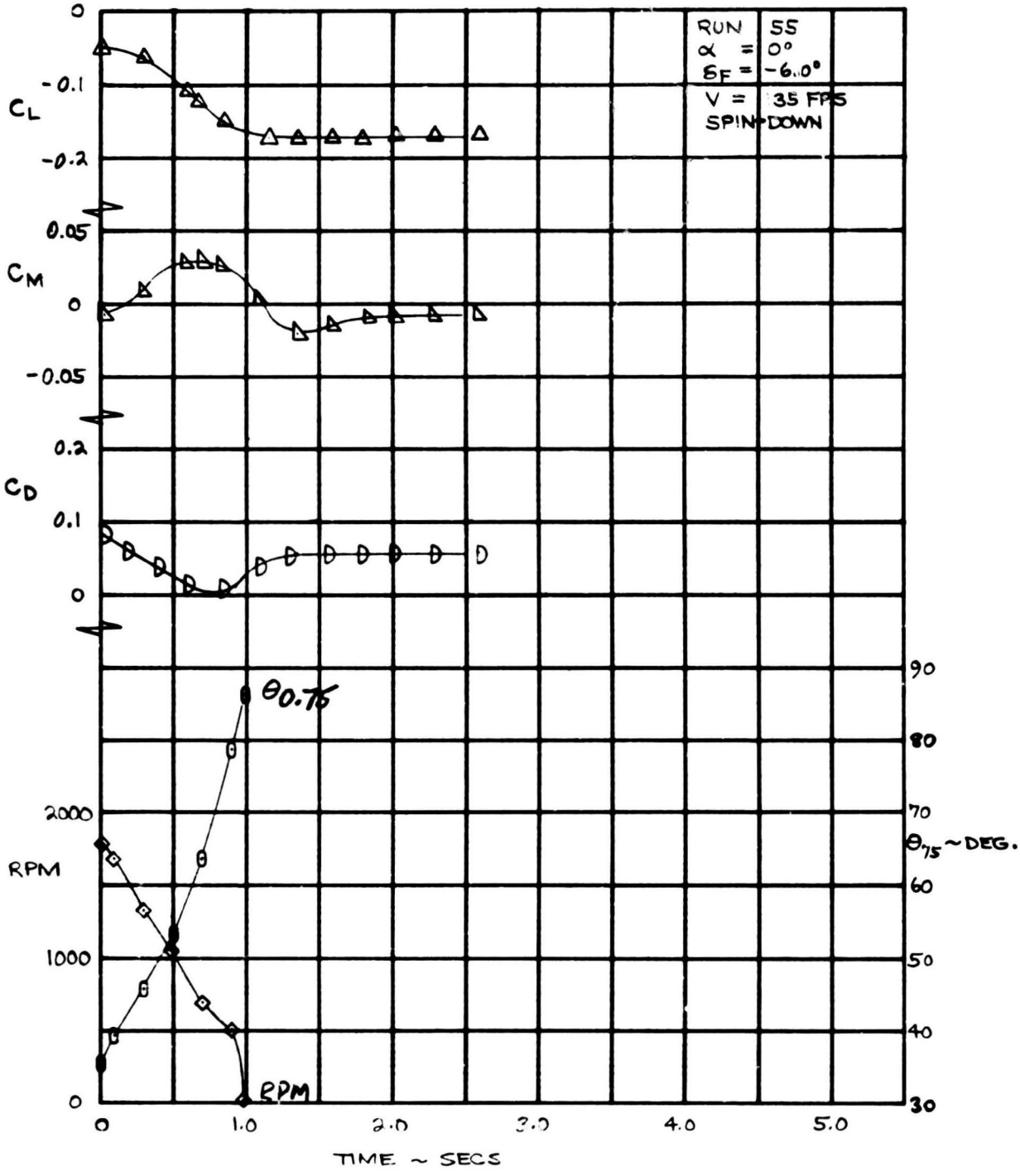

Figure 36. Drag, Lift and Pitching Moment for a 1.0 Second, 2 Step Linear Schedule, Feathering.

1.3.3 Effects of Angle of Attack and Flap Deflection

The nonlinear collective schedule shown in Figures 37 and 38 was believed to be the best that could be devised within the restraints of the test program, so this schedule was also tested to determine the effects of angle-of-attack variations and flap deflections. For the angle-of-attack variations, the transient data for lift, drag, and pitching moment are given in Figures 39 through 44. The same transient schedule was used to evaluate the effect of flap deflection and time histories of lift, drag, and pitching moment for flap deflections up to 30° are given in Figures 45 through 48. The transient drag increment is not affected significantly by flap deflection, although the total drag increases as expected.

1.4 STABILITY DERIVATIVES

The test data obtained have been analyzed to show the significance of the rotor normal force and pitching moment on the aircraft angle-of-attack stability. The contribution of the rotor is a function of the 1st harmonic blade dynamic response, which is collective pitch- and rpm-dependent. As a result, the stability derivatives change throughout the conversion process.

The rotor normal force derivate is largest when the rotor is feathered and is equal to 1.5 times the increase in lift on one blade due to an angle-of-attack change. The lift curve of the wing and nacelle can be computed from DATCOM methods. Figure 49 shows a comparison of the wing and feathered rotor data with this prediction. The test data, although scattered, indicate approximately the same slope. There is a zero-lift-angle discrepancy of one degree. This appears to be due to the wing aerodynamics. It is unlikely that the tunnel flow could be skewed enough to account for this discrepancy. The lift data for the model with the wing aerodynamic surface removed and the rotor feathered are shown in Figure 50. A similar comparison is shown for the rotor windmilling at 1,800 rpm in Figure 51. These data need further consideration, but the overall model lift curve slope can be predicted for the critical feathered-rotor condition.

The pitching moments measured about the balance centerline at zero rpm are produced by the normal force of the rotor since the hub pitching moment is zero when the rotor is feathered, as shown in Figure 52. Data for the windmilling rotor are shown in Figure 53. These data show that the pitching moment increases linearly with angle of attack.

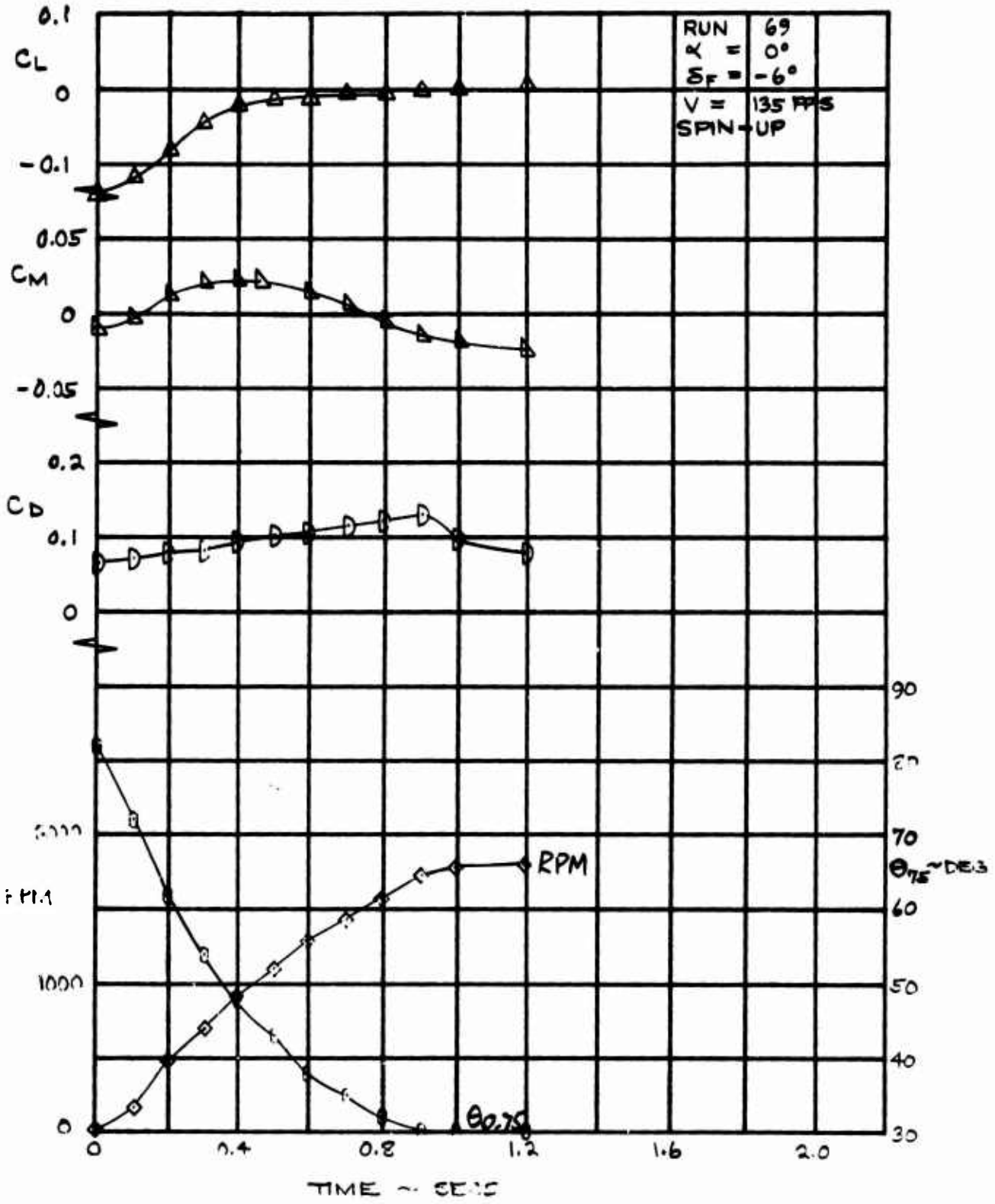

Figure 37. Drag, Lift and Pitching Moment for a 0.9 Second Nonlinear Schedule, Spin-Up.

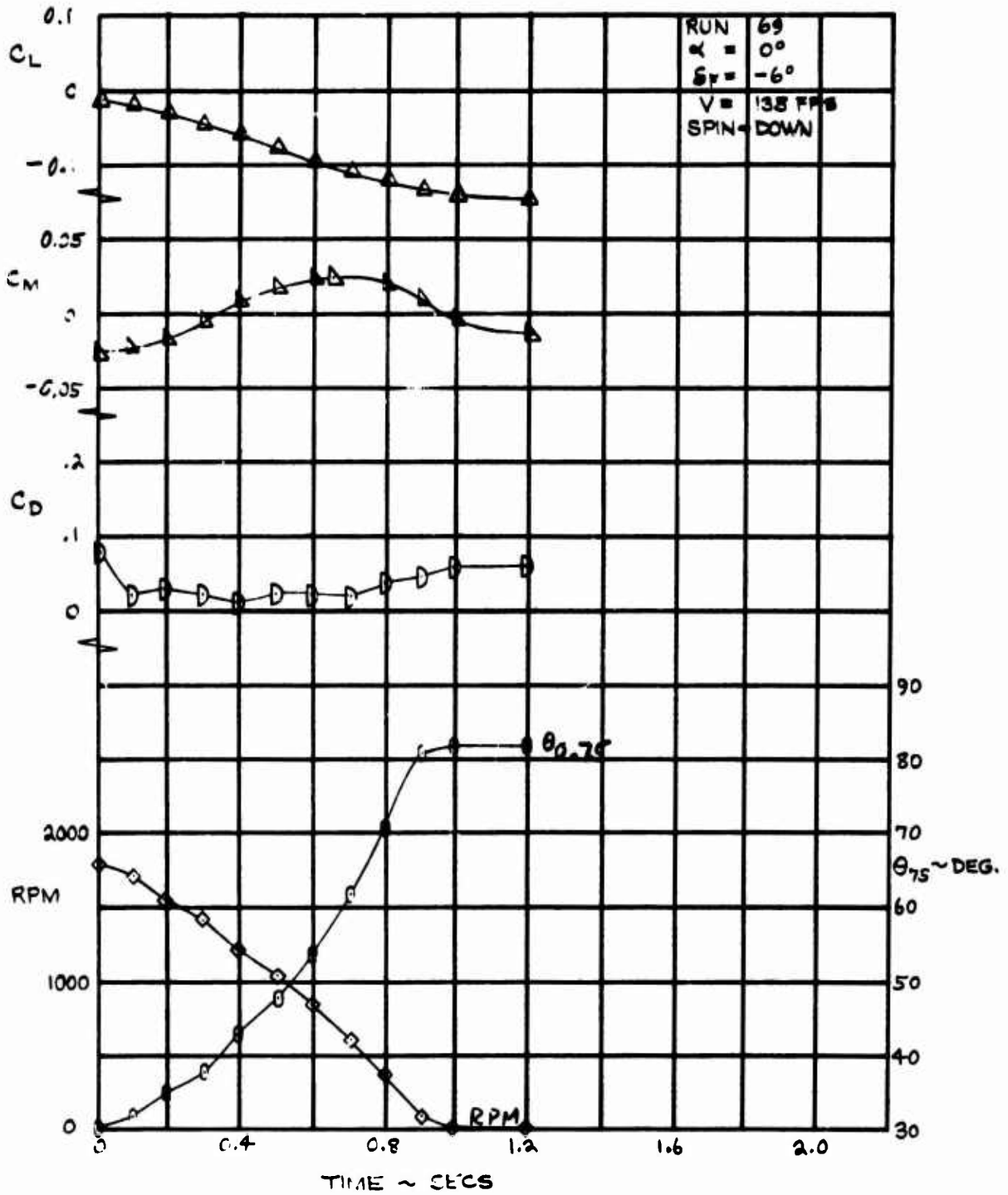

Figure 38. Drag, Lift and Pitching Moment for a 0.9 Second Nonlinear Schedule, Feathering.

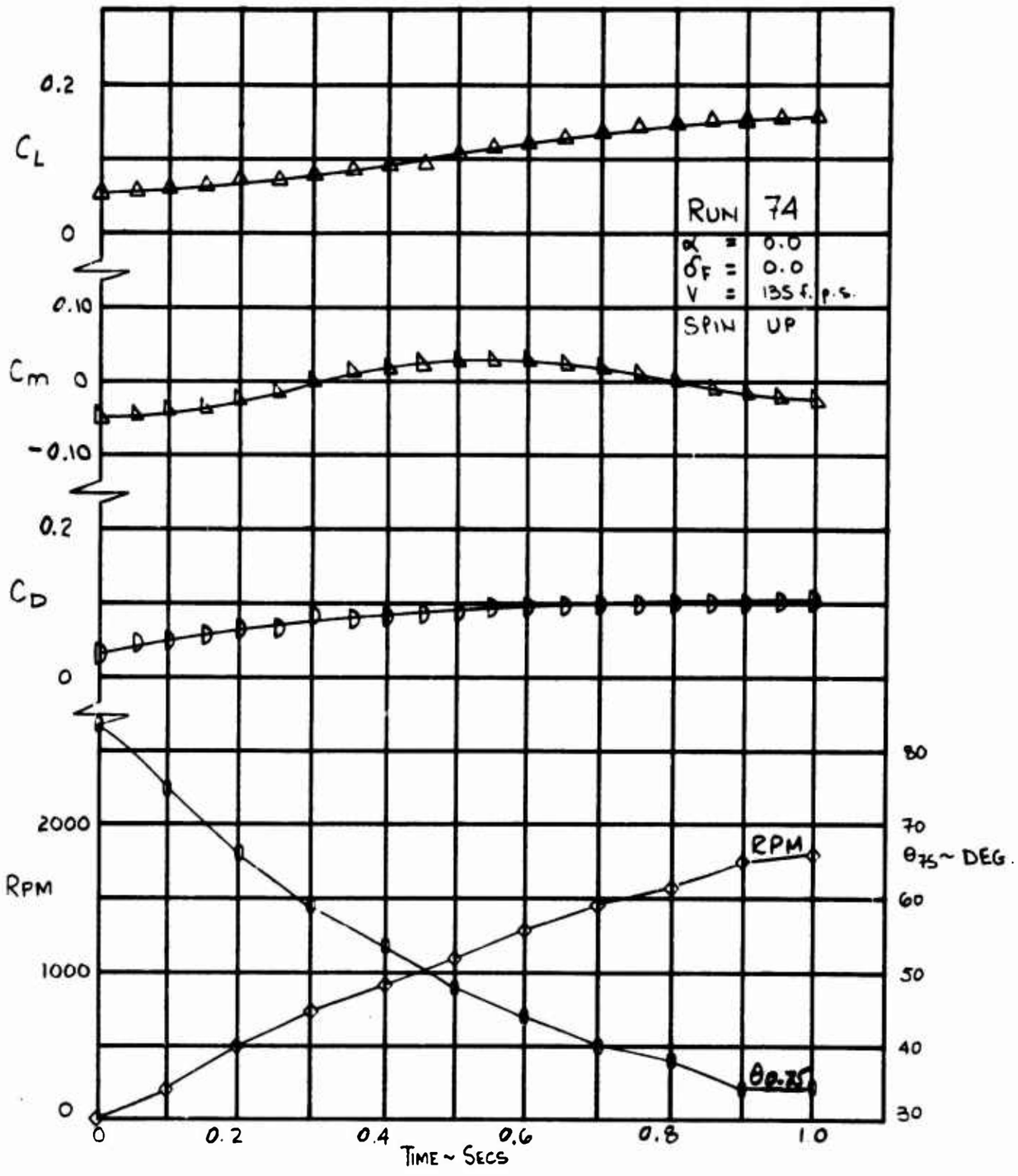

Figure 39. Drag, Lift and Pitching Moment for a 0.91 Second Nonlinear Schedule, Spin-Up at $\alpha = 0$.

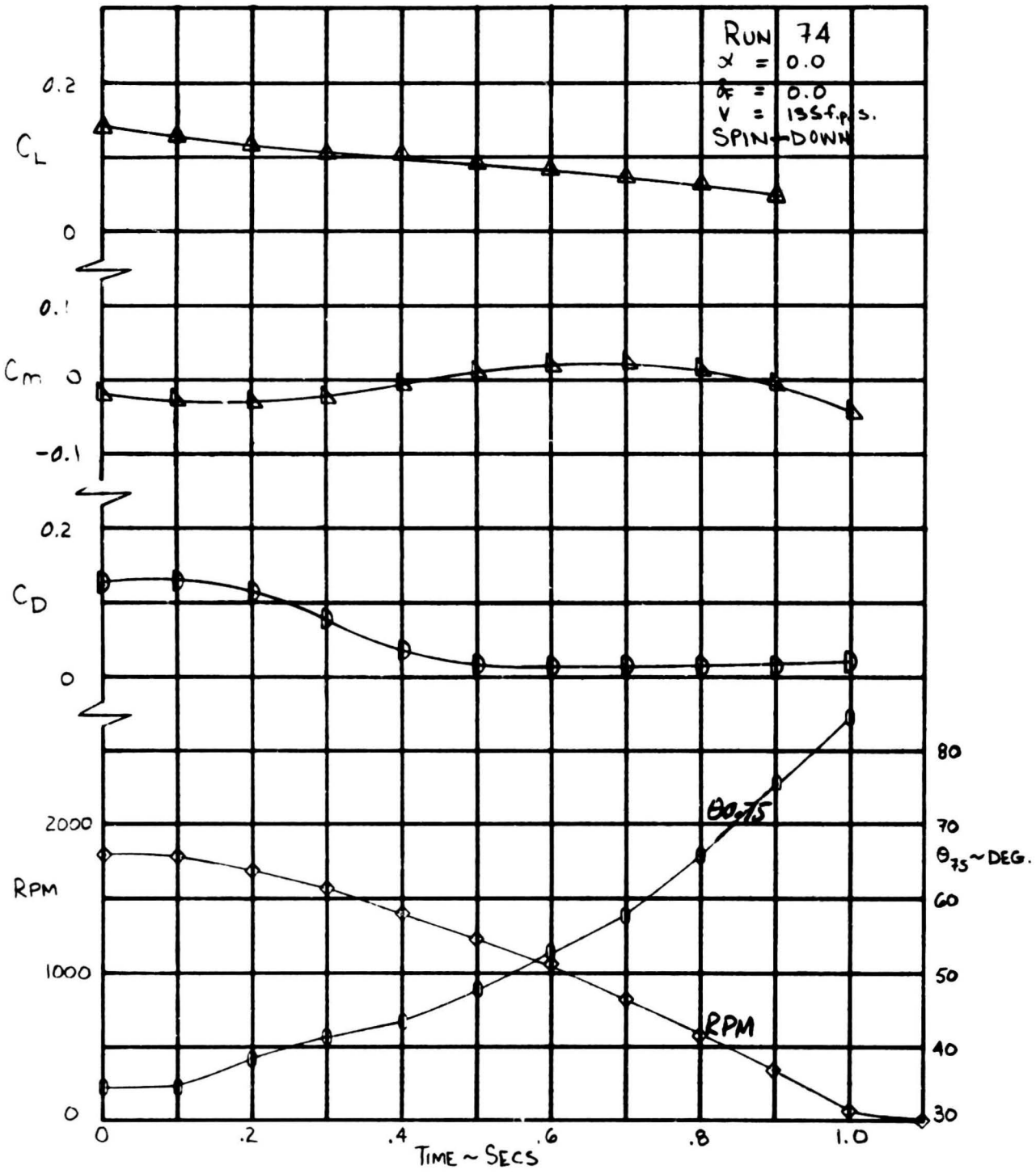

Figure 40. Drag, Lift and Pitching Moment for a 0.91 Second Nonlinear Schedule, Feathering at $\alpha = 0$.

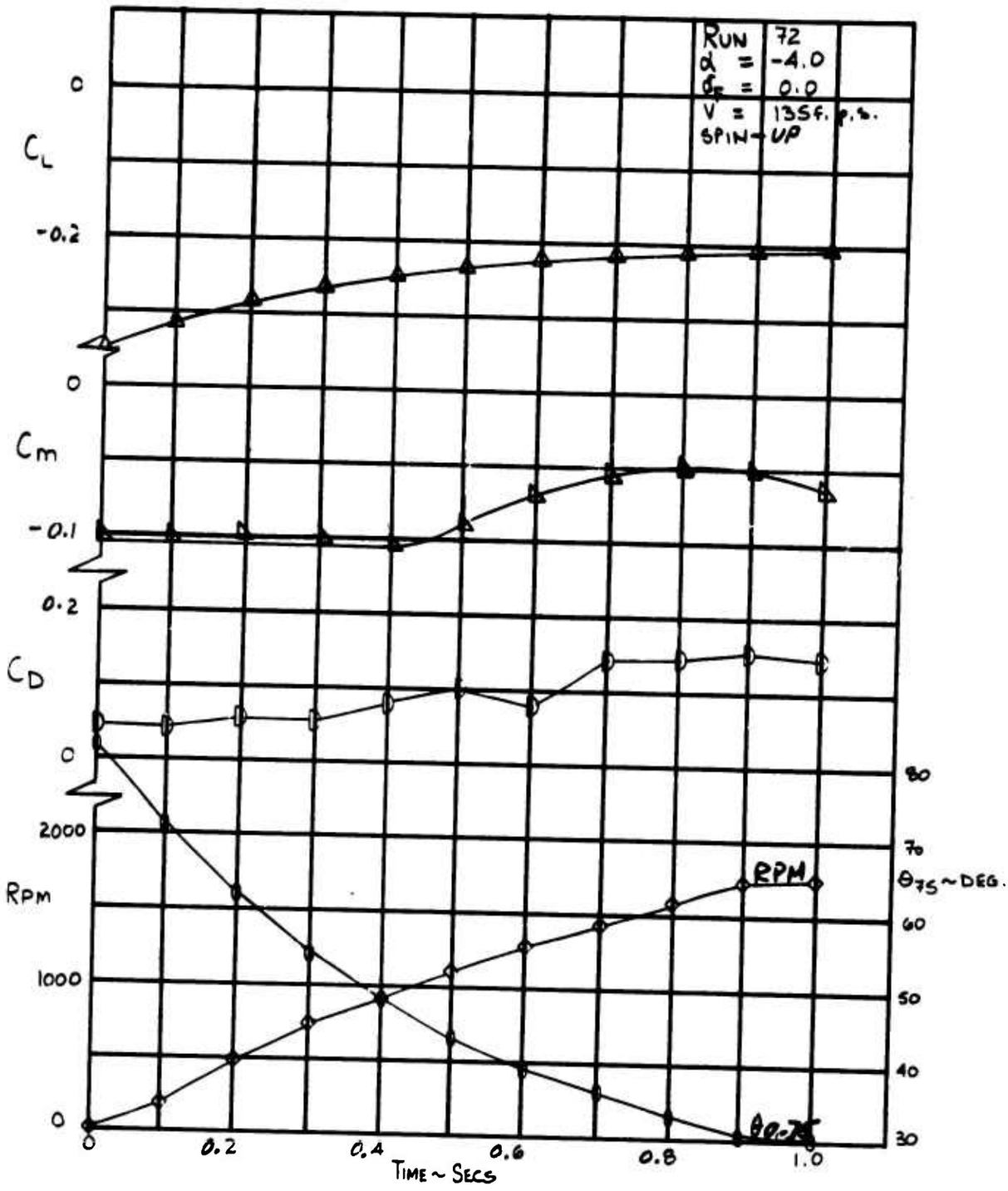

Figure 41. Drag, Lift and Pitching Moment for a 0.91 Second Nonlinear Schedule, Spin-up at α= -4.

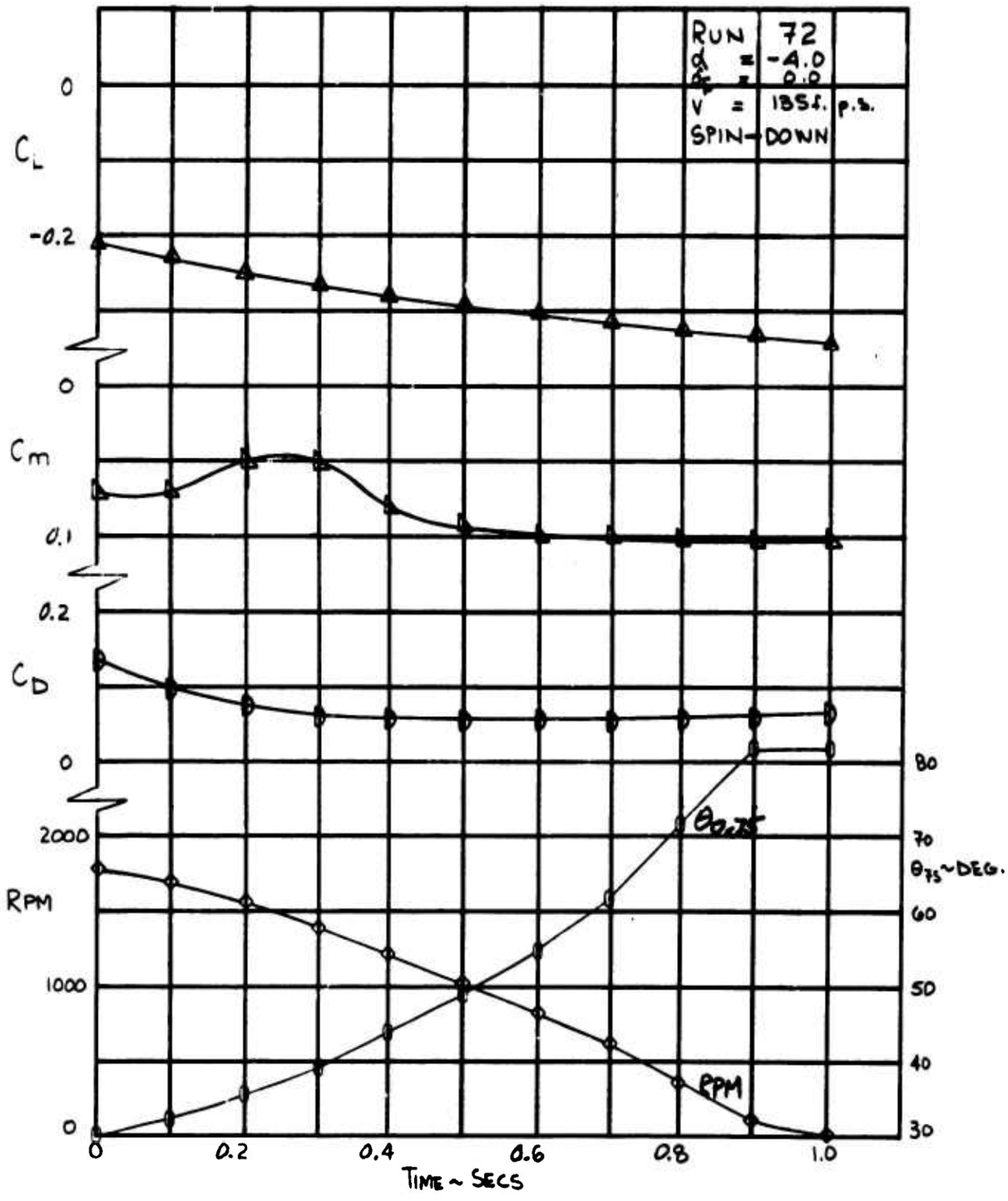

Figure 42. Drag, Lift and Pitching Moment for a 0.91 Second Nonlinear Schedule, Feathering at α = -4.

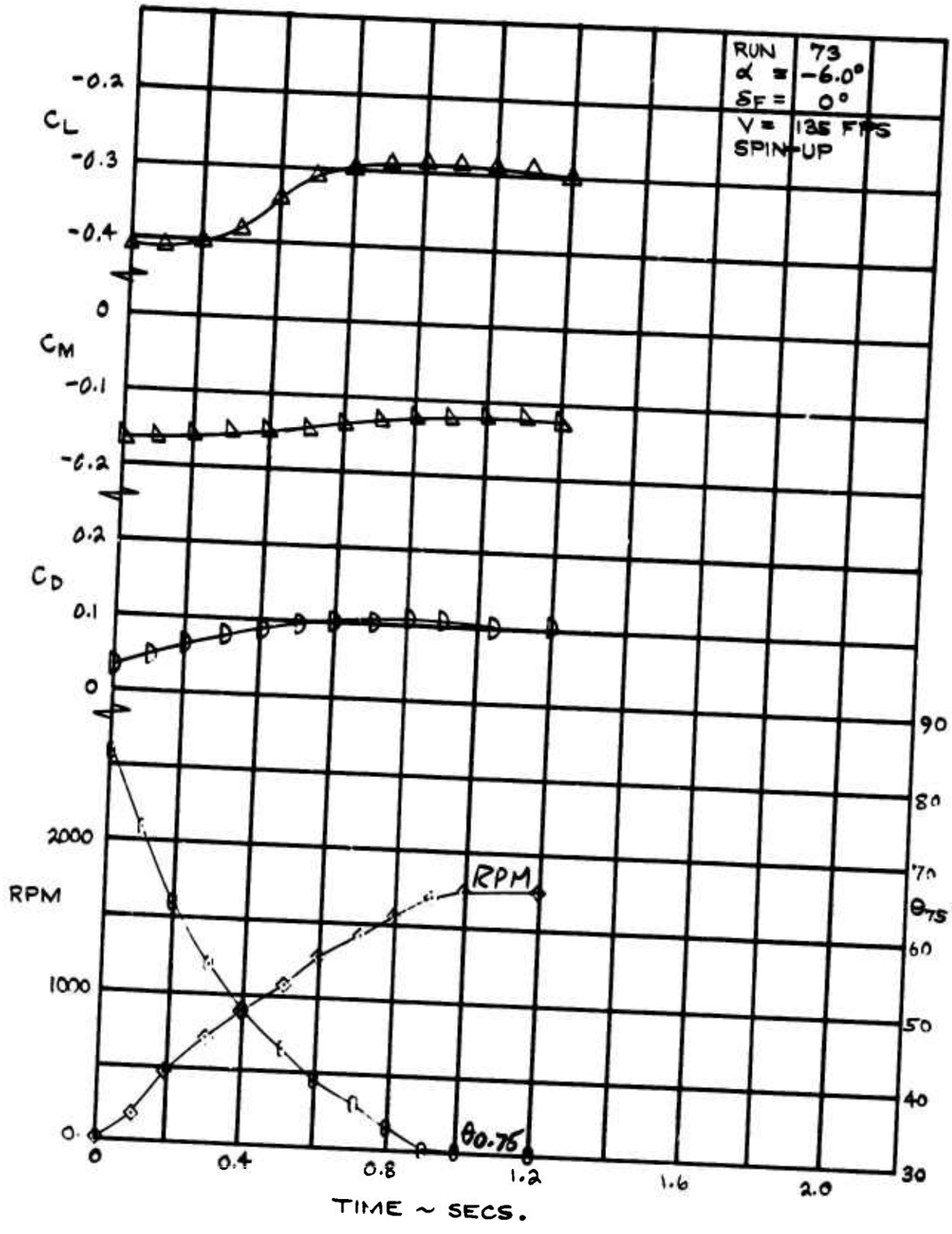

Figure 43. Drag, Lift and Pitching Moment for a 0.91 Second Nonlinear Schedule, Spin-Up at $\alpha = -6$.

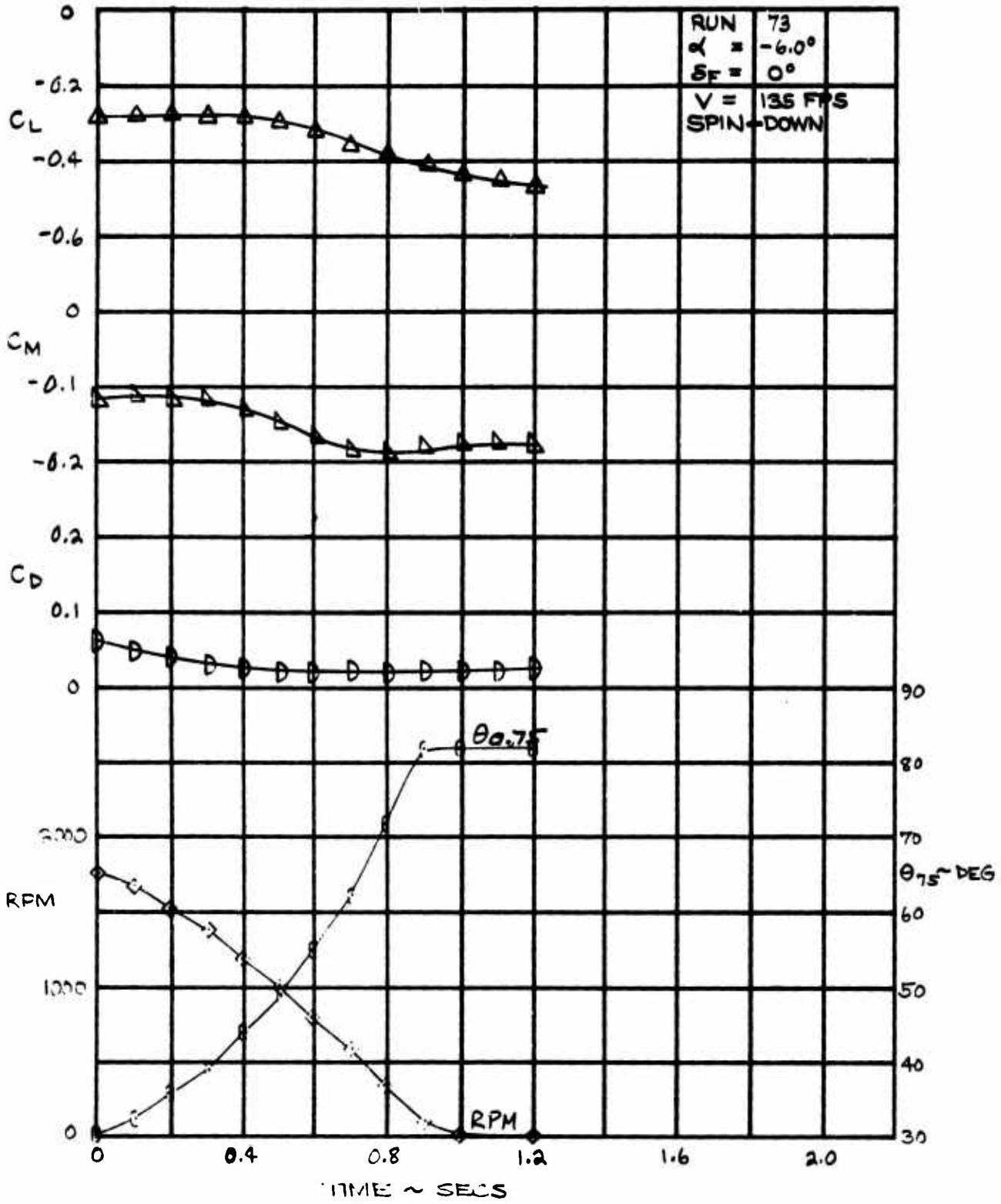

Figure 44. Drag, Lift and Pitching Moment for a 0.91 Second Nonlinear Schedule, Feathering at α = -6.

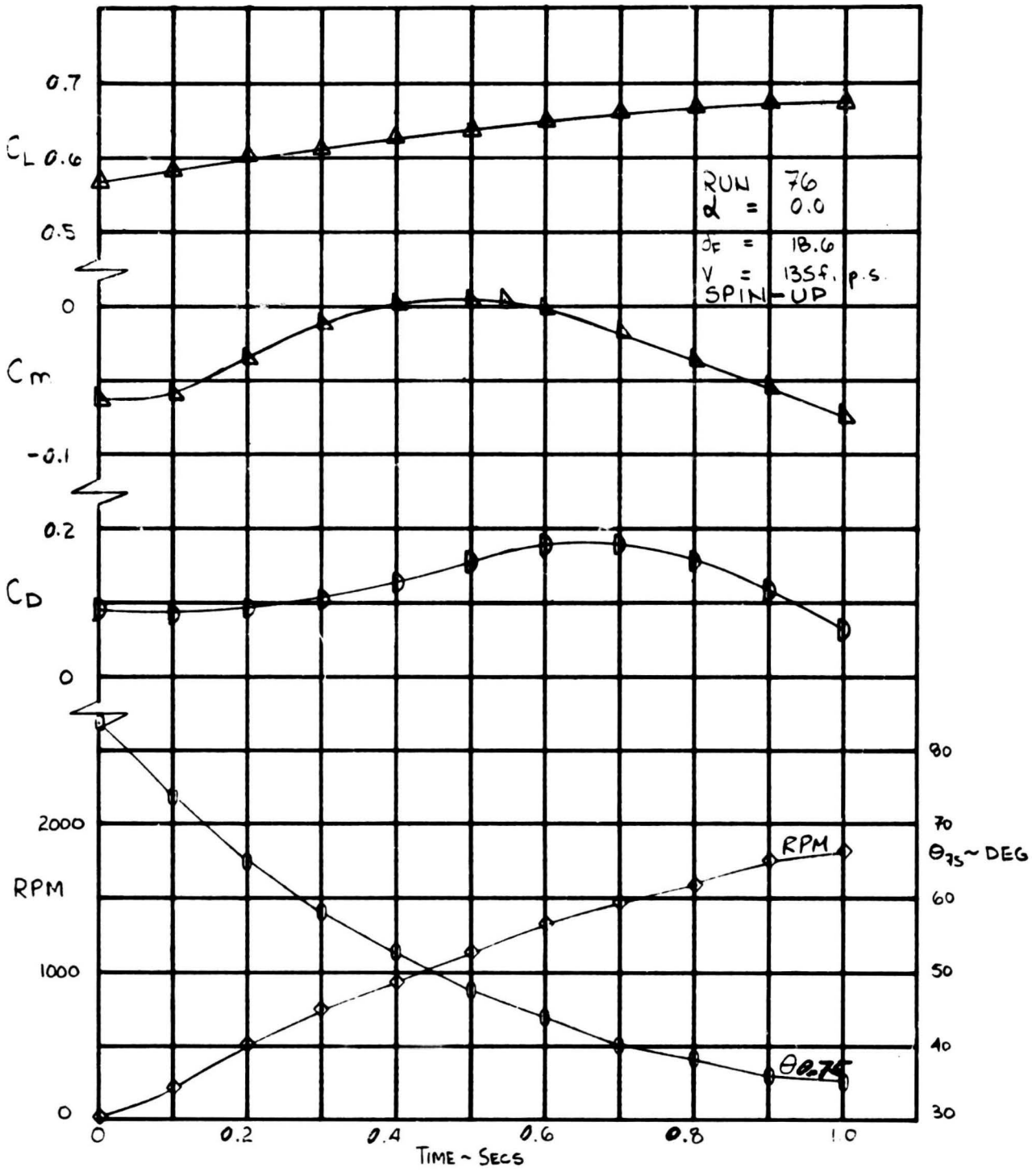

Figure 45. Drag, Lift and Pitching Moment for a 0.91 Second Nonlinear Schedule, Spin-Up at δf = 18.6.

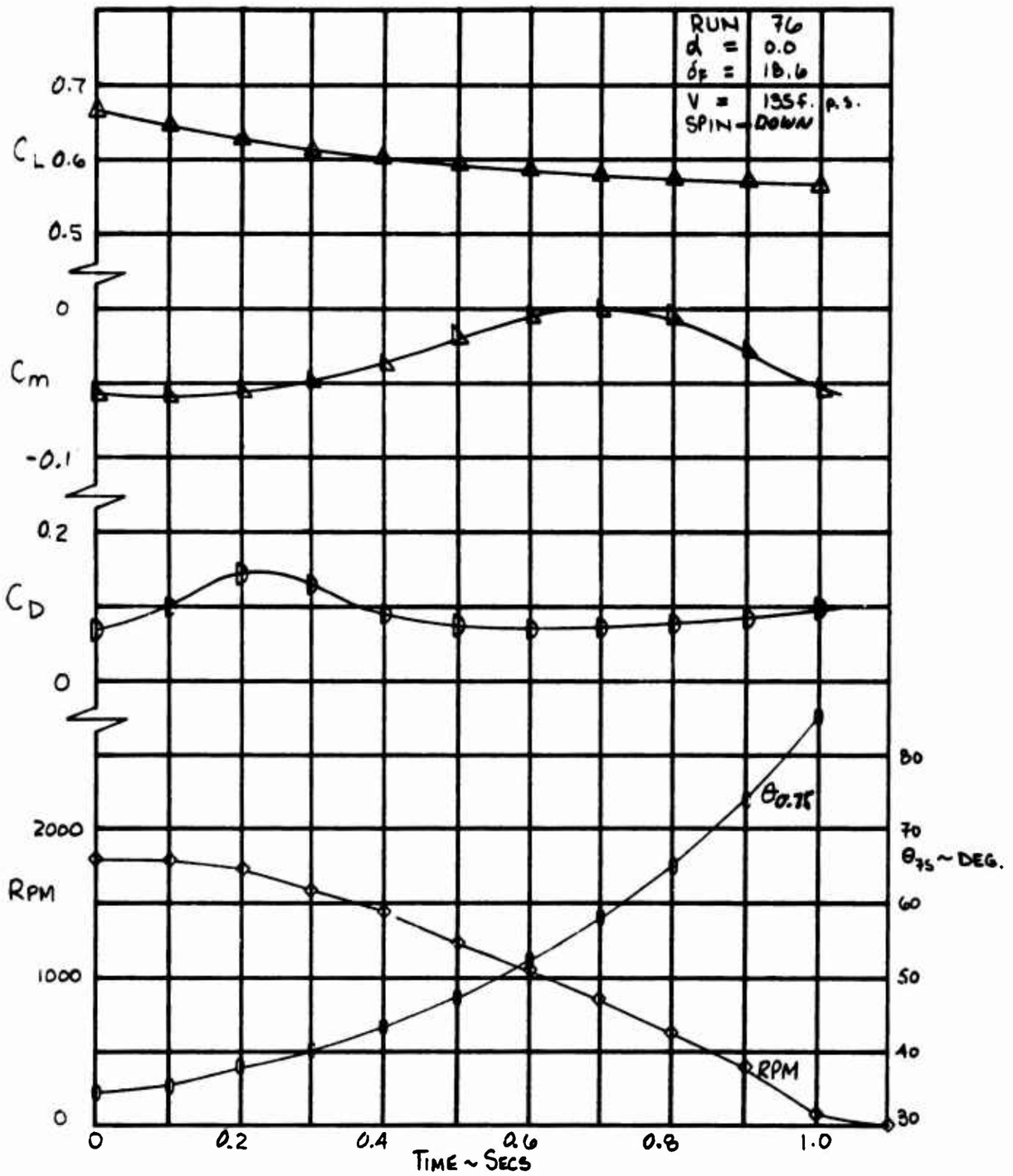

Figure 46. Drag, Lift and Pitching Moment for a 0.91 Second Nonlinear Schedule, Feathering at $\delta f = 18.6$.

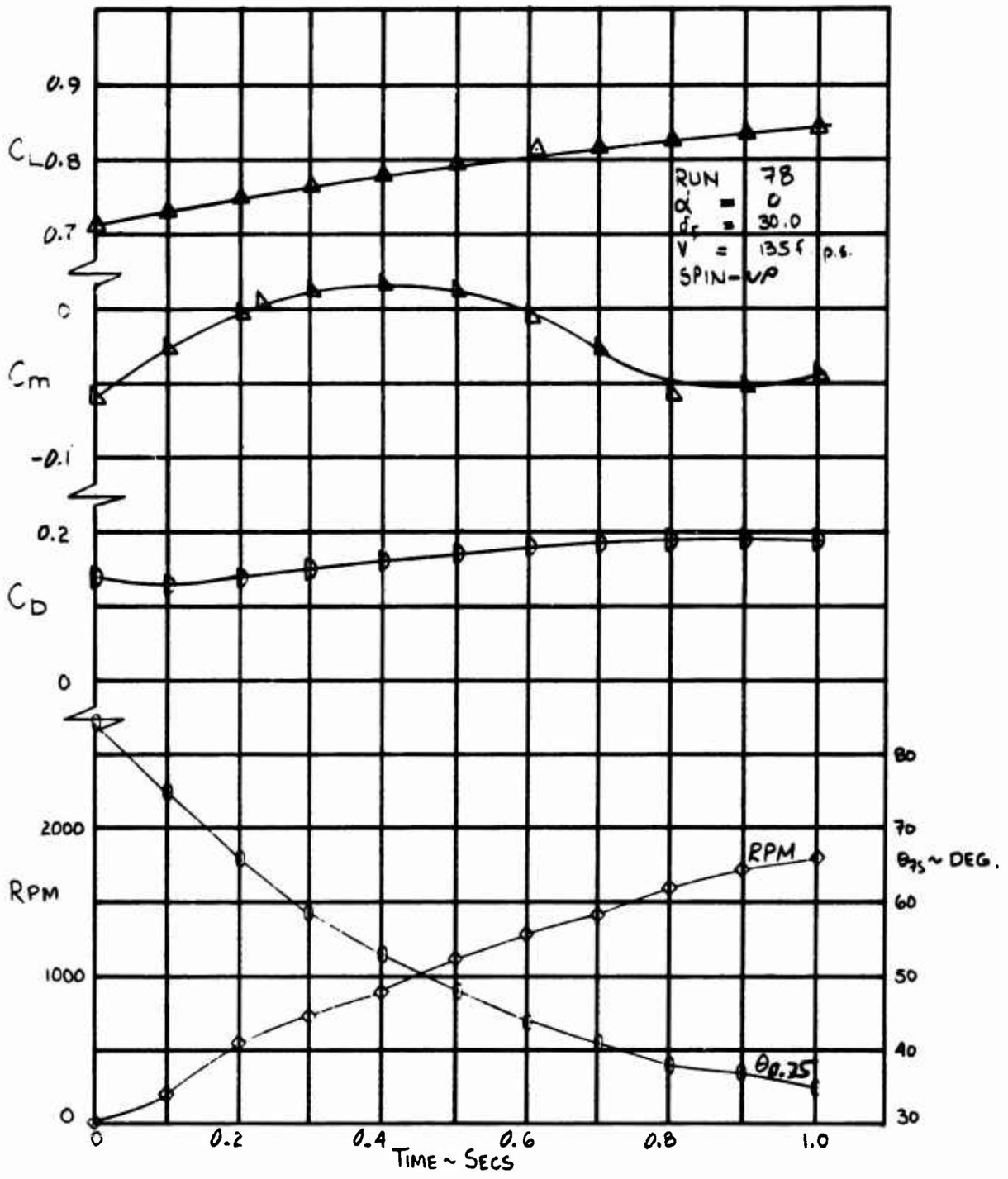

Figure 47. Drag, Lift and Pitching Moment for a 0.91 Second Nonlinear Schedule, Spin-Up at δ f = 30.

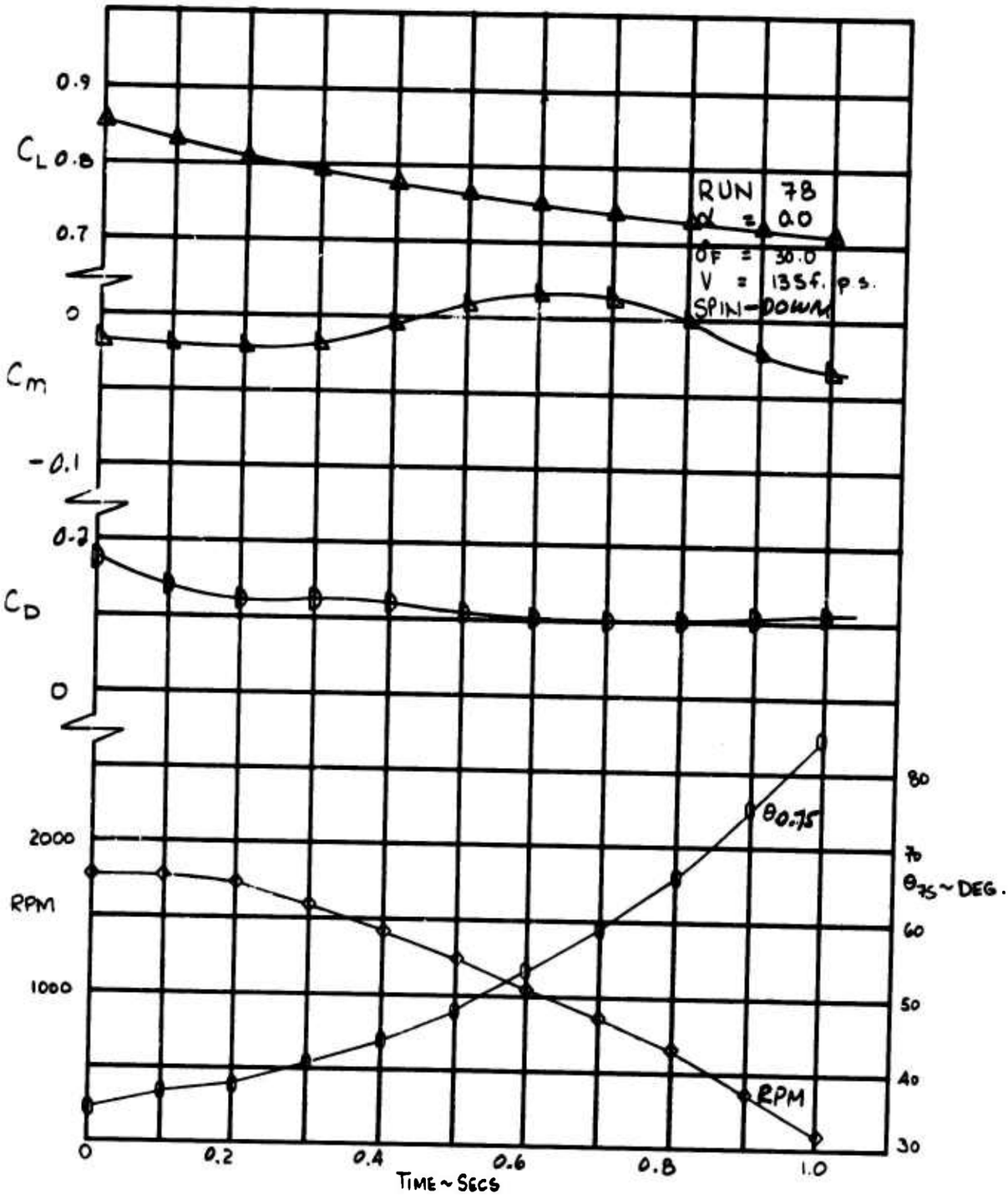

Figure 48. Drag, Lift and Pitching Moment for a .91 Second Nonlinear Schedule, Feathering at $\delta f = 30$.

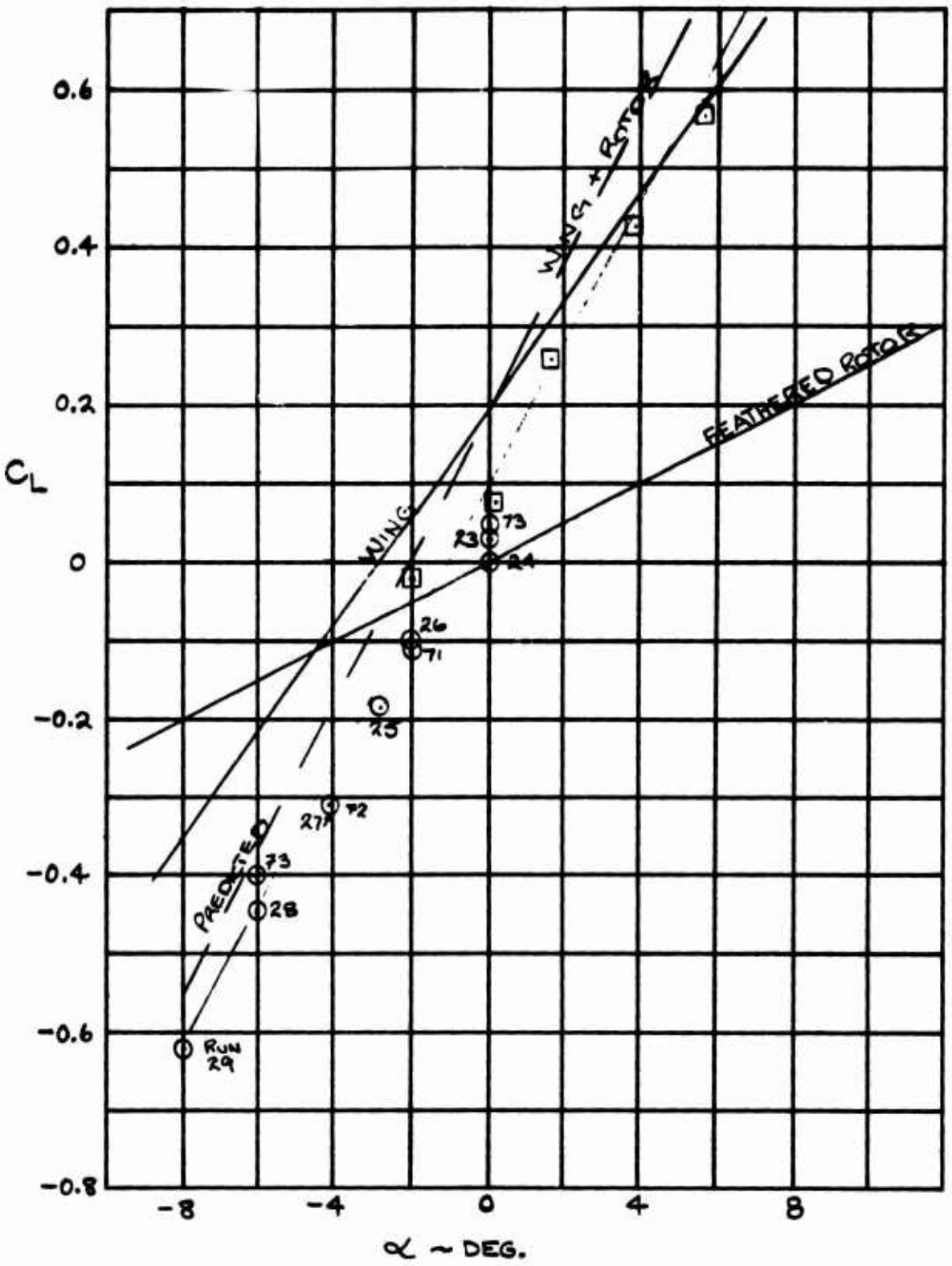

Figure 49. Contribution of Normal Force of Feathered Prop/Rotor to Aircraft Lift-Angle of Attack Relationship.

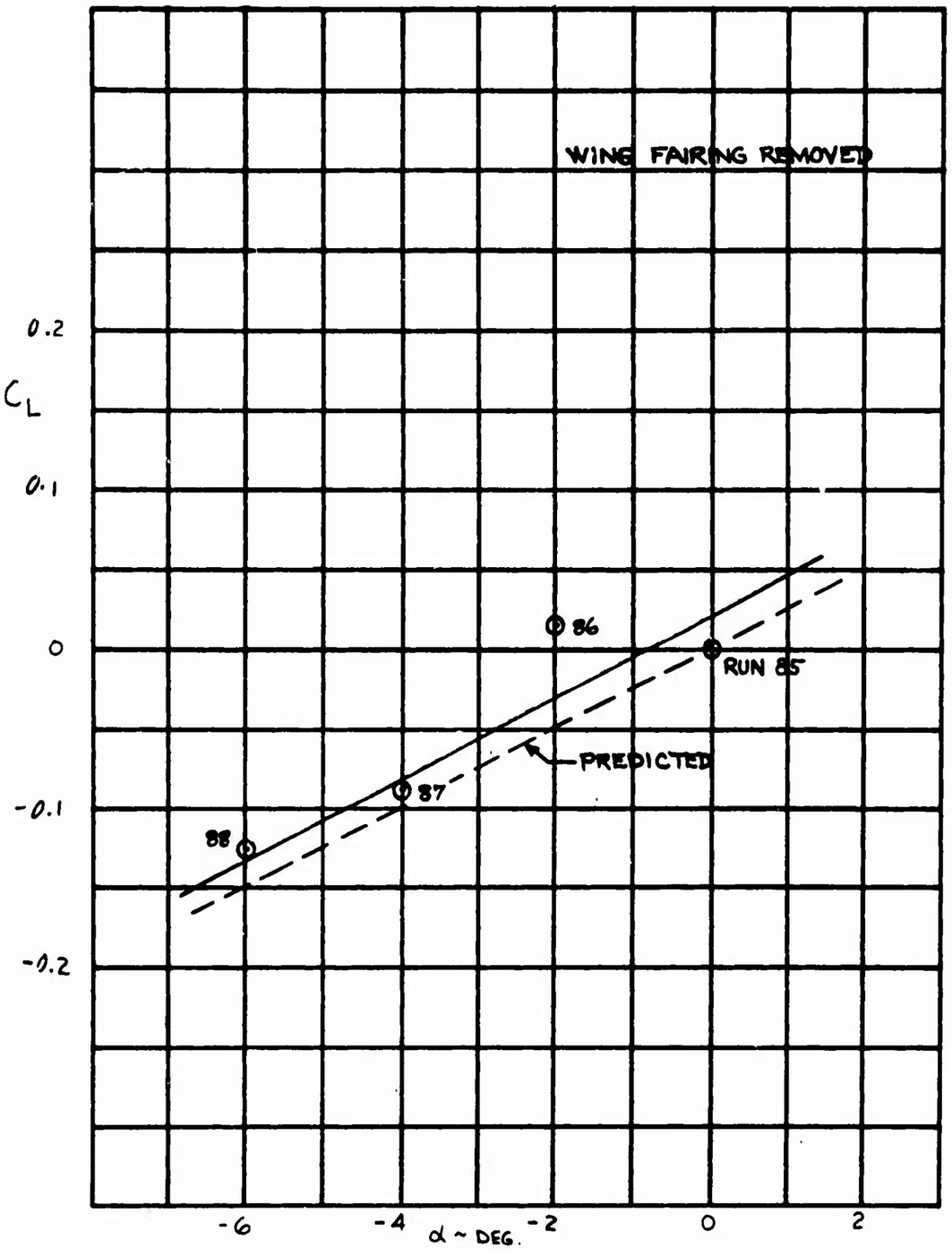

Figure 50. Lift Produced by Normal Force of Feathered Rotor.

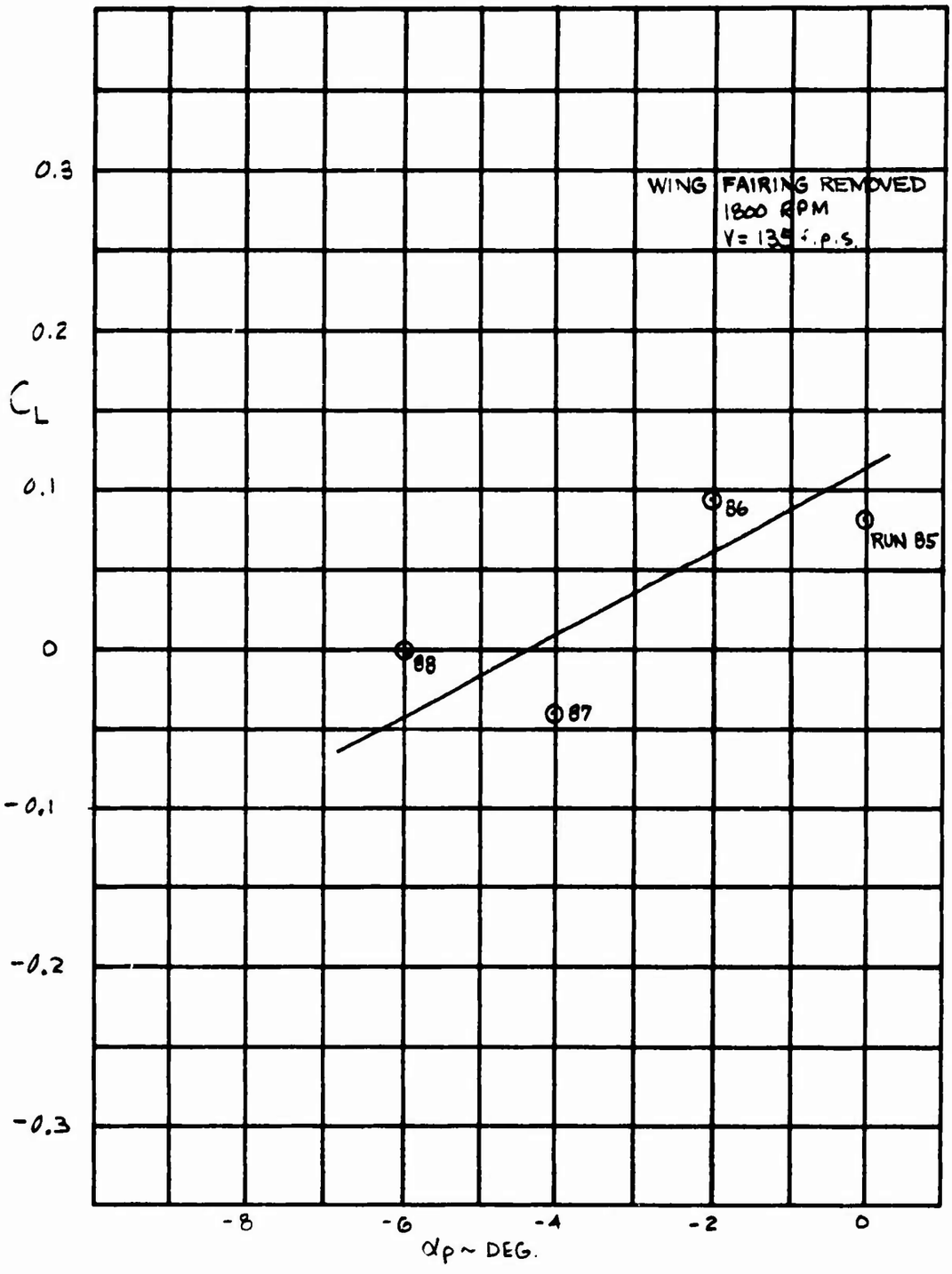

Figure 51. Lift Produced by Normal Force of Windmilling Rotor.

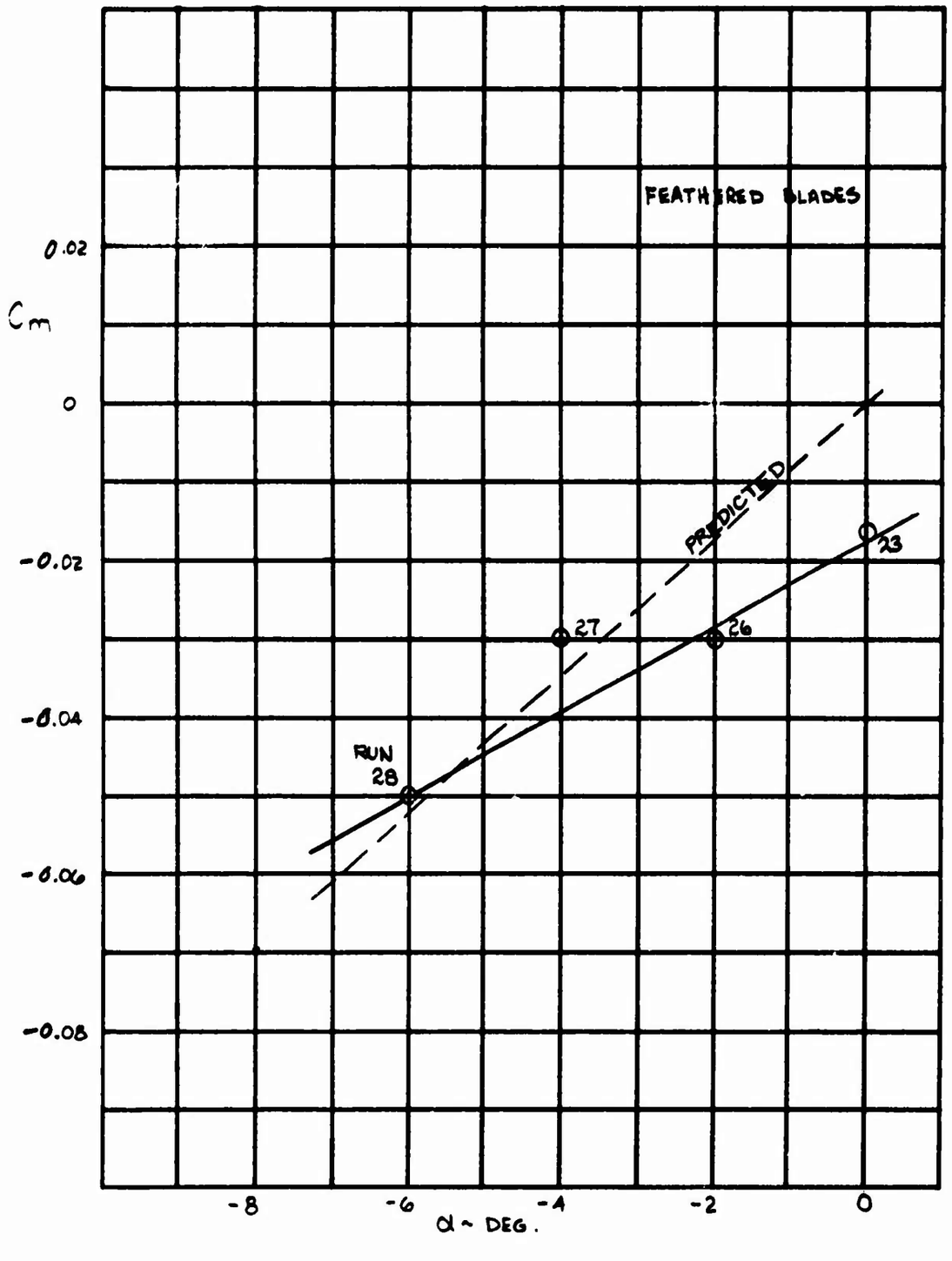

Figure 52. Pitching Moment Produced by Wing and Feathered Rotor.

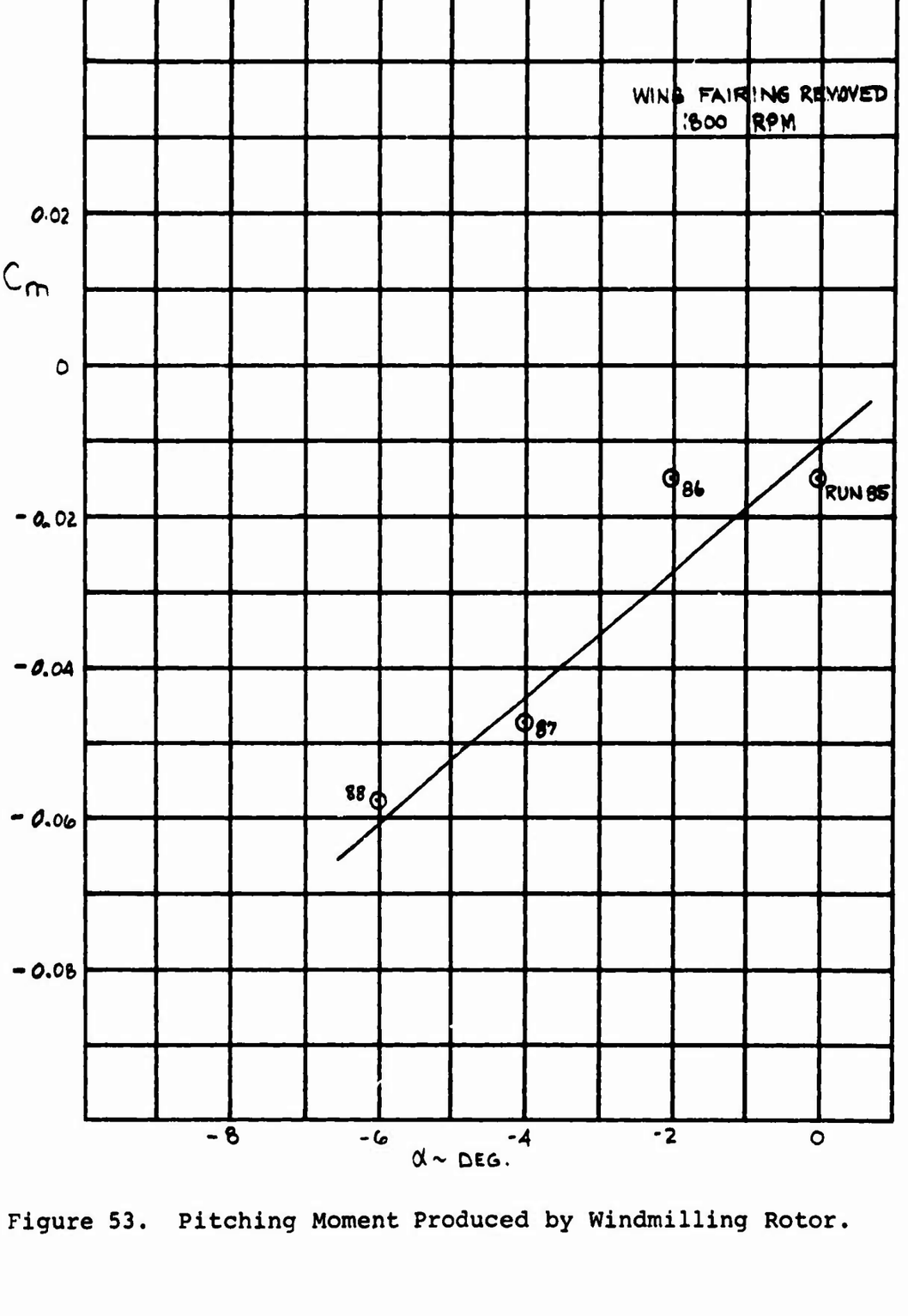

Figure 53. Pitching Moment Produced by Windmilling Rotor.

2. BLADE-BENDING MOMENTS

Optimization of the zollective pitch schedule for conversion included consideration of vibratory blade-bending moments so that a practical schedule could be devised. As shown in Figure 4, there is only a small change in blade loads in the conversion transient from steady operation at the same rpm. Collective schedule optimization is therefore unrestrained by blade loads.

Chordwise blade-bending moments during Phase I tests were high at the higher rotor speeds (1,400 to 1,800 rpm) because the chordwise frequency of the blade bending was approximately at 1.0 per rev rather than the desired 0.75 per rev.

2.1 SCALING OF MODEL BLADE-BENDING MOMENTS

From blade loads considerations, the major purposes of this test program were to investigate the need for restraints on the conversion collective schedule and to obtain data for substantiating the blade loads-prediction techniques. Since the model blade design was of a representative structure and this design included the proper frequency, inertia (Lock number), and geometry scaling, the data generated will be valuable for substantiating the analysis. The model blade dynamic scaling did not include Froude number equivalence and the model blade structure did not duplicate the full-scale design. It is therefore necessary to correlate the blade load measurements with analysis to determine the detailed significance of these data.

2.2 STEADY WINDMILLING

2.2.1 RPM and Dynamic Coupling Effects

Figures 54 and 55 present the variation of blade loads with rpm in steady windmilling conditions during Phase I tests. The vibratory chordwise bending reaches peaks at 400, 900, and 1,700 rpm. These rpm's correspond to the 4/rev, 2/rev, and 1/rev blade chordwise natural frequency integer crossings indicated by the baffle test data in Figure 19. The blade flapwise loads generally decrease as rpm increases; however, there are identifiable peaks at 250 rpm and 550 rpm corresponding to the 4/rev and 2/rev blade flapwise natural frequency crossings. At 900 rpm the loads peak due to coupling between the chord and flap blade modes.

In Phase II testing the blades were tuned as described in Section 3.1.4. A comparison of the blade loads data for the tuned and original blades is given in Figure 56. The peaks in the blade load curves occur at the rpm corresponding to the

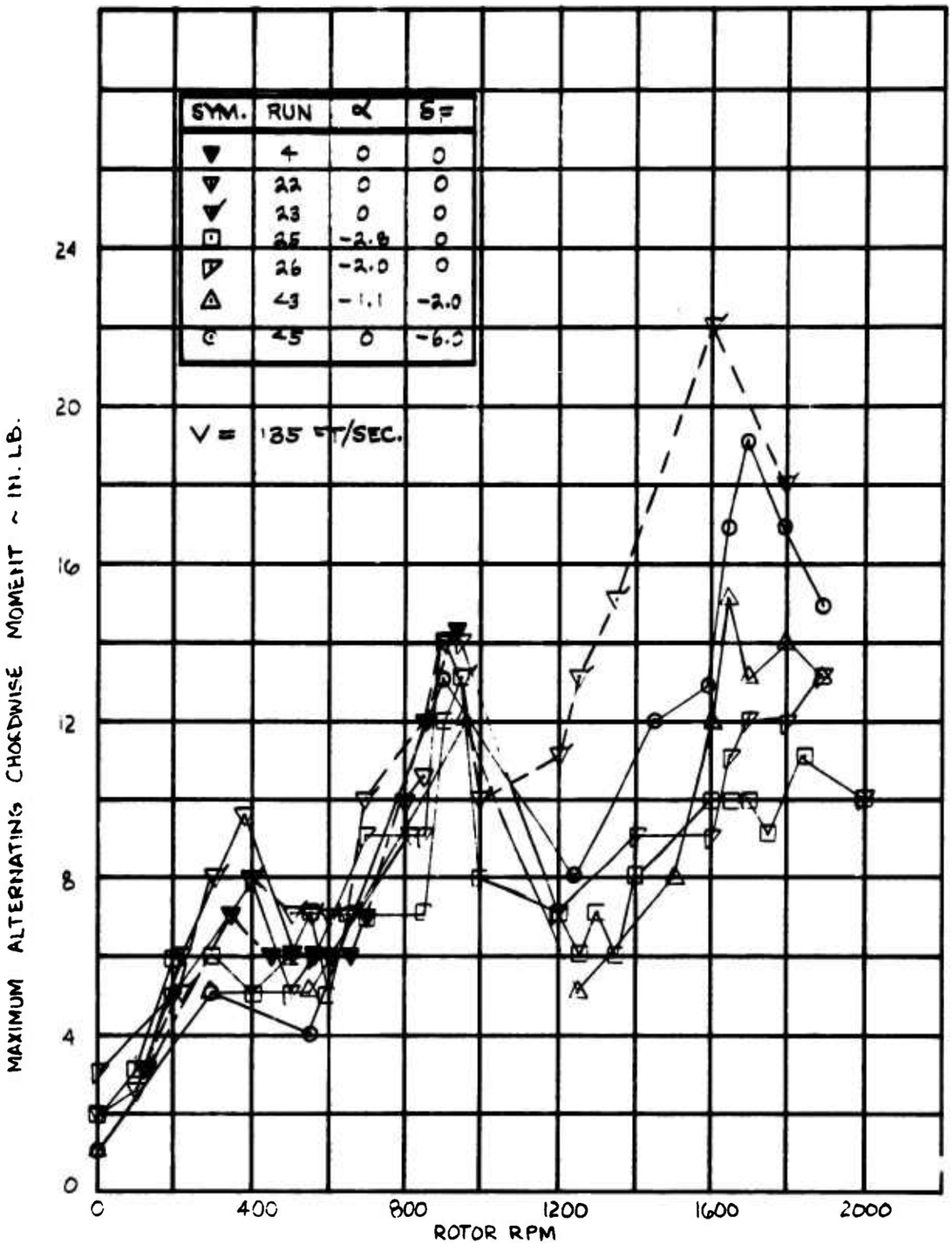

Figure 54. Alternating Chordwise Blade Bending Moment at 0.11R for Windmilling at Near Zero Lift Conditions.

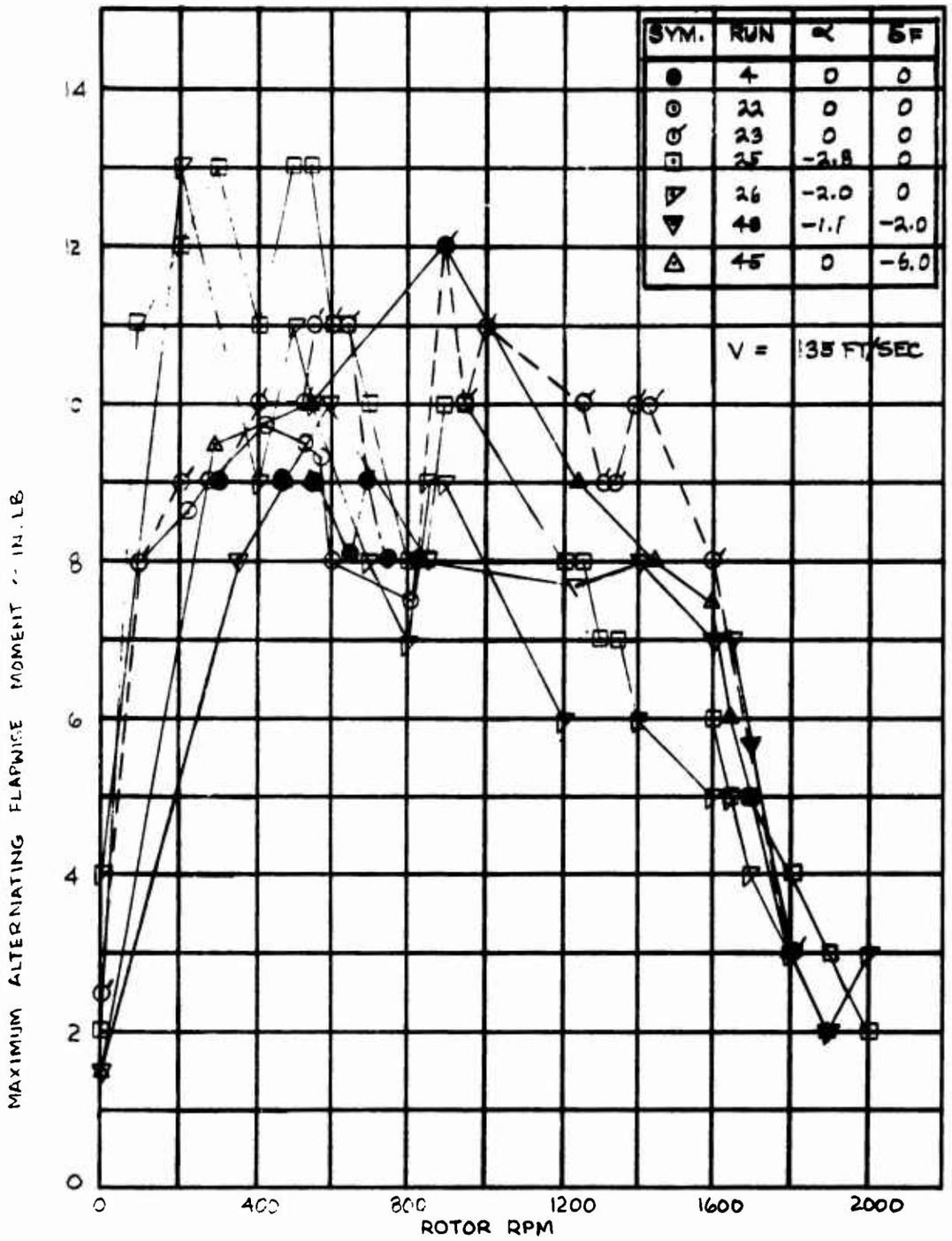

Figure 55. Alternating Flapwise Blade Bending Moment at 0.13R for Windmilling at Near Zero Lift Conditions.

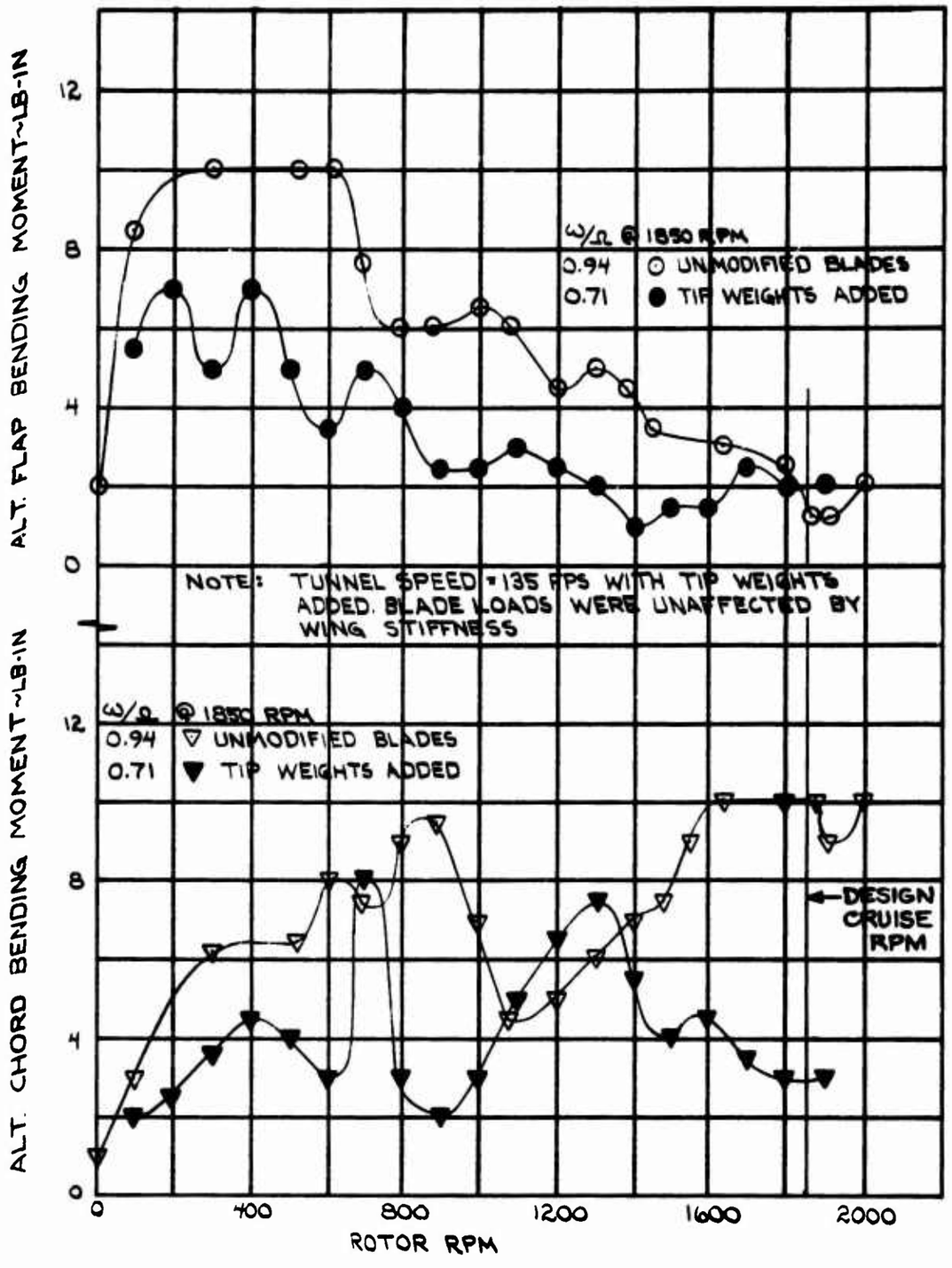

Figure 56. Effect of Inplane Frequency on Blade Loads Under Steady Windmilling.

integer frequency crossings for the tuned blades (see Figure 9). At the design cruise rpm of 1,850, both the flap and chord blade loads are low when the frequencies are close to the full-scale design values.

The impact of wing-rotor dynamics on blade loads can best be assessed by testing with different wing stiffnesses. Figure 57 shows blade loads over the rpm range for two wing stiffnesses. The braced wing was sufficiently stiff to raise all frequency crossings of the 1/rev line outside of the test rpm range, as reported in Section 3. This order-of-magnitude change in wing dynamics provided little change in measured blade loads at the design rpm. It must be concluded that rotor blade loads are not sensitive to wing stiffness and the coincidence of rotor and wing frequencies did not increase blade loads.

Blade alternating-torsion data measured in steady windmilling are of magnitudes less than one inch-pound and, with small angle of attack and flap deflection, these loads decrease approximately linearly with increasing rpm. When the angle of attack is not small or the flap is deflected to increase lift, the alternating torsion was constant or slightly increased with rpm. These data show some indication of coupling of the torsion with the occurrences of larger flapwise or chordwise blade moments. Alternating torsion measured on the green blade was always larger than that measured on the red blade. These data are presented in Volume II.

2.2.2 Effect of Wing Lift and Rotor Shaft Angle of Attack

Wing lift creates an induced velocity which alters the flowfield around the wing and rotor from the freestream velocity. The wing lift can be changed by changing flap incidence or wing angle of attack. When the aircraft angle of attack is changed, the rotor experiences a change in the flowfield apart from that caused by wing lift. A 1/rev sinusoidal change in blade section angle of attack is experienced due to rotor angle of attack. Test data obtained in steady windmilling indicate that the effect of wing lift on blade loads is small compared to the effect of rotor angle of attack, as shown in Figures 58 and 59. At a specific angle of attack, there is little difference between the blade loads data measured with and without the wing aerodynamic surface installed. The blade loads increase as the angle of attack is increased or decreased from -2 degrees. From these data, it appears that the rotor was skewed +2 degrees in the tunnel when the indicated angle of attack was zero. This is in line with the wing-off lift data of Section 1.2, which also showed zero lift at -2 degrees incidence. The model was rechecked for alignment before it was removed from the tunnel, but no misalignment was found.

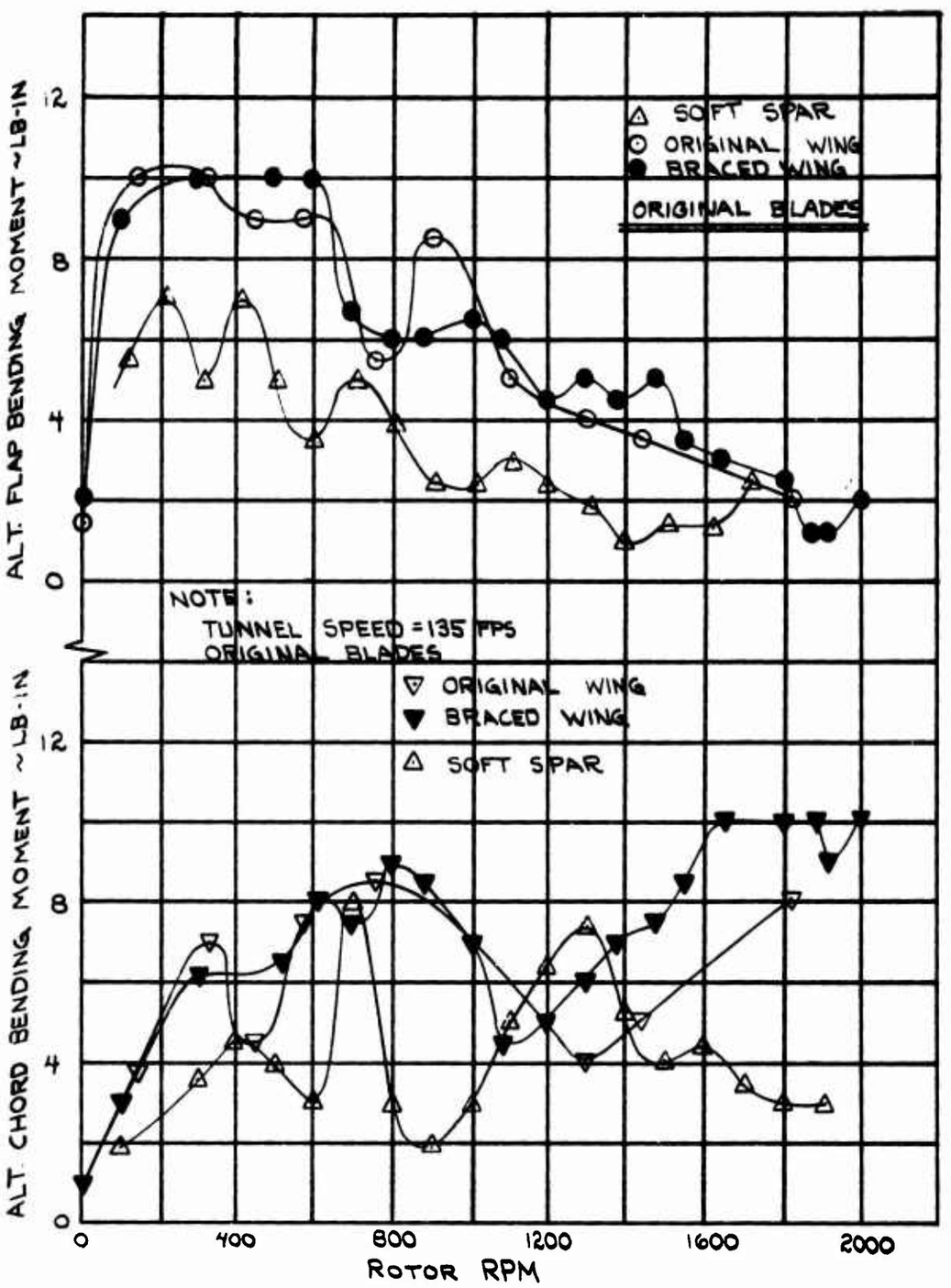

Figure 57. Effect of Stiffened Wing on Blade Loads Steady Windmilling.

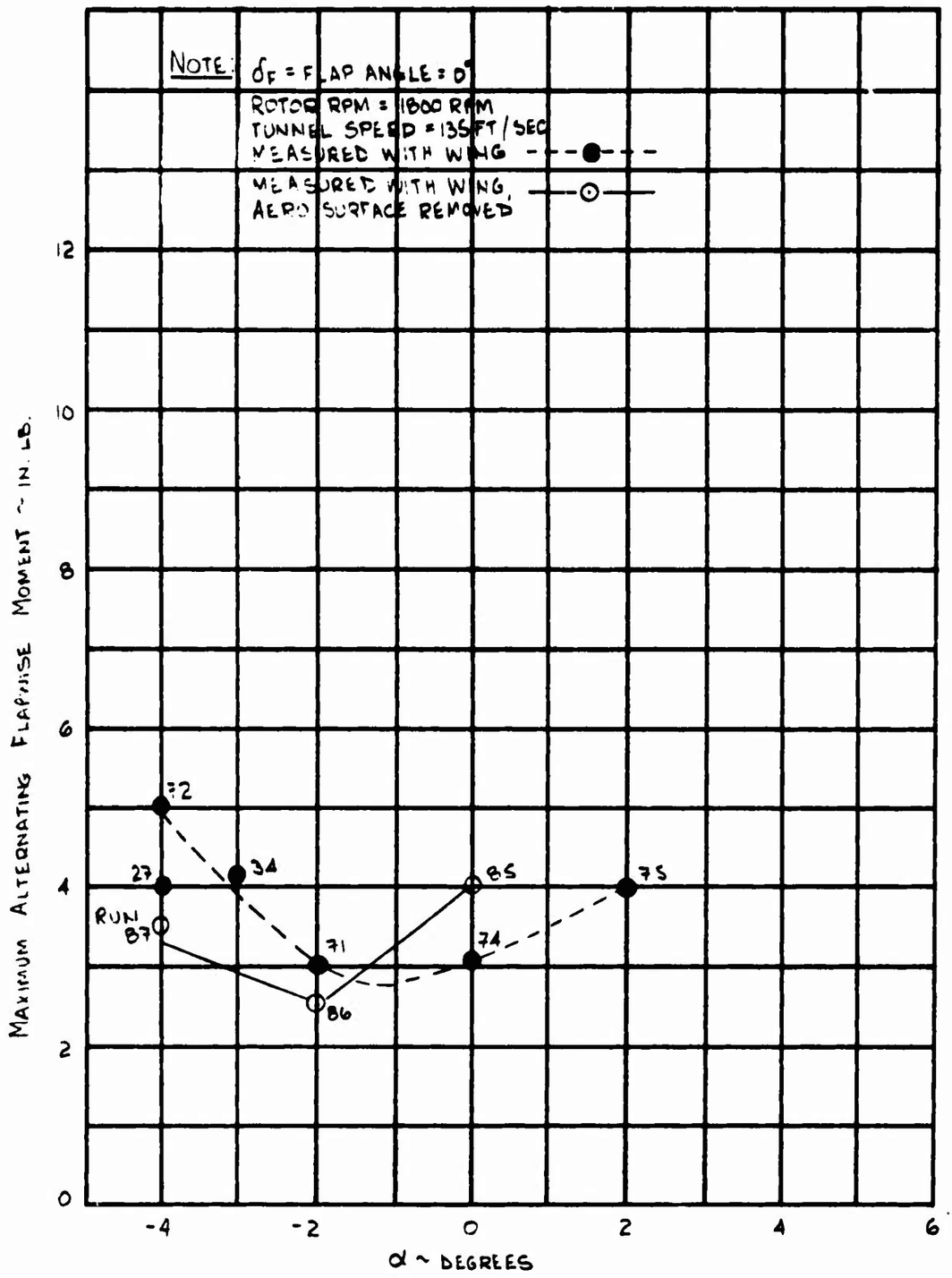

Figure 58. Alternating Flapwise Moment at 0.13R versus Rotor Shaft Angle of Attack.

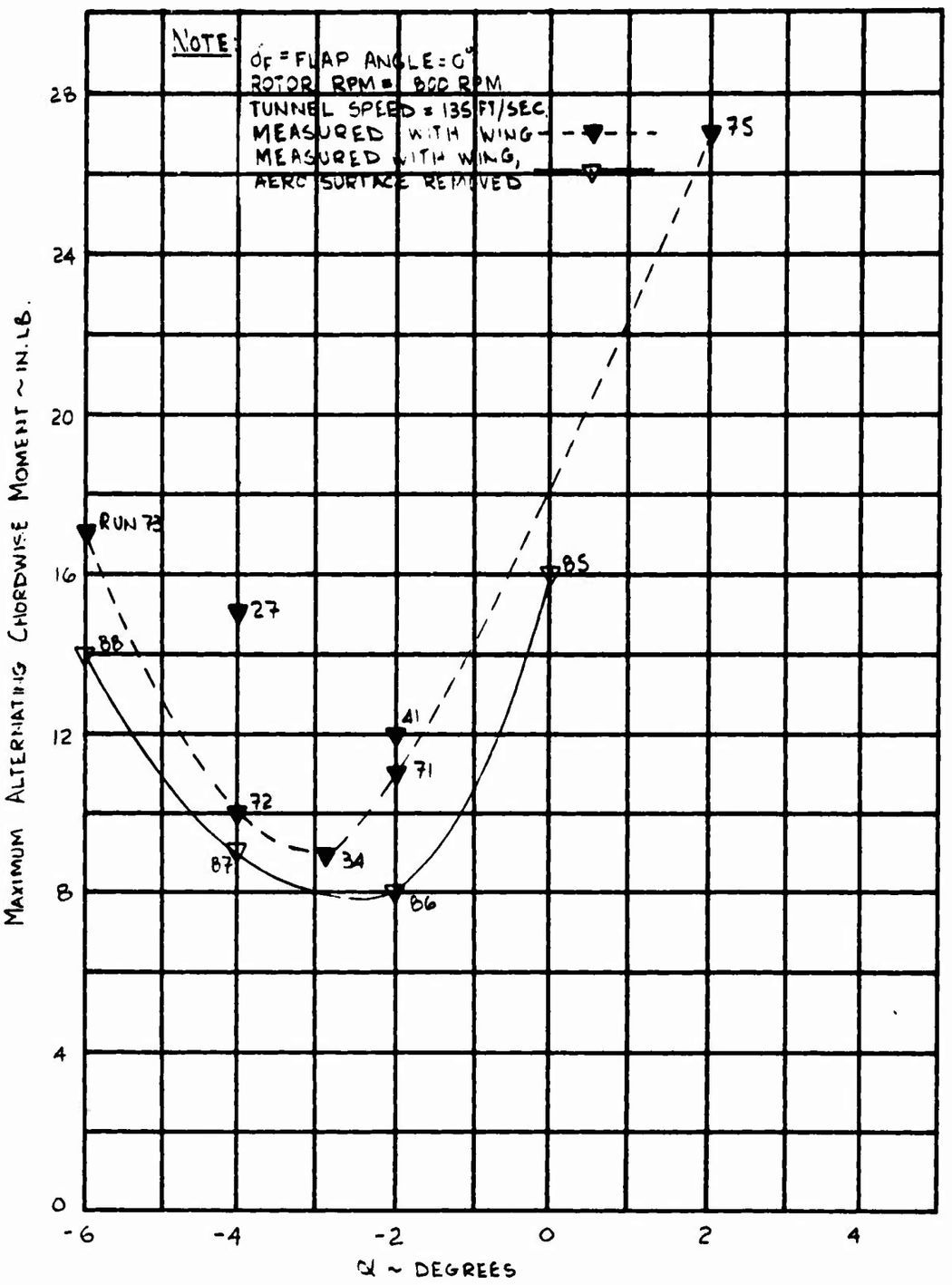

Figure 59. Alternating Chordwise Moment at 0.11R versus Rotor Shaft Angle of Attack.

The blade loads data to determine the effect of wing lift due to flap deflection indicate that alternating blade chord-bending loads and flap-bending loads increase slowly with flap-induced wing circulation. The flap-bending data in Figure 60 show 33% increase over the flap deflection test range. The chord-bending data in Figure 64 increase 33% as the wing flap incidence increases.

A comparison of the effects of rotor angle of attack and flap deflection on blade chord bending shows that one degree of rotor angle of attack produced alternating blade chord bending equivalent to that produced by more than 20 degrees of wing flap deflection. For the test conditions shown in Figures 59 and 61,

$$\left|\frac{\Delta \text{ Chord Bending}}{\Delta\ \alpha}\right| \gtrsim 4.0,$$

$$\left|\frac{\Delta \text{ Chord Bending}}{\Delta\ \delta_F}\right| \gtrsim 0.19.$$

This indicates that the conversion maneuver should be performed with the largest appropriate flap deflection, thereby allowing minimum angle of attack and producing minimum blade loads.

2.2.3 Hub Precone Variations

To determine the effect of the hub precone angle on the alternating blade loads during steady windmilling, the rotor was tested with precone angles of +5, +2.5, and zero degrees at zero angle of attack without the wing surface during the Phase I tests. The effect of precone angle on blade loads throughout the rpm range is shown in Figure 62. Change in hub precone had no effect on blade flap bending. Positive precone slightly reduced blade chord bending at the peak value. Figure 63 is a crossplot of the effect of precone on blade chord bending at three typical rotor speeds. The variations shown are not believed to be of significant magnitude to influence the design of a prop/rotor.

2.3 CONVERSION

When the rotor rpm is varying rapidly during the conversion transient, it would be expected that the dynamic transients would introduce virtual damping into the system. The test data generally show this tendency, particularly at the lower rotor speeds. A major objective of this test program was to find out how the conversion collective schedule should be tailored for minimum alternating blade-bending moments. Figure 64 presents the results of the peak blade loads measured

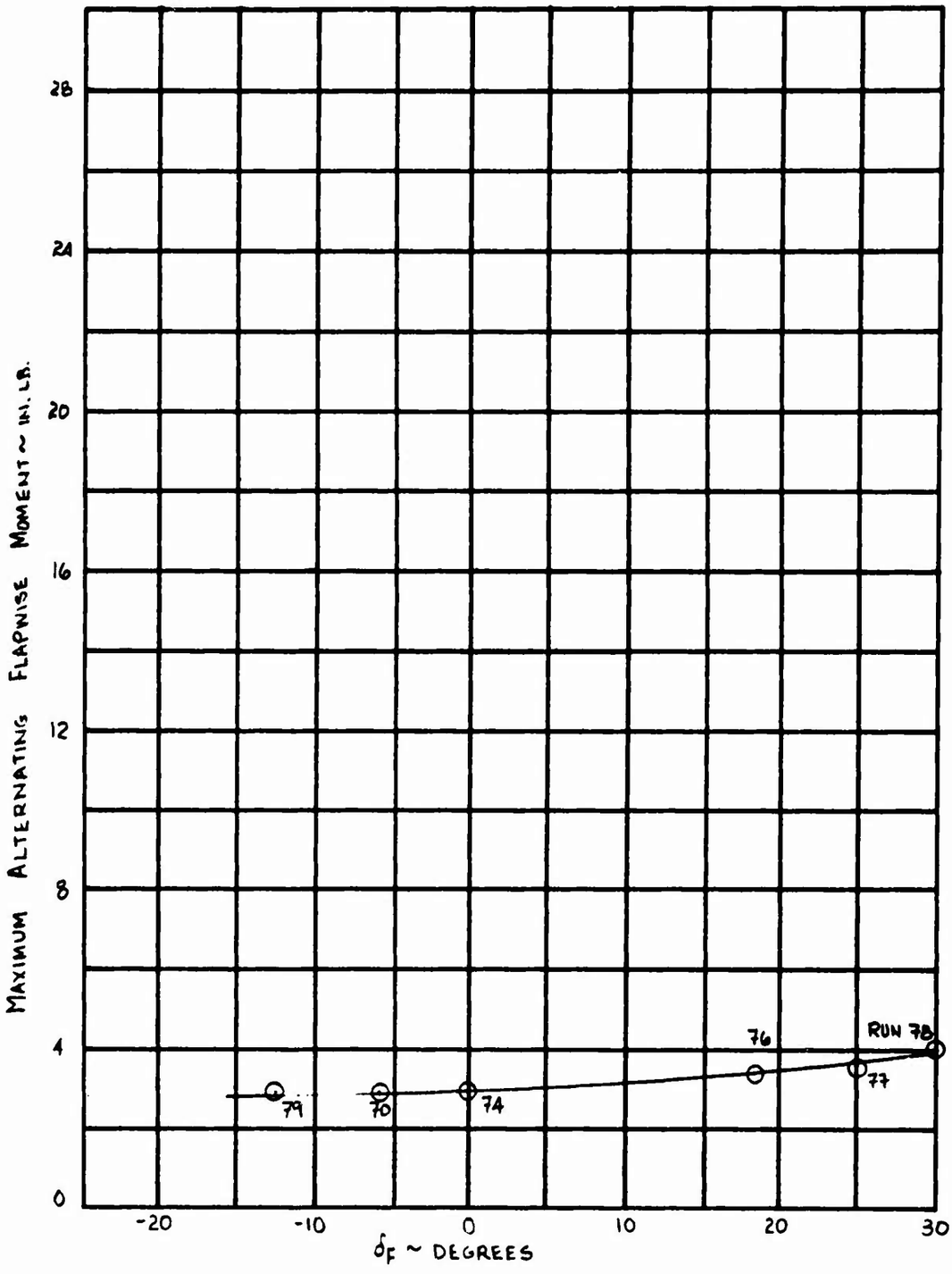

Figure 60. Effect of Flap Deflection on Alternating Flapwise Moment at 0.13R During Steady Windmilling at α = 0.

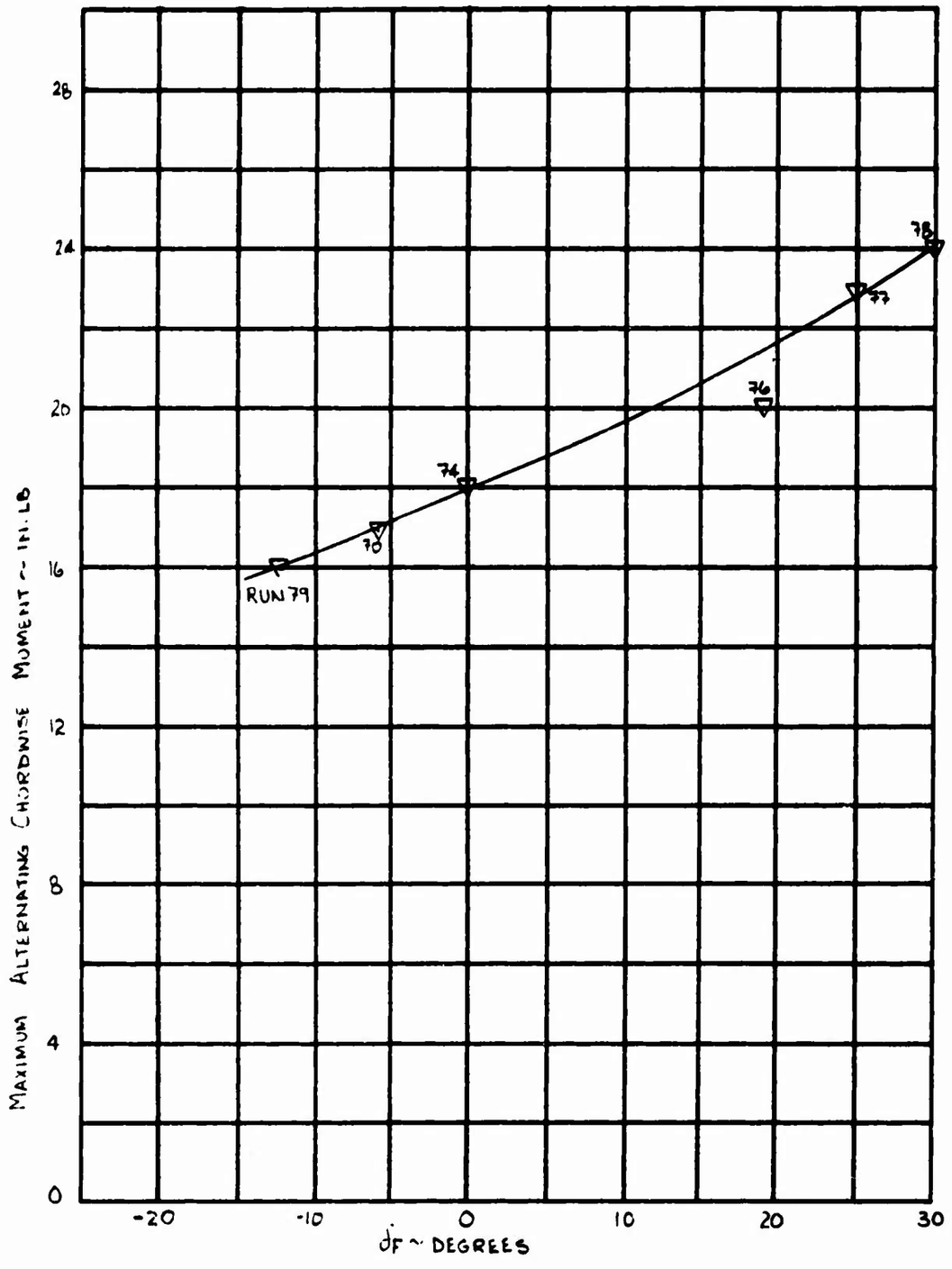

Figure 61. Effect of Flap Deflection on Alternating Chordwise Bending Moment at 0.11R During Steady Windmilling at $\alpha = 0$.

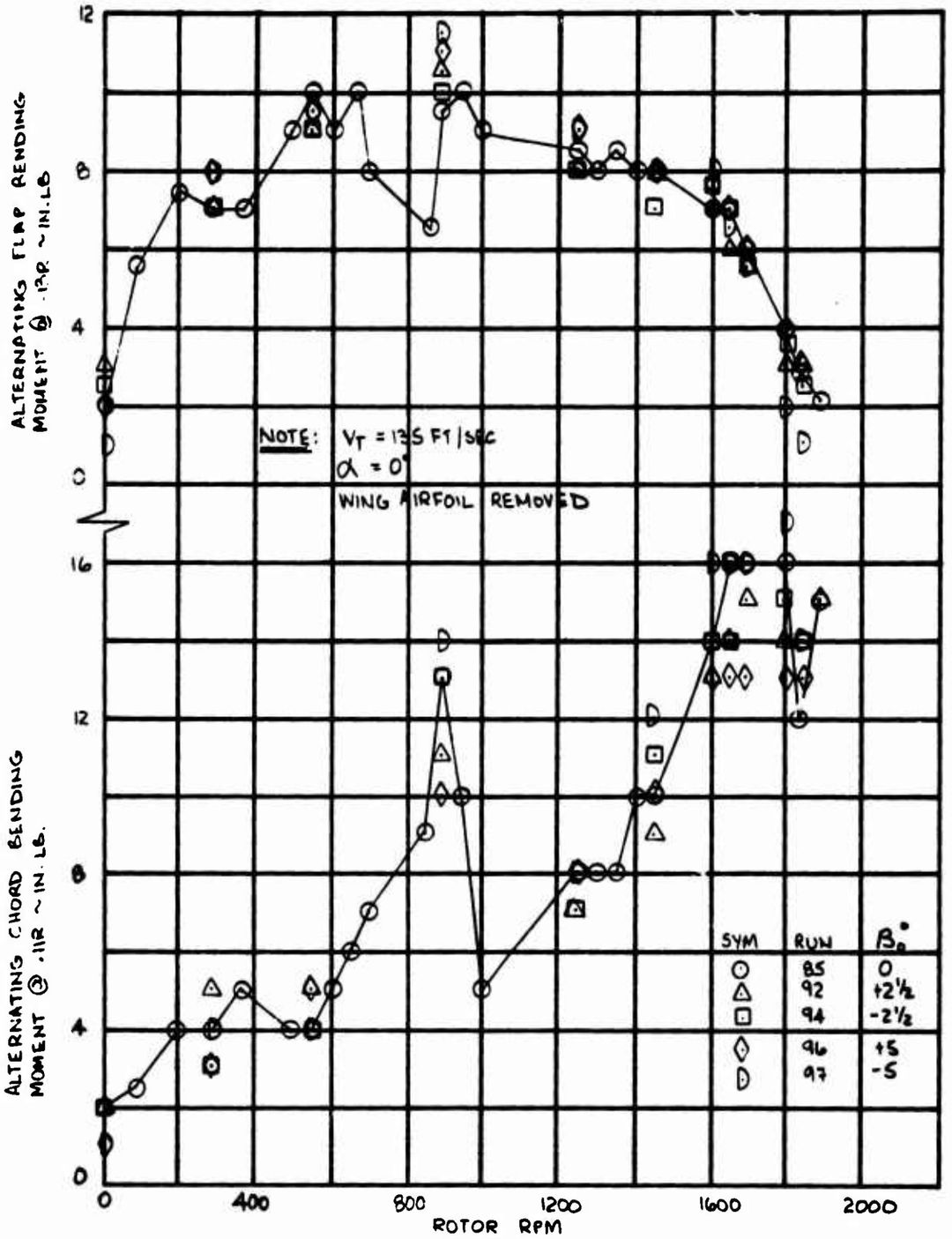

Figure 62. Chordwise and Flapwise Bending Moments versus RPM for Various Pre-cone Angles.

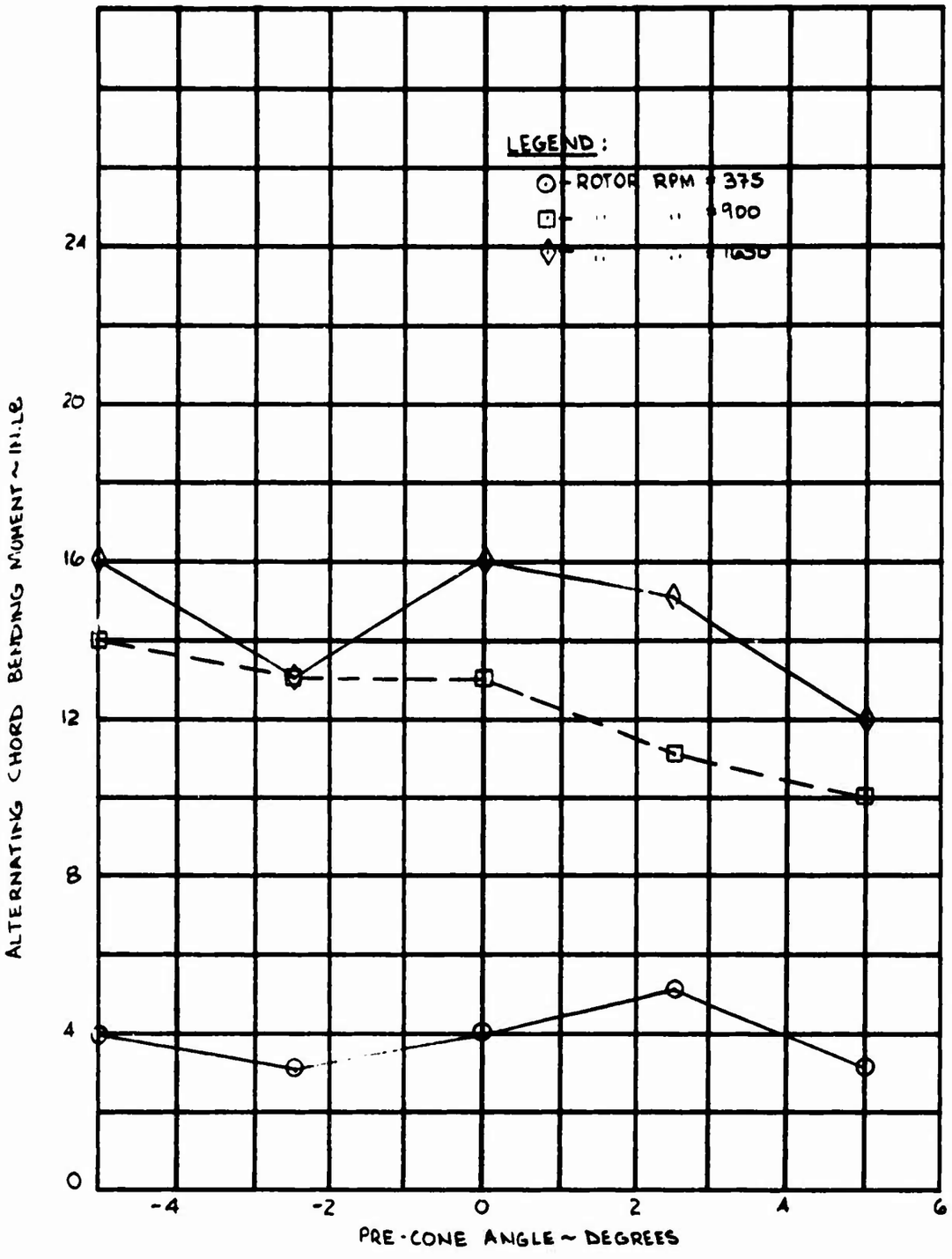

Figure 63. Effect of Pre-cone Angle on Alternating Chord Bending Moment.

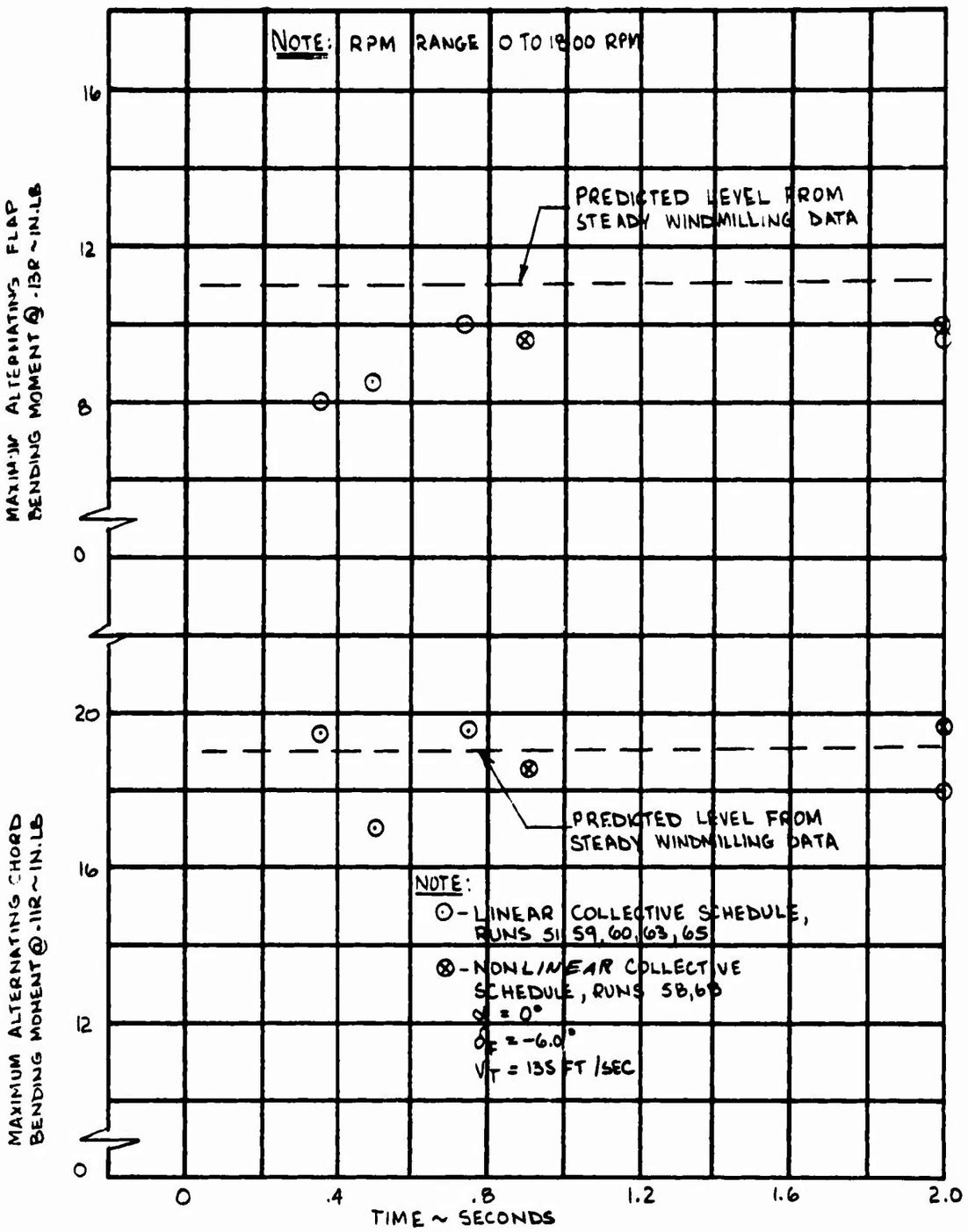

Figure 64. Effect of Conversion Time and Collective Pitch Schedule on Maximum Alternating Blade Loads, $\alpha = 0$, $\delta f = -6$.

during conversion with various conversion times and schedules. These data are for $\alpha = 0$, $\delta_f = -6$, so the model lift is approximately zero. The test data indicate that conversion time and rate of change of collective did not significantly affect peak transient blade loads over the test range. Peak values are approximately the same or less than the peak values measured in steady conditions.

The effect of angle-of-attack variations on peak blade loads in conversion is shown in Figures 65 and 66. The alternating chordwise bending moments are shown to be essentially the same as the moments measured in steady conditions, Figure 59. Flapwise bending moments are somewhat larger in conversion (Figure 65) than those measured in equivalent steady conditions (Figure 58). These alternating flapwise loads also vary with the direction of the conversion; that is, spin-up causes lower flapwise loads than feathering. This difference between spin-up and feathering may be due to the larger angular acceleration at 900 rpm than was produced during spin-up.

The effect of flap deflection on blade loads during conversion is shown in Figures 67 and 68. Flap deflection in conversion causes similar variations in blade loads as given previously for steady windmilling. Again, an increase in wing lift by flap deflection causes a much smaller increase in blade loads than an equivalent angle-of-attack change. The change in blade loads caused by flap deflection as a function of rpm is shown in Figure 4. These data show reduced blade loads at low rpm and somewhat increased loads near the design rpm.

To determine the effect of drive system inertia on blade loads during conversion, the normal rotor hub was replaced by a geometrically similar hub that increased the total rotating inertia by 5 percent. A comparison of the blade loads data for the two hubs is shown in Figures 69 through 72. These data indicate that a 5-percent change in drive system inertia has no significant effect on flap and chord bending during spin-up or feathering.

2.4 STOPPED-BLADE LOADS

The measured steady blade moments for the feathered-rotor conditions are shown in Figure 73. Differences between the prediction and the data are believed to be due to the aerodynamic flowfield of the wing which was not included in the prediction. Subsequent detail study of these steady blade loads data must include accounting for the effects of blade azimuth position.

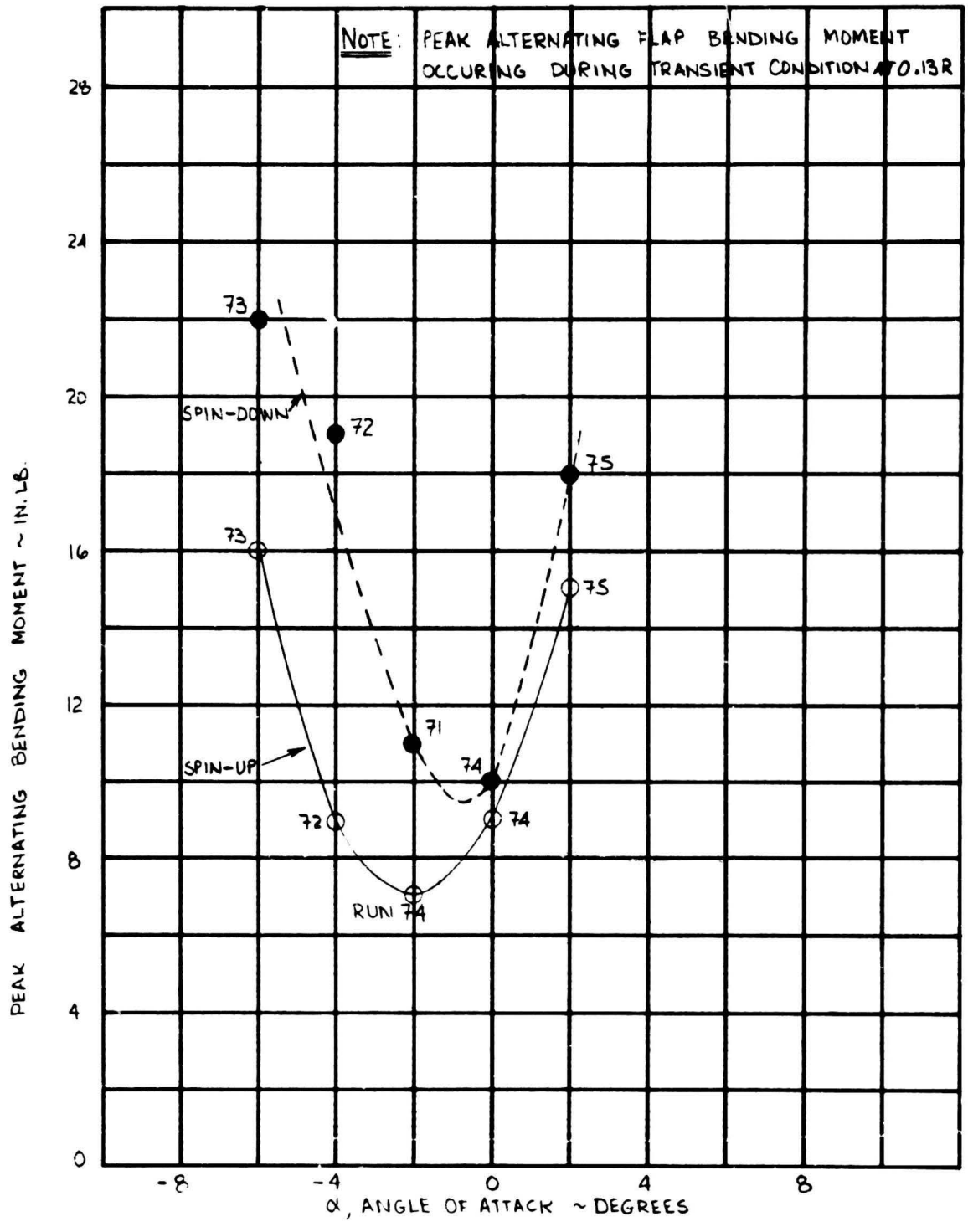

Figure 65. Effect of Angle of Attack on Blade Flap Bending Moment During Conversion.

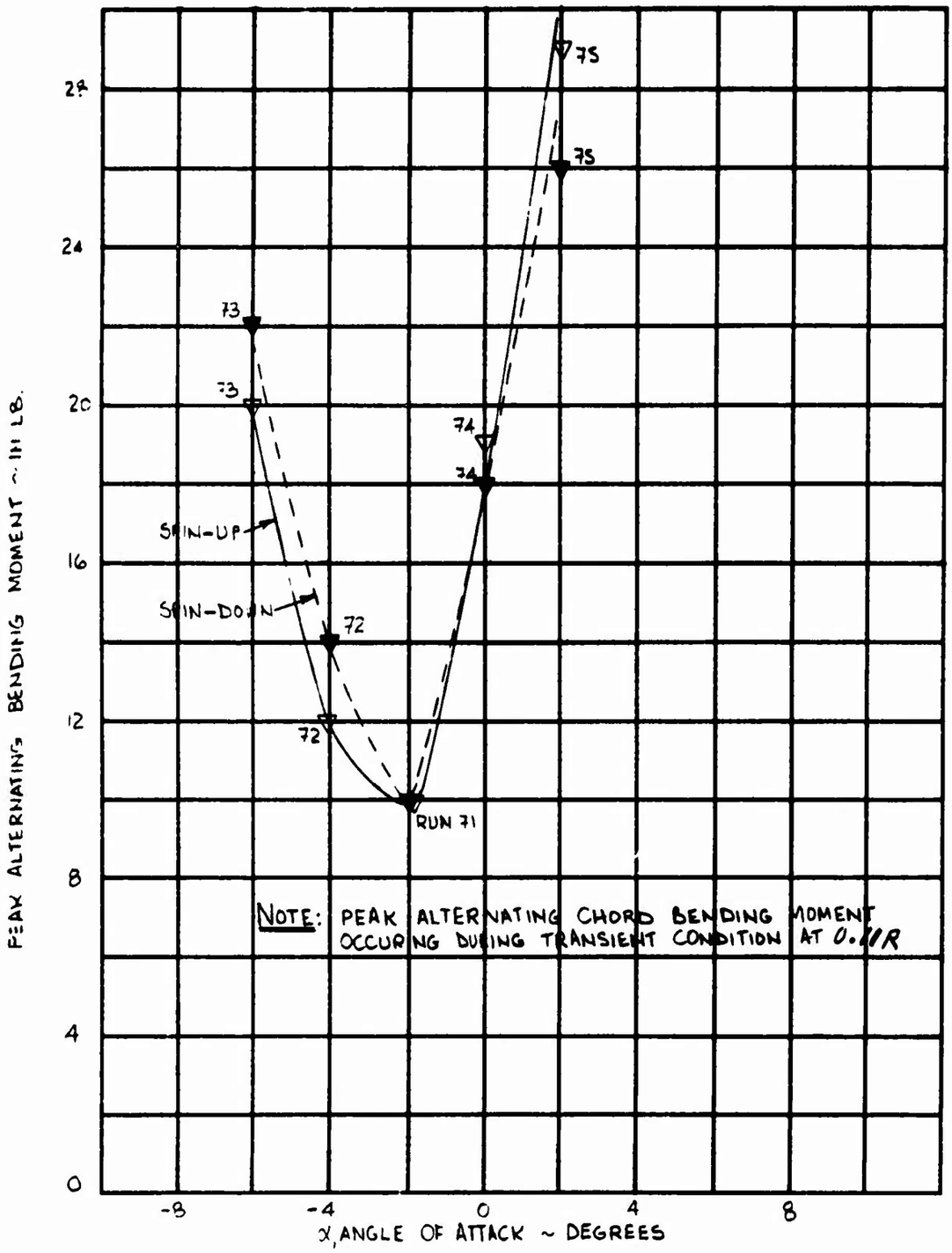

Figure 66. Effect of Angle of Attack on Blade Chord Bending Moment During Conversion.

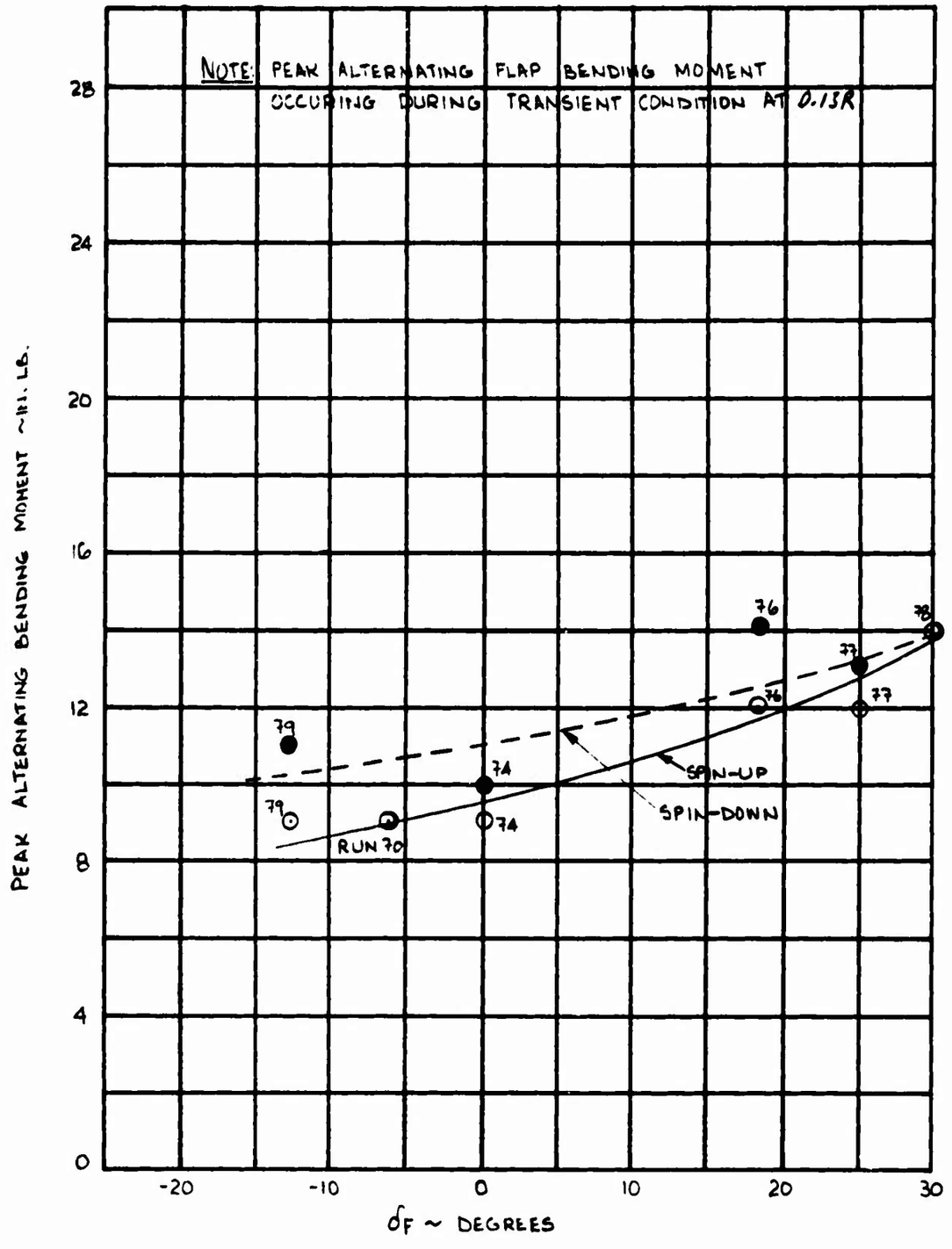

Figure 67. Effect of Flap Deflection on Blade Flap Bending Moment During Conversion, $\alpha = 0$.

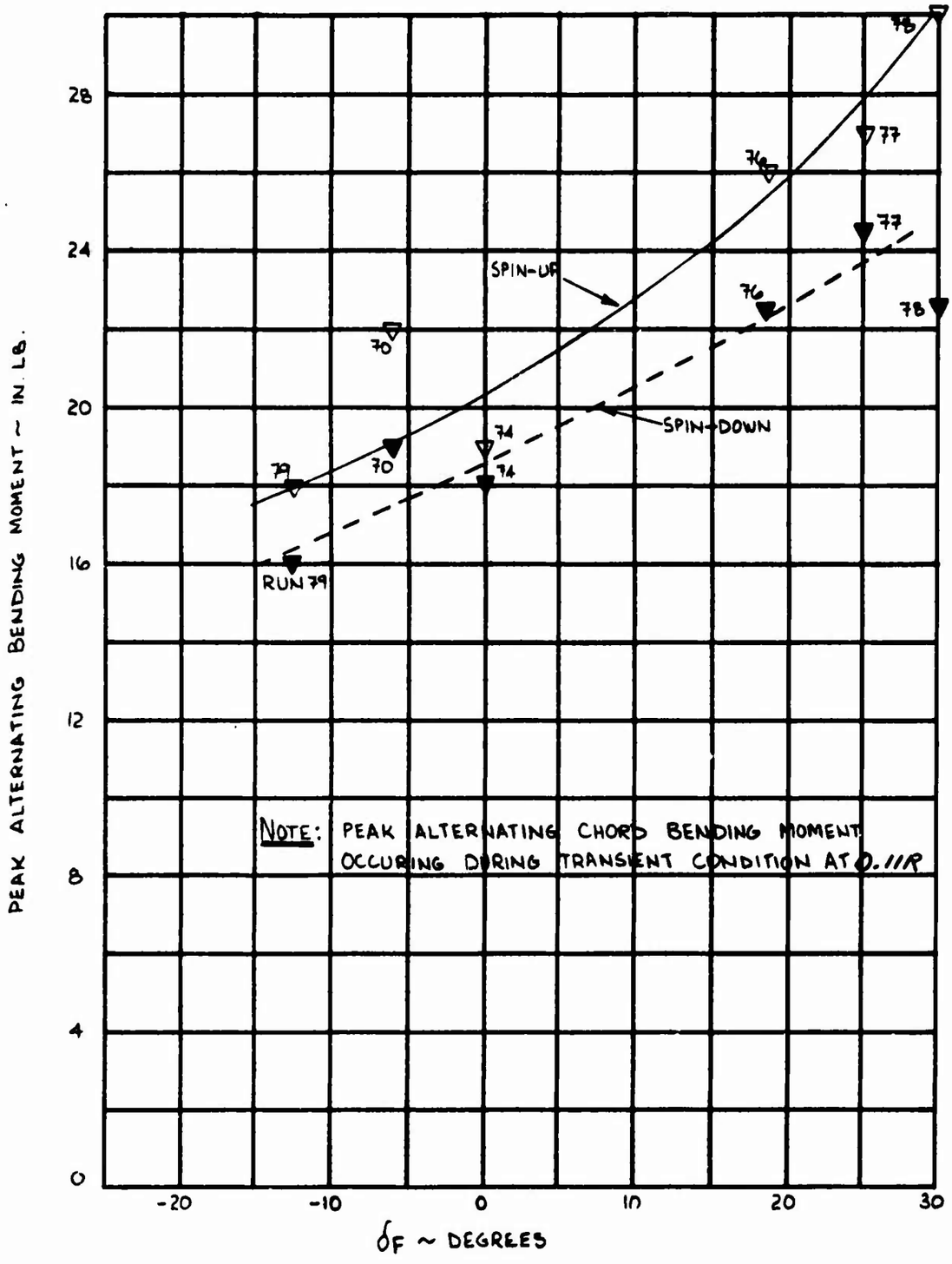

Figure 68. Effect of Flap Deflection on Blade Chord Bending Moment During Conversion, $\alpha = 0$.

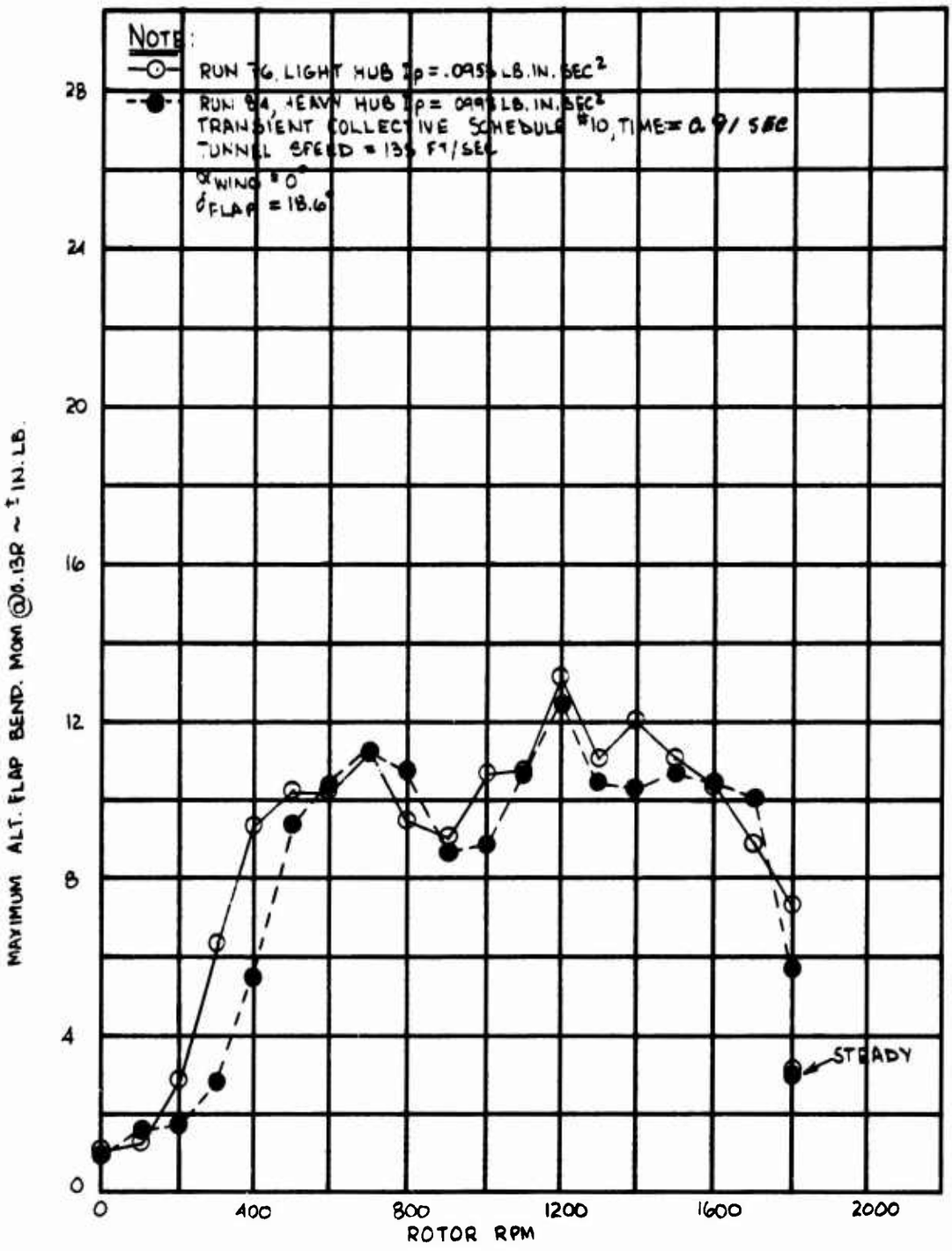

Figure 69. Effect of Hub Inertia on Alternating Blade Flap Bending During Rotor Spin-up.

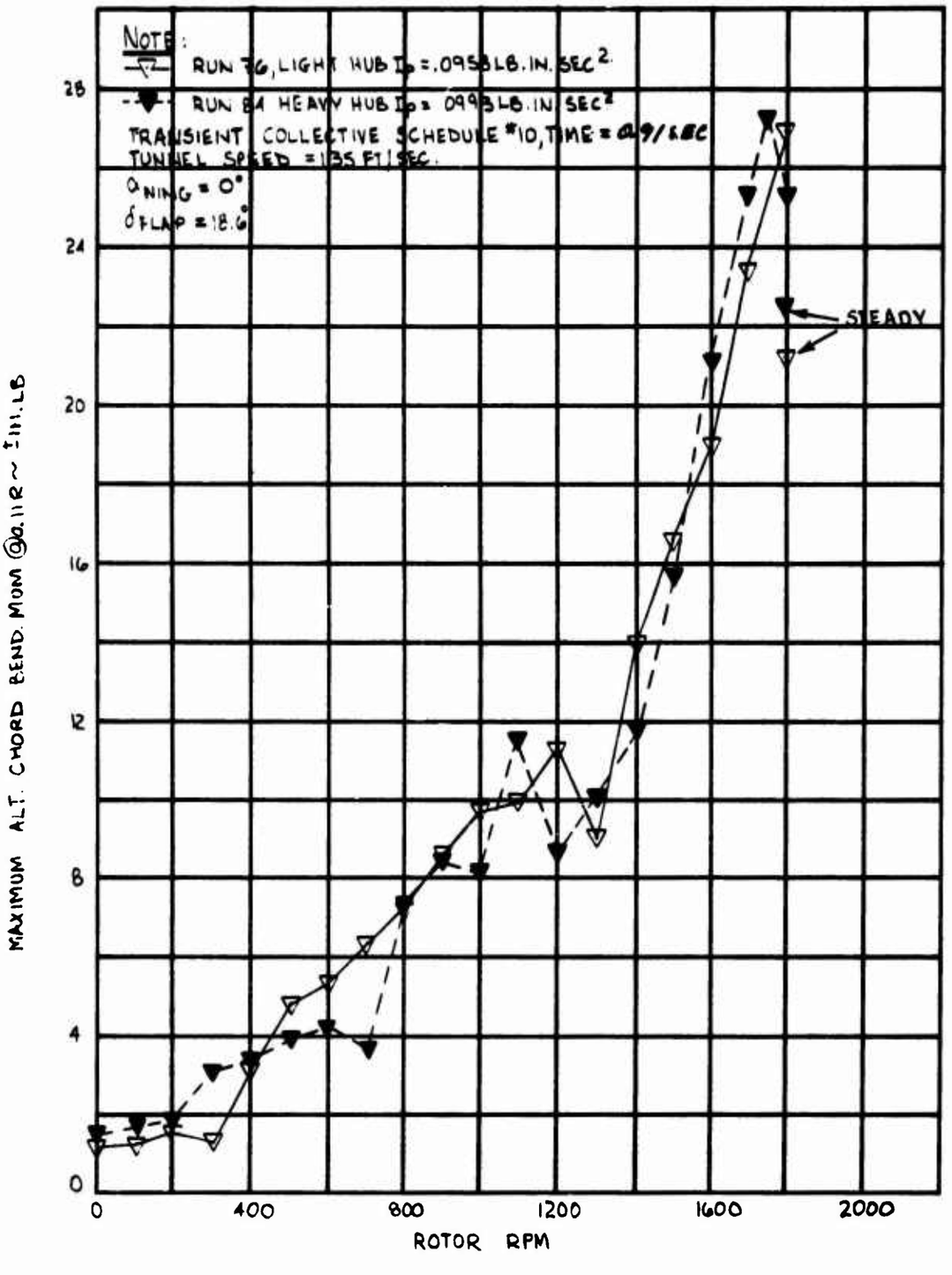

Figure 70. Effect of Hub Inertia on Alternating Blade Chord Bending During Rotor Spin-Up.

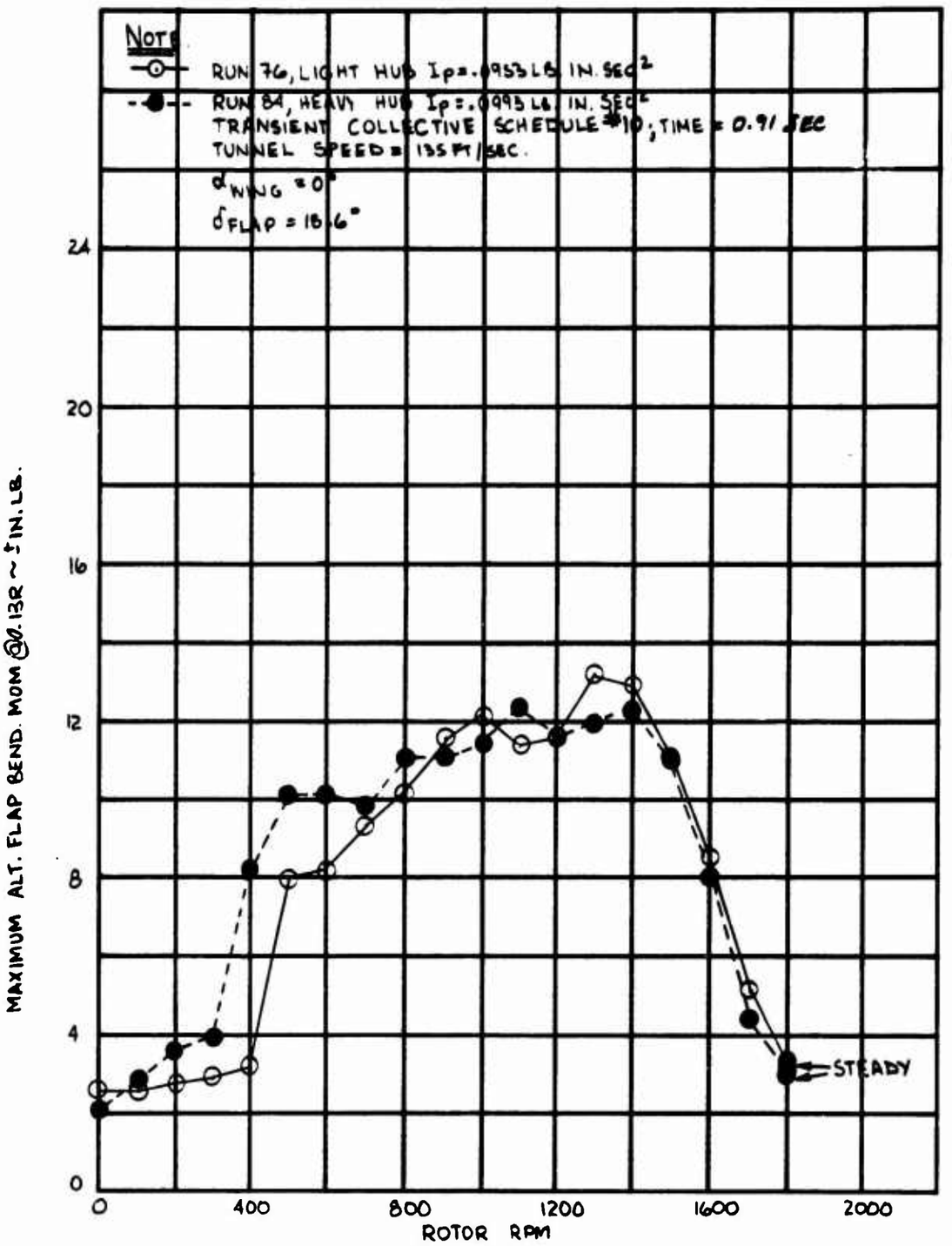

Figure 71. Effect of Hub Inertia on Alternating Blade Flap Bending During Feathering.

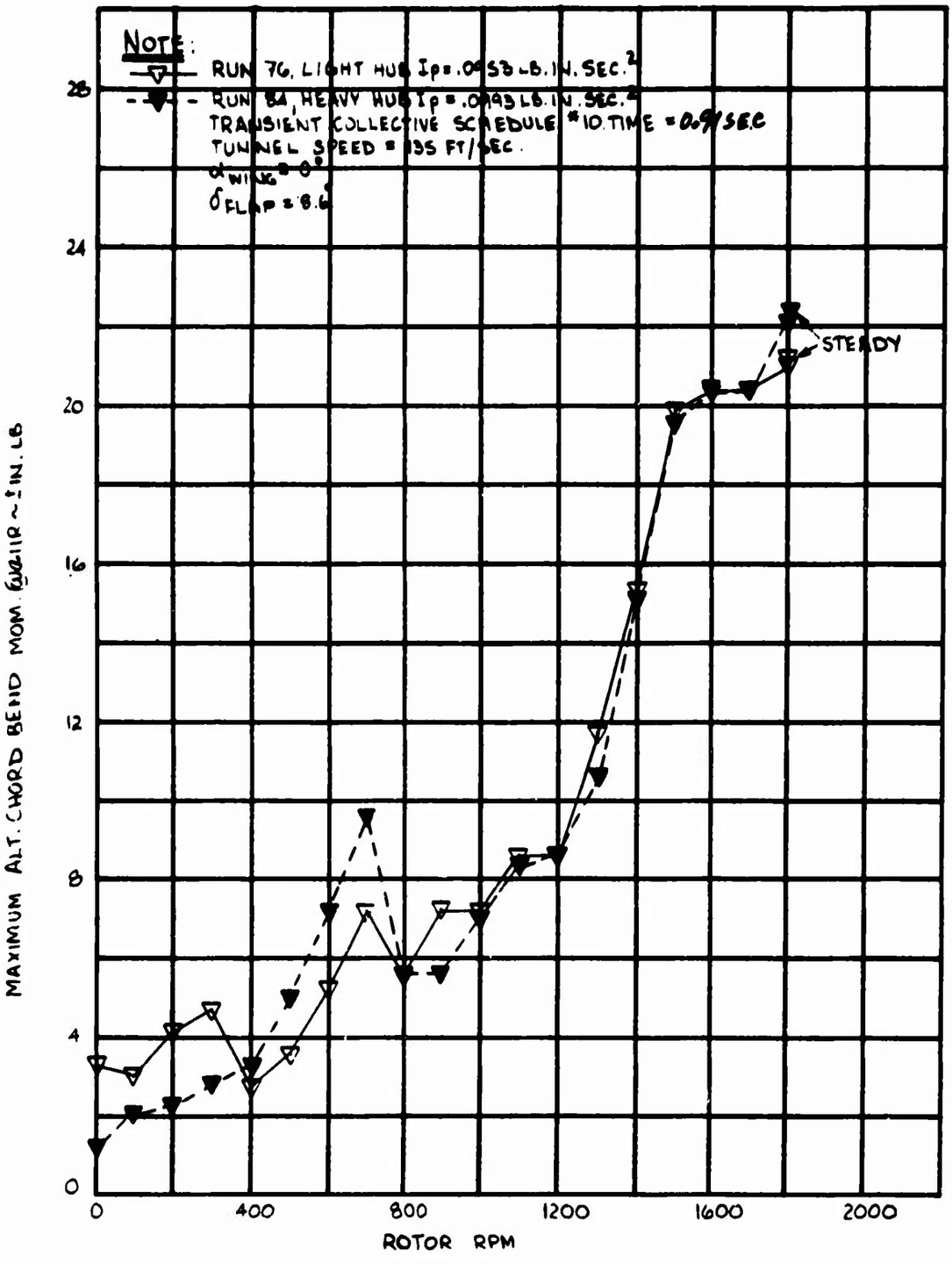

Figure 72. Effect of Hub Inertia on Alternating Blade Chord Bending During Feathering.

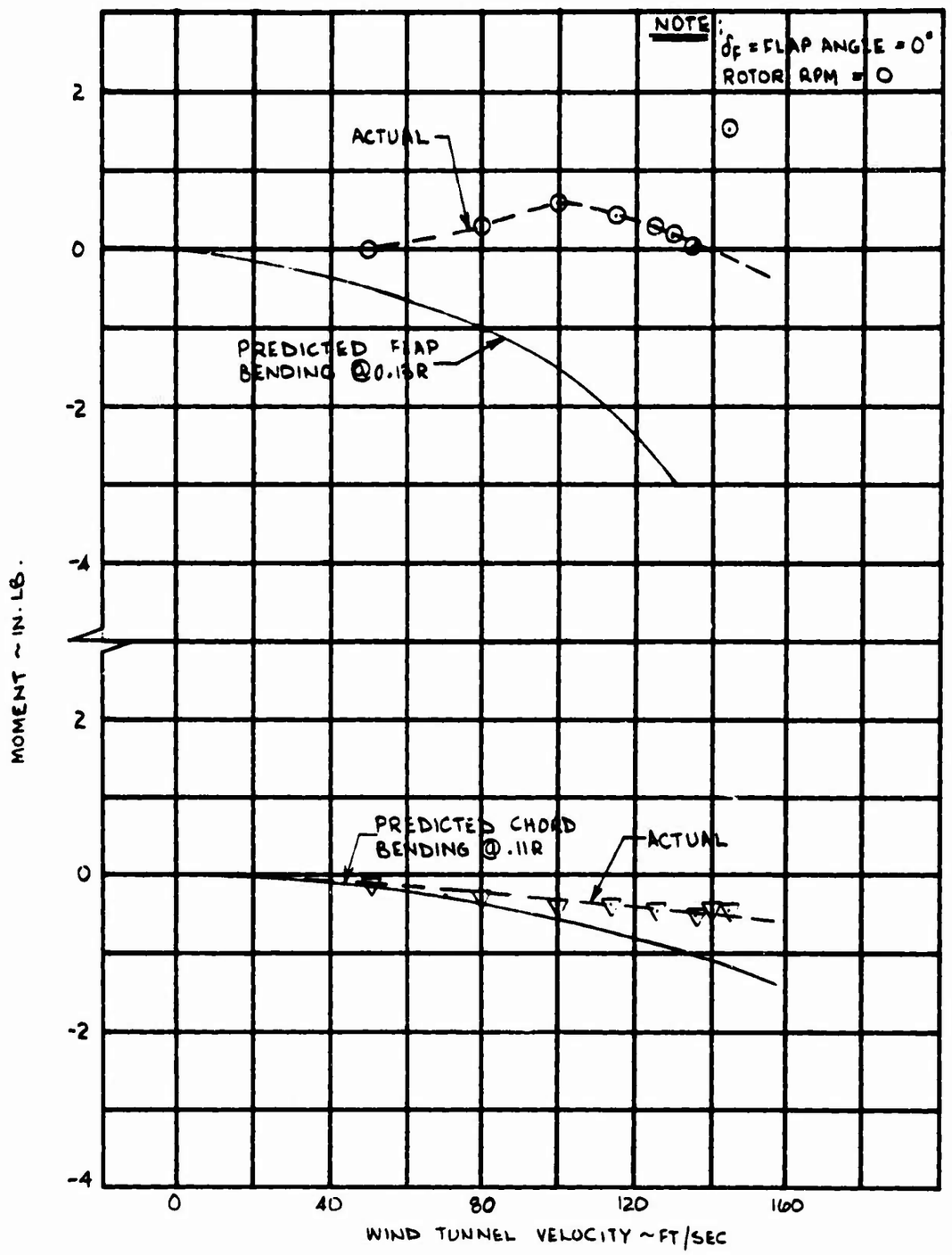

Figure 73. Predicted and Actual Steady Flap and Chord Moments for the Feathered Condition.

3. MODEL DYNAMIC CONSIDERATIONS

An analysis of the air- and ground-resonance characteristics of the model as tested shows the dynamic couplings involved with this model. This analysis was updated following the test to include the results of the wing and blade natural frequency data. Other model parameters used in the analysis are given in Table III. The analysis provides the proper couplings between the dynamic modes as a result of the rotating rotor.

The results of this analysis are presented in Figures 74 and 75. Positive damping (stable) was predicted for all modes, as seen in Figure 75.

The predicted-frequency plot can be used to help understand measured wing loads. As can be seen from Figure 76, wing torsion response is prominent at 850 rpm. Figure 74 shows that this rotor speed is very close to the predicted speed for coincidence between the wing torsion mode, flap frequency plus rotational speed, and the 3/rev rotor speed. Thus, it appears that near 850 rpm the 3/rev rotor frequency is forcing the wing torsional mode at its natural frequency. As shown in Table IV, the response of the wing at 850 rpm is predominantly 3/rev.

Another significant wing response is the vertical bending response near 1,400 rpm as shown in Figure 76. Table IV shows that the wing lift at this rotor speed is predominantly 1/rev. An examination of Figure 74 shows the predicted coincidence between the wing vertical-bending mode and 1/rev at 1,400 rpm, thus exciting the wing vertical bending response. The 3/rev, 2/rev, and 1/rev crossings of wing chord frequency are clearly identifiable in Figure 76, as are the 5/rev wing torsion and the 3/rev wing vertical bending, though none of these show loads approaching those of the multiple interaction previously discussed. The identification of these crossings lends credence to the dynamic analysis.

Figure 77 shows a drop in chordwise blade loads for rpm greater than 1,680 for tests up to Run 25. For Runs 25 and subsequent the peak chordwise load has shifted to a higher rpm (1,800). This is caused by the increase in flap stiffness when the blades were reworked after Run 22 to increase their load capacity. Since the blade is highly twisted and at high incidence, the flapwise stiffness at low blade incidence contributed to chordwise stiffness at high blade incidence.

TABLE III

MODEL CHARACTERISTICS USED IN DYNAMIC ANALYSIS

Slope of lift curve	5.73 per degree
Reference chord	1.8125 in.
Blade radious	16.875 in.
Blade mass moment of inertia	0.01873 lb-sec^2-in.
Air density	0.002378 slugs/ft^3
Tunnel airspeed	135 ft/sec
Rotor speed (varies)	1,600 to 2,200 rpm
Distance from nacelle pivot to hub center	6.15 in.
Distance from nacelle pivot to effective wing root	22.2 in.
Distance from nacelle pivot to system cg	0.85 in.
Rotor-nacelle pitch inertia about pivot	1.35 lb-sec^2-in.
Total weight (rotor-nacelle)	11.0 pounds
Wing-torsion frequency	43 cps
Wing-chordwise frequency	30 cps
Wing vertical frequency	23 cps
Blade frequency (varies with rpm)	24.167 to 28.333 cps
Number of blades	3

TABLE III - Continued

Root cutout	0.15
Root collective (varies with rpm)	63.34 to 55.02 degrees
Angle of attack at 3/4 span	0 degrees
Blade twist at 3/4 span	-25.96 degrees
Percent pitch damping	2
Percent yaw damping	2
Percent roll damping	2
Percent blade damping	1

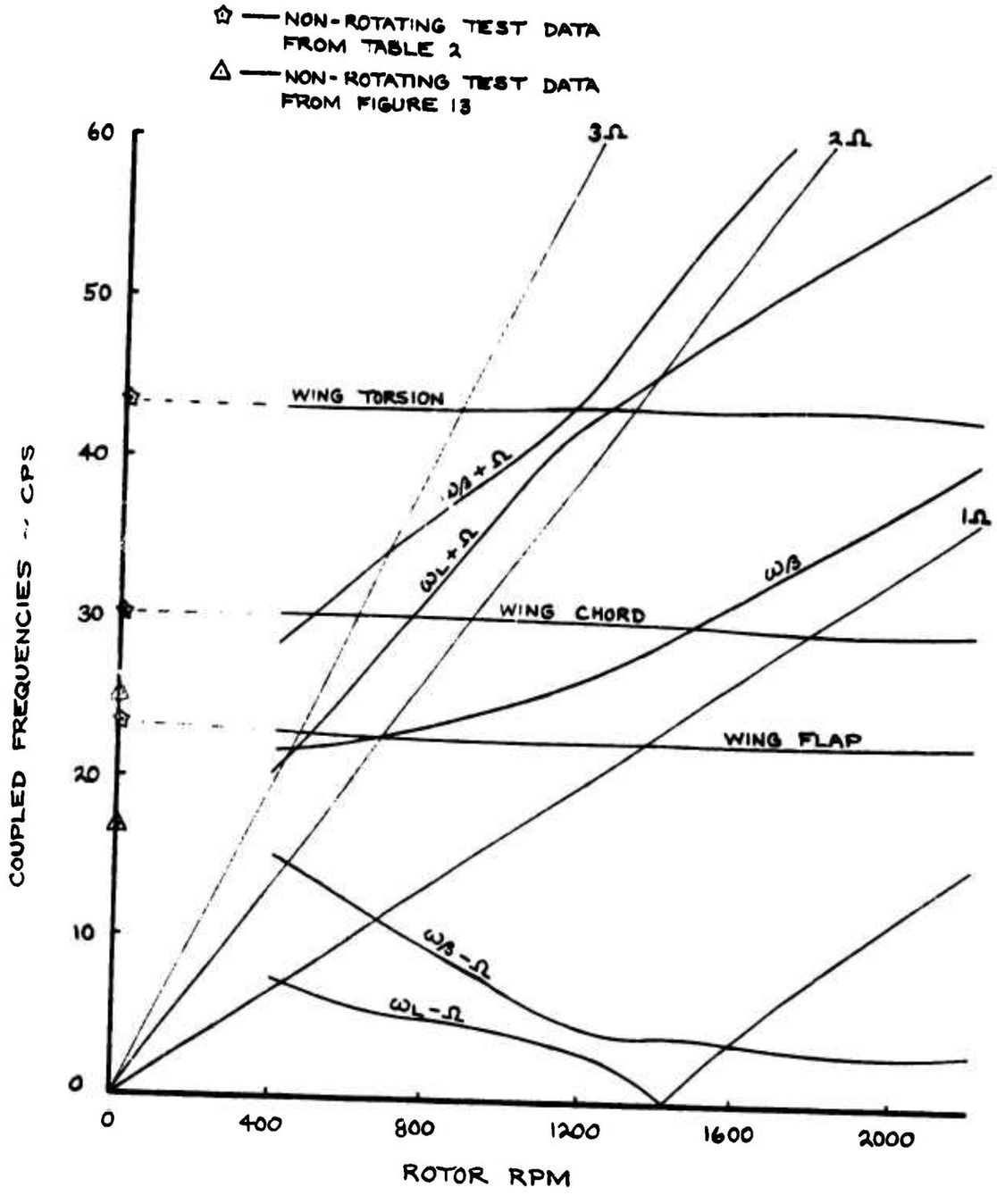

Figure 74. Calculated Frequencies of the Coupled Dynamic Modes of the Wing and Rotor System of the Model as Tested.

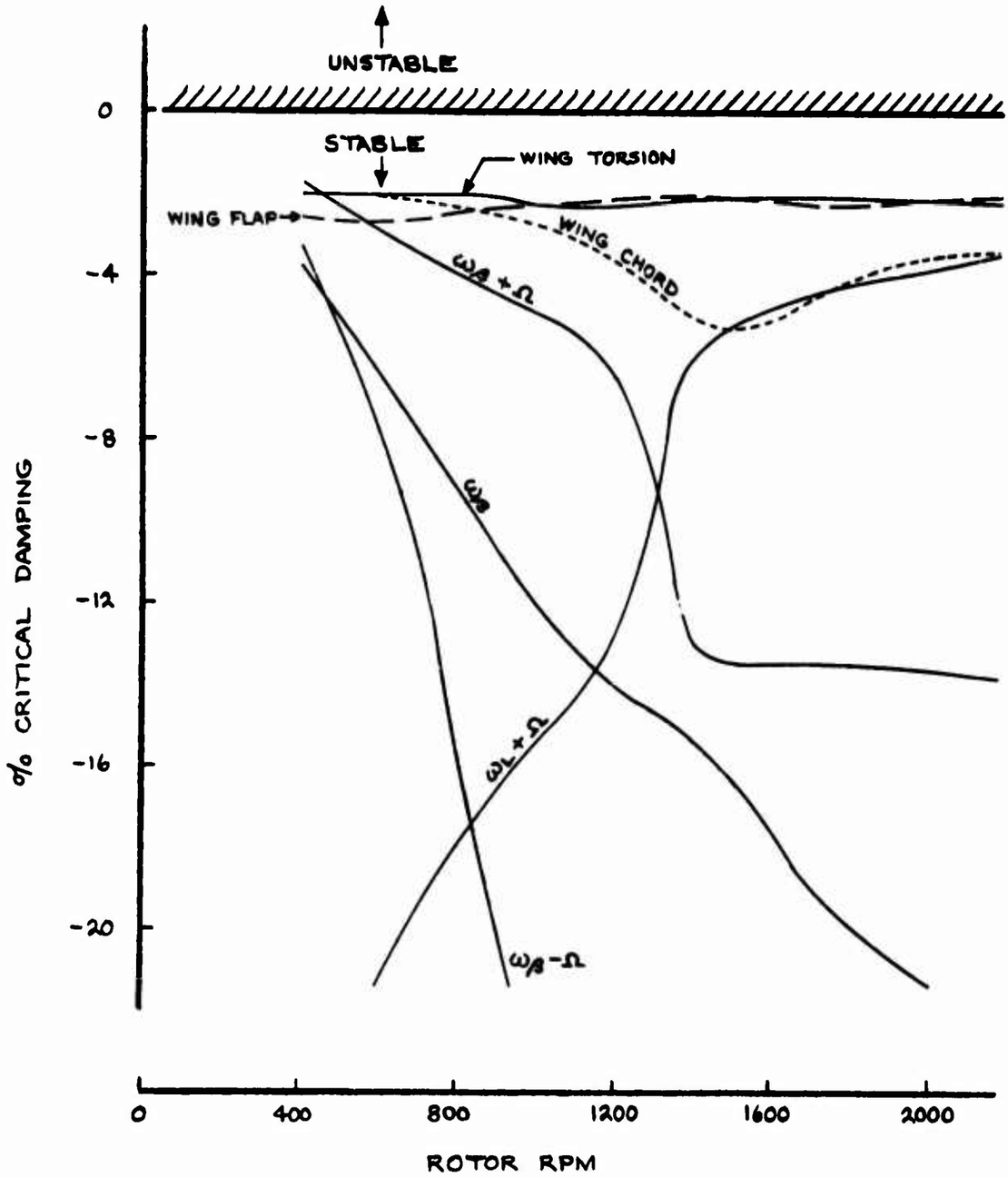

Figure 75. Calculated Damping of Coupled Dynamic Modes of Model as Tested.

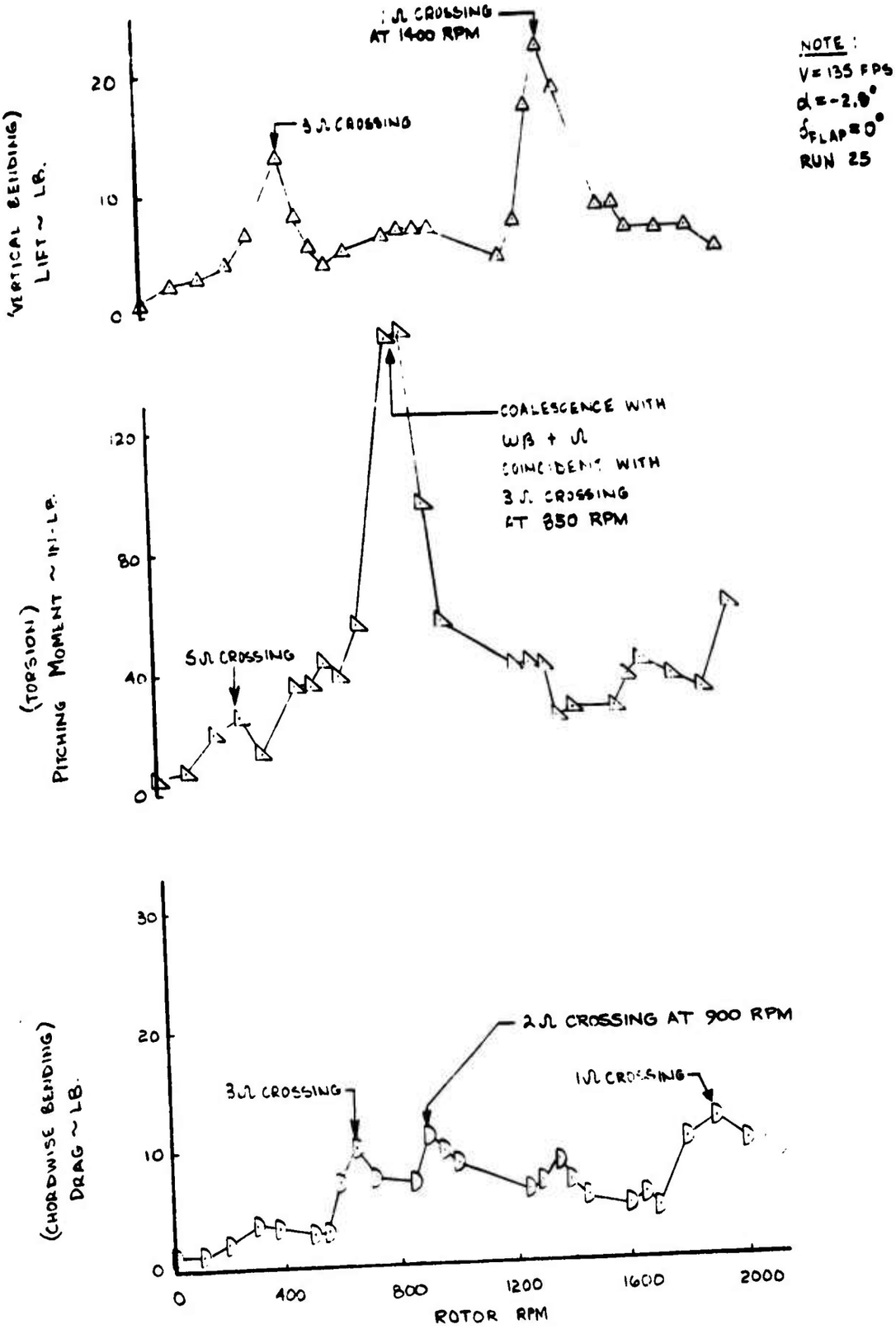

Figure 76. Alternating Wing Loads Data Show Good Correlation with Dynamic Predictions.

TABLE IV

DOMINANT FREQUENCIES OF WING AND BLADE ALTERNATING LOADS DURING STEADY WINDMILLING

RPM	WING LIFT CYCLES/ REV	WING DRAG CYCLES/ REV	WING PITCHING MOMENT CYCLES/REV	RED BLADE CHORD BENDING AT 0.11R CYCLES/REV	RED BLADE FLAP BENDING AT 0.13R CYCLES/REV	GREEN BLADE CHORD BENDING AT 0.2R CYCLES/REV
200	3	3	3	5	1	5
300	5	5	5	5	1	5
370	3	5	4	3	1	3
500	3	3	3	3	1	1
550	3	3	3	1	1	1
600	3	3	3	1	1	1
650	3	3	3	1	1	1
720	3	3	3	2	2	2
850	1	3	3	2	2	2
900	1	3	3	2	2	2
950	1	3	3	2	2	2
1,000	1	3	3	1	1	1
1,250	1	1	1	1	1	1
1,300	1	1	1	1	1	1
1,350	1	1	1	1	1	1
1,400	1	1	1	1	1	1
1,450	1	1	1	1	1	1
1,600	1	1	1	1	1	1
1,650	1	1	1	1	1	1
1,700	1	1	1	1	1	1
1,800	1	1	1	1	1	1
1,890	1	1	1	1	1	1
2,000	1	1	1	1	1	1

NOTES: Run 25
Tunnel Speed = 135 fps
$\alpha = 2.8°$
$\delta_{FLAP} = 0°$

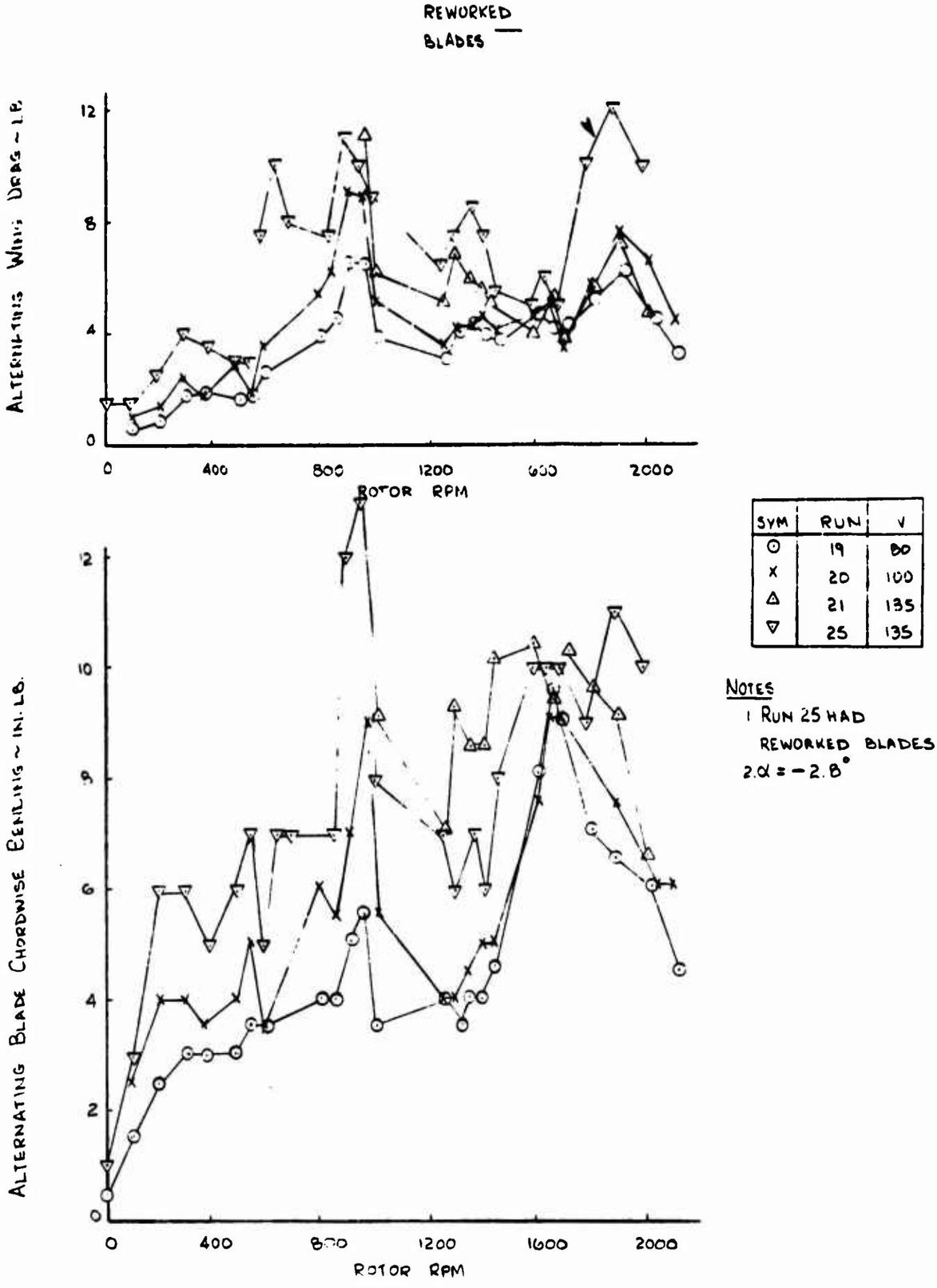

Figure 77. Airspeed Variations Show Inter-Dependence of Wing Drag and Chordwise Blade Bending.

SECTION VI

CONCLUSIONS

1. A properly tailored collective schedule makes it possible to execute the spin-up/feathering conversion operation in approximately 1/3 seconds model scale (10 seconds full scale) with less than 0.05 g aircraft acceleration.

2. 0.1 g aircraft acceleration produced linear schedules of approximately the same time.

3. The collective schedule which minimizes transient drag and rate of change of drag for a rapid conversion is a nonlinear schedule

4. Maximum transient drag is predicted conservatively by simple blade element analysis.

5. Transient drag is increased as spin times are reduced.

6. Wing lift and angle of attack increase the transient drag increment.

7. Lift and pitching-moment data are rpm-dependent but are little affected by spin time.

8. The rotor derivatives measured agree with the predictions within the data scatter.

9. Alternating blade loads did not vary enough at a given rpm between the transient operation of conversion and steady windmilling operation to indicate that blade loads should be any constraint in the development of a collective pitch schedule for conversion.

10. Alternating flapwise and chordwise blade loads are not sensitive to interactions of wing-rotor dynamics.

11. Blade loads peak at integer blade frequency crossings.

12. In nearly axial flow, high chordwise alternating moments will be experienced if the blade chordwise frequency is greater than about 0.8 times the rotor speed.

13. Lower blade alternating loads at the same C_L are obtained by using flaps instead of increasing angle of attack of the aircraft basic wing.

14. Rotor hub pre-cone variations from +5 to -5 degrees did not cause a significant change in alternating flapwise or chordwise blade loads.

15. Bench test data show a relatively large coupling of blade torsional deflections as a result of chordwise bending. This coupling was approximately equivalent to one degree of cyclic pitch for the conditions tested and was such as to reduce the stability of the in-plane blade bending. For the rotor tested, the significance of this coupling appears to have been small since hub pre-cone variation effects were small.

16. A drive system inertia change did not cause a significant change in alternating flapwise and chordwise blade load during a conversion transient.

17. Steady blade loads for a feathered rotor were found to be of smaller magnitude than predicted.

SECTION VII

RECOMMENDATIONS

Based on the results of this test, it is recommended that:

1. Effort be continued to show detailed substantiation of prediction techniques and use of this analysis for detailed refinement of the best schedule tested.

2. Studies be conducted of control system design to minimize complexity. These should include trades of peak acceleration and deceleration transients against control complexity.

3. Further testing be performed to better define the variation of rotor derivatives in conversion and to identify the contribution of wing-rotor interference.

4. Further test data be generated by this program and analyzed to include items such as refinement of rotor blade aeroelastic properties including prediction of mounting deflections.

5. Rotating-blade frequencies be measured prior to all test programs. Baffle testing is one way this can be done successfully.

APPENDIX I

TEST LOG

1/16 SCALE MODEL 213 PROP/ROTOR SEMISPAN CONVERSION MODEL W/T TEST

NOT REPRODUCIBLE

RUN NO.	CONFIGURATION *	TYPE OF RUN	α DEG.	δ_{FLAP} DEG	V FT/SEC	$\theta_{.75}$ DEG.	RPM	PRE-CONE DEG.	HUB INERTIA **	DATE/TIME
1	W, N, B	STOPPED BLADE LOADS	0	0	VARY	88	0	0	1	4/15/70
2	"	"	0	0	VARY	86	0	0	1	4/16
3	"	VARIABLE AZIMUTH BLADE LOADS	0	0	135	VARY	0	0	1	4/16
4	"	STEADY RPM BLADE LOADS	0	0	135	VARY	VARY	0	1	4/16
5	"	"	0	0	100	"	"	0	1	4/16
6	"	"	0	0	80	"	"	0	1	4/16
7	"	"	0	0	80	"	"	0	1	4/16
8	"	"	0	-12.7	100	"	"	0	1	4/17
9	"	"	-2.8	0	100	"	"	0	1	4/17
10	"	"	0	0	80	"	"	0	1	4/17

TEST LOG

NOTES: * W ~ WING
N ~ NACELLE
B ~ BLADES

** 1 IS THE STANDARD ALUMINUM RING

RUNS 1 THRU 10 : LIGHTS IN TUNNEL
RUN 1 : STILL PICTURES
RUN 4 : MOTION PICTURES

1/16 SCALE MODEL 213
PROP/ROTOR SEMISPAN
CONVERSION MODEL W/T TEST

RUN NO.	CONFIGURATION	TYPE OF RUN	α DEG.	δ_{FLAP} DEG.	V FT/SEC	$\theta_{.75}$ DEG.	RPM	PRE-CONE DEG.	HUB INERTIA	DATE/TIME
11	W,N,B	STEADY RPM BLADE LOADS	0	0	100	VARY	VARY	0	1	4/17/70
12	"	"	0	0	50	"	"	0	1	4/17
* 13	"	"	0	0	—	"	"	0	1	4/17
14	"	"	0	0	80	"	"	0	1	4/17
15	"	"	0	0	70	"	"	0	1	4/17
16	"	"	0	0	60	"	"	0	1	4/17
17	"	"	-2.85	0	135	"	"	0	1	4/17
18	"	"	"	0	80	"	"	0	1	4/17
19	"	"	"	0	"	"	"	0	1	4/17
20	"	"	"	0	100	"	"	0	1	4/17

TEST LOG

NOTES: * RUN 13 ABORTED, NO DATA
RUNS 11 THRU 20: LIGHTS IN TUNNEL

1/16 SCALE MODEL 213
PROP/ROTOR SEMISPAN
CONVERSION MODEL W/T TEST

RUN NO.	CONFIGURATION	TYPE OF RUN	α DEG.	δ_{FLAP} DEG.	V FT/SEC	$\theta_{.75}$ DEG.	RPM	PRE-CONE DEG.	HUB INERTIA	DATE/TIME
21	W, N, B	STEADY RPM BLADE LOADS	-2.85	0	135	VARY	VARY	0	1	4/17/70
22	"	"	0	0	"	"	"	0	1	4/17
*23	"	"	0	0	"	"	"	0	1	4/20
24	"	"	0	0	100	"	"	0	1	4/20
25	"	"	-2.8	0	135	"	"	0	1	4/20
26	"	"	-2.0	0	"	"	"	0	1	4/20
27	"	"	-4.05	0	"	"	"	0	1	4/20
28	"	"	-6.05	0	"	"	"	0	1	4/20
29	"	"	-8.1	0	"	"	"	0	1	4/20
**30	"	"	0	0	80	"	"	0	1	4/21

TEST LOG

NOTES: * STARTING WITH RUN 23 BLADES HAVE BEEN REWORKED TO GIVE NEW ALLOWABLES :

$C_{.11}$ = 17.6 IN-Lbs
$F_{.13}$ = 25.1 IN-Lbs

RCAL EQUIV. CHANGED TO:

$C_{.11}$ RCAL EQ = OLD RCAL X 2.0
$C_{.2}$ " = " X 2.5
$F_{.13}$ " = " X 2.0

** TORSION @ .2R ON GREEN BLADE REMOVED AND REPLACED BY FLAP BENDING @ .5R

RUNS 21 THRU 29 : LIGHTS IN TUNNEL
RUN 28 : STILL PICTURES

1/16 SCALE MODEL 213
PROP/ROTOR SEMISPAN
CONVERSION MODEL W/T TEST

TEST LOG

RUN NO.	CONFIGURATION	TYPE OF RUN	α DEG.	δ_{FLAP} DEG.	V FT/SEC	$\theta_{.75}$ DEG.	RPM	PRE-CONE DEG.	HUB INERTIA	DATE/TIME
31	W, N, B	STEAD RPM BLADE LOADS	0	0	100	VARY	VARY	0	1	4/21/70
32	"	"	-2.9	0	"	"	"	0	1	4/21
33	"	"	-2.9	0	125	"	"	0	1	4/21
*34	"	BLADE LOADS /800 RPM WITH α	VARY	0	135	35.0	1800	0	1	4/21
**35	"	WING LIFT (0 RPM)	0	VARY	"	86.6	0	0	1	4/21
36	"	STEADY RPM BLADE LOADS	0	18.6	"	VARY	VARY	0	1	4/21
37	"	"	0	25.0	"	"	"	0	1	4/21
38	"	"	0	30.0	"	"	"	0	1	4/21
39	"	"	0	-0.5	"	"	"	0	1	4/21
40	"	"	0	-2.0	"	"	"	0	1	4/21

NOTES: * RUN 34 α'S = -2.9, -4.15, -5.2, -4.05, -2.8, -0.6, -2.8

** RUN 35: δ FLAPS = -30, -20 (UNTAPED FLAP)
δ FLAPS = -20, -15, -12.7, -7, -4, 0, 5, 10 (TAPED FLAP)

RUN 37: LIGHTS IN TUNNEL
STILL PICTURES

1/16 SCALE MODEL 213 PROP/ROTOR SEMISPAN CONVERSION MODEL W/T TEST

TEST LOG

RUN NO.	CONFIGURATION	TYPE OF RUN	α DEG.	δ_{FLAP} DEG.	V FT/SEC	$\theta_{.75}$ DEG.	RPM	PRE-CONE DEG.	HUB INERTIA	DATE/TIME
41	W, N, B	STEADY RPM BLADE LOADS	-2.1	-2.0	135	VARY	VARY	0	1	4/21/70
42	"	"	0	-4.0	"	"	"	0	1	4/22
43	"	"	-1.1	-2.0	"	"	"	0	1	4/22
44	"	"	0	-6.0	"	"	"	0	1	4/22
* 45	"	COLLECTIVE VARIATION WITH TIME	0	"	"	$\frac{\delta\theta}{\delta \text{TIME}}$	$\frac{\delta \text{RPM}}{\delta \text{TIME}}$	0	1	4/22
46	"	TRANSIENT SCHEDULE # 1 (SEE FIG. 79)	0	"	"	VARY	VARY	0	1	4/22
47	"	"	0	"	"	"	"	0	1	4/22
48	"	"	0	"	"	"	"	0	1	4/22
49	"	"	0	"	"	"	"	0	1	4/22
** 50	"	TRANSIENT SCHEDULE # 5	0	"	"	"	"	0	1	4/22

NOTES: * RUN 45 : COLLECTIVE WAS VARIED MANUALLY FROM FEATHER TO 1800 RPM ; TIME ~ 7 SEC.

** RUN 50 : TUNNEL DOOR IN FLOOR WAS OPEN

RUNS 48 THRU 50 : FILTER ON WING DRAG (≈ 45 CPS FREQUENCY RESPONSE)

RUN 47 : LIGHTS IN TUNNEL, MOTION PICTURES

1/16 SCALE MODEL 213
PROP/ROTOR SEMISPAN
CONVERSION MODEL W/T TEST

RUN NO.	CONFIGURATION	TYPE OF RUN TRANSIENT SCHEDULES:	α DEG.	δ_{FLAP} DEG.	V FT/SEC	$\theta_{.75}$ DEG.	RPM	PRE-CONE DEG.	HUB INERTIA	DATE/TIME
51	W, N, B	# 5 (SEE FIG. 79)	0	-6.0	135	VARY	VARY	0	1	4/22/70
52	"	"	0	"	"	"	"	0	1	4/22
53	"	# 4	0	"	"	"	"	0	1	4/22
54	"	"	0	"	"	"	"	0	1	4/23
55	"	"	0	"	"	"	"	0	1	4/23
56	"	# 3	0	"	"	"		0	1	4/23
57	"	"	0	"	"	"	"	0	1	4/23
58	"	"	0	"	"	"	"	0	1	4/23
59	"	# 6	0	"	"	"	"	0	1	4/23
60	"	# 7	0	"	"	"	"	0	1	4/24

TEST LOG

NOTES: RUNS 51 THRU 59 : FILTER ON WING DRAG (≈ 45 CPS FREQUENCY RESPONSE)
RUN 60 : NEW GALVO ON WING DRAG (30 CPS FREQUENCY RESPONSE)
RUN 56 THRU 59 : GAIN CHANGED ON WING DRAG
RUN 52, 53, 57, 59, 60 : LIGHTS IN TUNNEL, MOTION PICTURES

1/16 SCALE MODEL 213
PROP/ROTOR SEMISPAN
CONVERSION MODEL W/T TEST

TEST LOG

RUN NO.	CONFIGURATION	TYPE OF RUN TRANSIENT SCHEDULES	α DEG.	δ_{FLAP} DEG	V FT/SEC	$\theta_{.75}$ DEG.	RPM	PRE-CONE DEG.	HUB INERTIA	DATE/TIME
61	W, N, B	# 7 (SEE FIG. 79)	0	-6.0	135	VARY	VARY	0	1	4/24/70
62	"	"	0	"	"	"	"	0	1	4/24
63	"	# 8	0	"	"	"	"	0	1	4/24
64	"	# 9	0	"	"	"	"	0	1	4/24
65	"	"	0	"	"	"	"	0	1	4/24
66	"	# 10	0	"	"	"	"	0	1	4/24
67	"	"	0	"	"	"	"	0	1	4/24
68	"	"	0	"	"	"	"	0	1	4/24
69	"	"	0	"	"	"	"	0	1	4/27
70	"	"	0	"	"	"	"	0	1	4/27

NOTES: RUN 69 : NEW GALVO ON WING DRAG (30 CPS FREQUENCY RESPONCE)
RUNS 61 THRU 70 : LIGHTS IN TUNNEL
RUN 63, 64, 66 : MOTION PICTURES

1/16 SCALE MODEL 213
PROP/ROTOR GEMINI-PAN
CONVERSION MODEL W/ [illegible]

RUN NO.	CONFIGURATION	TYPE OF RUN	α DEG.	δ_{FLAP} DEG	V FT/SEC	$\theta_{.75}$ DEG.	RPM	PRE-CONE DEG.	HUB INERTIA	DATE/TIME
71	W, N, B	TRANSIENT SCHEDULE # 10 (SEE FIG. 79)	-1.95	0	135	VARY	VARY	0	1	4/27/70
72	"	"	-4.0	0	"	"	"	0	1	4/27
73	"	"	-6.0	0	"	"	"	0	1	4/27
74	"	"	0	0	"	"	"	0	1	4/27
75	"	"	+1.9	0	"	"	"	0	1	4/27
76	"	"	0	18.6	"	"	"	0	1	4/27
77	"	"	0	25.0	"	"	"	0	1	4/27
78	"	"	0	30.0	"	"	"	0	1	4/27
79	"	"	0	-12.7	"	"	"	0	1	4/27
80	"	"	+1.95	18.6	"	"	"	0	1	4/27

TEST LOG

NOTES: RUNS 71 THRU 80 : LIGHTS IN TUNNEL
RUN 80 : STILL PICTURES

1/16 SCALE MODEL 213
PROP/ROTOR SEMI-SPAN
CONVERSION MODEL W/ TEST

RUN NO.	CONFIGURATION	TYPE OF RUN	α DEG.	δ_{FLAP} DEG.	V FT/SEC	$\theta_{.75}$ DEG.	RPM	PRE-CONE DEG.	HUB INERTIA	DATE/TIME
81	W, N, B	TRANSIENT SCHEDULE # 11 (SEE FIG. 79)	0	30.0	135	VARY	VARY	0	1	4/27/70
82	"	"	0	"	100	"	"	0	1	4/27
83	"	"	0	"	"	"	"	0	1	4/27
* 84	"	TRANSIENT SCHEDULE # 10	0	18.6	135	"	"	0	2	4/27
85	N, B	STEADY RPM	0	—	"	"	"	0	1	4/28/70
86	"	"	-2.05	—	"	"	"	0	1	4/28
87	"	"	-4.0	—	"	"	"	0	1	4/28
88	"	"	-6.0	—	"	"	"	0	1	4/28
89	"	"	+2.1	—	"	"	"	0	1	4/28
90	"	"	4.0	—	"	"	"	0	1	4/28

TEST LOG

NOTES: * RUN 84 : INCREASED DRIVE SYSTEM INERTIA (BRASS RING)
RUNS 81 THRU 90 : LIGHTS IN TUNNEL
RUN 85 : MOTION AND STILL PICTURES

NOT REPRODUCIBLE

1/16 SCALE MODEL 213
PROP/ROTOR SEMISPAN
CONVERSION MODEL W/ WING TEST

RUN NO.	CONFIGURATION	TYPE OF RUN	α DEG.	δ_{FLAP} DEG.	V FT/SEC	$\theta_{.75}$ DEG.	RPM	PRE-CONE DEG.	HUB INERTIA	DATE/TIME
91	N_2B	STEADY RPM	6.0	—	135	VARY	VARY	0	1	4/28/70
92	"	"	0	—	"	"	"	2.5	1	4/29/70
*93	"	"	0	—	"	"	"	-2.5	1	4/29
94	"	"	0	—	"	"	"	"	1	4/29
**95	"	"	0	—	"	"	"	"	1	4/29
96	"	"	0	—	"	"	"	5.0	1	4/29
97	"	"	0	—	"	"	"	-5.0	1	4/29
		END OF PHASE 1 TESTS								

TEST LOG

NOTES: * RUN 93: BLADES OUT OF TRACK

** RUN 95: WING SPAR STIFFENED IN DRAG BY WIRES (ATTEMPT TO CHANGE WING DRAG FREQUENCY)

RUNS 91 THRU 97 : LIGHTS IN TUNNEL

RUNS 92 THRU 97 : MOTION PICTURES

NOT REPRODUCIBLE

THE BOEING COMPANY

PREPARED BY:
CHECKED BY:
DATE:

NUMBER
REV LTR
MODEL NO.

TEST LOG 1/6 SCALE CONVERSION MODEL

RUN NO.	CONFIGURATION	TYPE RUN	V	COLL	RPM	α	β F	DATE
98	W.N.L	CORRELATION	0	VAR	0 To 1800	-1.9	0	1/26/71
99	WNE	1/REV SWEEP	135	VAR	0 To 1800	-1.9	0	1/26/71
100	WNE	1/REV SWEEP	60	VAR	0 To 1800	-1.9	0	1/26/71
101	WNE	1/REV SWEEP	60	VAR	0 To 1800	-1.9	0	1/26/71
102	WNE	4/REV SWEEP	60	VAR	0 To 1800	-1.9	0	1/26/71
103	WNE	4/REV SWEEP	135	VAR	0 To 1800	-1.9	0	1/26/71
104	WNE	WING BRACED	135	VAR	0 To 1800	-1.9	0	1/27/71
105	WNE	WING BRACED	60	VARY	0 To 2000	-1.9	0	1/27/71

BLADES REMOVED AND TUNED WITH WEIGHTS

98 START OF WING BRACE TESTS - CHECK RUN.

99 TO 103 } BAFFLE TEST OF ORIGINAL BLADES TO IDENTIFY ROTATING FREQUENCIES.

104 105 } WING BRACED TO INCREASE WING STIFFNESS

THE BOEING COMPANY

PREPARED BY:
CHECKED BY:
DATE:

NUMBER
REV LTR
MODEL NO.

FORM 11180 (8/67)

TEST 106 1/2 SCALE CONFIGURATION MODEL

SHEET 119

RUN NO.	MODEL CONFIGURATION	TYPE OF RUN	V q	COLL	RPM	α	δ_F	DATE
106	WNB	WING BRACED	80	VARY	0 To 2000	-1.9	0	1/28/71
107	WNB	WING BRACED 2/REV CAFFLE	80	VARY	0 To 2000	-1.9	0	1/28/71
108	WNB	WING BRACED 4/REV CAFFLE	80	VARY	0 To 2000	-1.9	0	1/28/71
109	WNB	SOFT WING RPM SWEEP	60	VARY	0 To 2000	-1.9		2/1/71
110	WNB	" "	100	VARY	0 To 2000	-1.9		2/1/71
111	WNB	" "	135	VARY	0 To 1900	-1.9		2/1/71
112	WNB	SOFT WING RPM AT VARIOUS SPEEDS	135	VARY	0 To 1900	-1.9 To +5.8		2/1/71
113	WNB	SOFT WING RPM AT VARIOUS SPEEDS	135	VARY	0 To 1900	-1.9 To +5.8		2/2/71
114	WNB	SOFT WING FLAP 30°	135	VARY	0 To 1900	-1.9 To +3.9	30°	2/2/71
115	WNB	SOFT WING	135	—	—	-2 To +12	0	2/2/71

106, 107, 108 } BLADE FREQUENCY CHECK AFTER TUNING

THE BOEING COMPANY

PREPARED BY:
CHECKED BY:
DATE:

NUMBER
REV LTR
MODEL NO.

RUN NO.	MODEL CONFIGURATION	TYPE OF RUN	V	COLL	RPM	α	δF	DATE
116	WING	SOFT WING 50 PRE-ROVE	60	VARY	6700 2020	-1.9	0	2/2/71
		END OF TEST						

TEST LOG 1/16 SCALE CONFIGURATION MODEL

FORM 11180 (6/67)

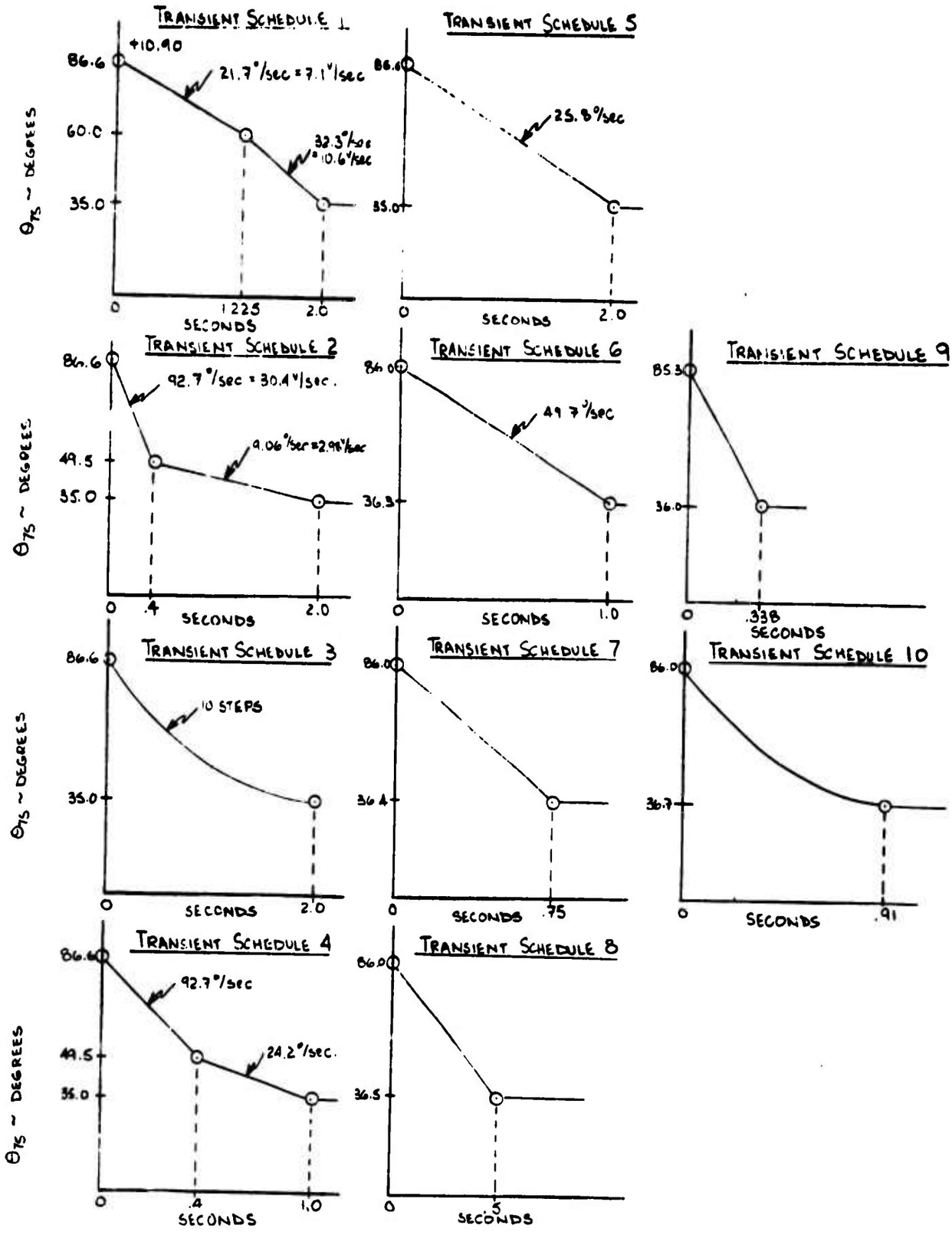

Figure 78. Transient Schedules.